DNA Nanoparticles as Ocular Drug Delivery Platform

Jan Willem de Vries

DNA Nanoparticles as Ocular Drug Delivery Platform

Jan Willem de Vries
PhD thesis
University of Groningen

September 2015

Zernike Institute PhD thesis series 2015-12
ISSN: 1570-1530
ISBN (print): 978-90-367-8015-5
ISBN (electronic): 978-90-367-8014-8

The research described in this thesis was carried out in the Polymer Chemistry and Bioengingeering group at the Zernike Institute for Advanced Materials, University of Groningen, The Netherlands. This work was funded by The Netherlands Organization for Scientific Research (NWO) and the European Research Council

Cover design: Annika Geurtsen
Printed by: Ipskamp Drukkers B.V. Enschede

rijksuniversiteit
groningen

DNA Nanoparticles as Ocular Drug Delivery Platform

Proefschrift

ter verkrijging van de graad van doctor aan de
Rijksuniversiteit Groningen
op gezag van de
rector magnificus prof. dr. E. Sterken
en volgens besluit van het College voor Promoties.

De openbare verdediging zal plaatsvinden op

vrijdag 18 september 2015 om 16.15 uur

door

Jan Willem de Vries

geboren op 26 mei 1987
te Bolsward

Promotor

Prof. dr. A. Herrmann

Beoordelingscommissie

Prof. dr. A.S.S. Dömling

Prof. dr. G. Molema

Prof. dr. S. Otto

Few are those who see with their own eyes
and feel with their own hearts.

Albert Einstein

Contents

1. Drug delivery systems based on nucleic acid nanostructures

1.1 Introduction

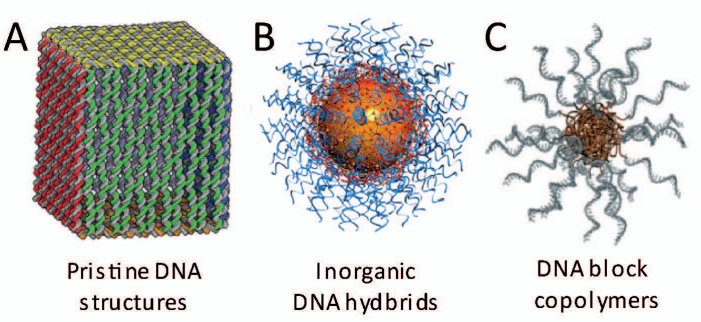

Figure 1.1 Different classes of DNA nanostructures including (A) pristine DNA nanoobjects[9], (B) inorganic-DNA hybrid materials[24] and C) assemblies of amphiphilic DNA block copolymers.

Since the discovery of the DNA double helix in 1953 many researchers have been intrigued not only by its role and the processes involved in storing genetic information but also by its utilization as a building block for

Parts of this chapter were published in: *J. Control. Rel.*, **2013**, *172*, 467-483

nanostructures[1]. This trend has been fuelled by the introduction of automated solid phase synthesis, polymerase chain reaction and molecular cloning techniques allowing to produce oligonucleotides (ODNs) and long nucleic acid strands and make them available for a wide scientific community at an affordable price or effort. The versatile fabrication methods and the notion about the position of each atom within double-stranded (ds) DNA in combination with the unique self-recognition properties of DNA have made nucleic acids one of the most popular construction materials for nano-scale objects[2]. Early models of DNA self-assembly relied on the hybridization of single-stranded (ss) ODNs into double strands to form nucleic acid junctions[3-4]. Each junction is composed of four DNA sequences and contains short ss overhangs called "sticky ends" (See Fig. 1.2A). These units provide a toehold for controlled assembly of multiple junctions, thereby creating a lattice of squares. In a similar way, a cube can be formed by catenating six circular DNA strands mediated by hybridization and ligation (See Fig. 1.2B)[5].

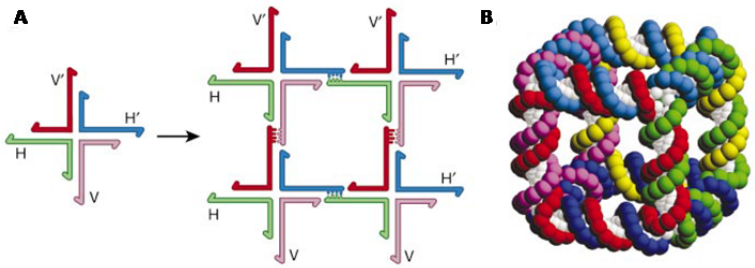

Figure 1.2 (A) On the left a representation of a nucleic acid junction formed from four ss DNA sequences is shown and on the right the corresponding lattice formed by hybridization of the sticky ends is depicted. (B) DNA cube formed by catenated circular DNA strands[4].

However, these assembly processes did not yield rigid junctions with defined angles and hence the geometry of the resulting structures was not well defined. To overcome these shortcomings two methods were developed to obtain well defined and structurally stable DNA nanoobjects. The first one involves DNA tiles that utilize the helical turn of DNA to form crossovers between two or more double strands within its structure (See Fig. 1.3A).

This design principle yields more rigid building blocks of high structural integrity that can be used for the construction of larger crystals of DNA[6-7]. Later this method was greatly expanded and generalized to allow the assembly of DNA into any desired shape like squares, triangles, star shapes or even smilies using a single viral DNA strand and many short ones that function as connecting elements, the ”staple strands”[8]. An example of a 3D structure is a DNA box that contains a controllable lid (See Fig. 1.1A)[9]. To date these DNA origami structures can easily be designed and synthesized and are applied for detection of biomolecules like proteins or DNA and for performing reactions at the nanometer scale[10-12].

The second method to obtain rigid DNA nanoobjects relies on the tensegrity principle (See Fig. 1.3B)[13-14]. The squares considered earlier were unstable due to flexible junctions. DNA triangles, however, do not face this shortcoming and when the edges are composed of this motif rigid structures are obtained[15]. Therefore, many researchers have used this principle to construct a large number of DNA nanocages resistant to deformation like tetrahedra, octahedra, dodecahedra and icosahedra[16-20].

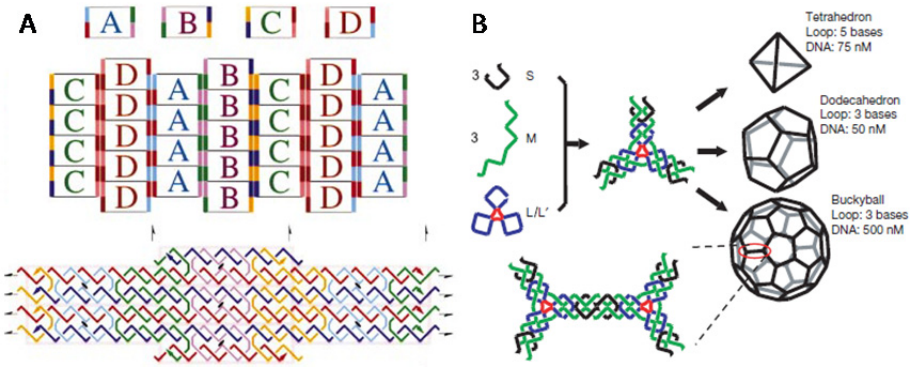

Figure 1.3 Assemblies based on DNA tiles. (A) A 2D-pattern of DNA that is based on four different tiles named A, B, C and D[6]. The colors at the vertical edges represent overhangs that hybridize with overhangs of other tiles with the same color (top). Example of a single DNA tile (bottom). (B) DNA tiles that self-assemble into 3D-nanoobjects[20].

Aside from using pristine DNA as building block inorganic nanoparticles (NPs) have been used as template for the organization of ODNs. One very

appealing template for this purpose is colloidal gold that was first used in 1996 when DNA functionalized gold nanoparticles (DNA-Au NPs) were introduced[21]. Thiol-terminated ODNs readily react with the surface of Au NPs and subsequent hybridization gives access to assemblies of higher order[22-23]. DNA-Au NPs offer some extra features like magnetic properties, plasmonic effects or the ability of fluorescence quenching, which represent a significant extension to the functionality of pristine DNA nanoobjects[24]. These characteristics are important in the field of bio-imaging and biomedicine; hence DNA-Au NPs have become a very popular template for the assembly of nanoobjects and currently find use in imaging, detection and as transfection agents and gene regulation materials[25-28].

In addition to DNA nanoparticles with an inorganic core such structures can be produced with a soft interior. The realization of these structures implies the use of synthetic organic polymers. The first DNA polymer conjugates date back to the late 1980s, where poly(L-Lysine)-*block*-DNA was used as anti-viral agent[29-30]. Nowadays, nucleic acid-polymer hybrid materials are already in clinical use[31]. Thereby, a hydrophilic synthetic macromolecule component was connected to an aptamer for increasing the *in-vivo* stability of the nucleic acid. For the realization of DNA polymer nanoobjects hydrophobic polymers need to be attached to the DNA units to achieve self-assembly into larger aggregates. The first example of such an amphiphilic biodegradable DNA block copolymer (DBC) contained poly(D,L-lactic-*co*-glycolic acid) as a hydrophobic polymer block[32]. These compounds form micellar structures that exhibit a hydrophobic core and a hydrophilic corona of ss DNA. More recently, several groups realized such micellar morphologies and in addition showed that the overall structure can be altered from spherical to cylindrical assemblies by stimuli like changes in pH, addition of endonucleases or through hybridization with complementary DNA[33-34]. Due to these unique properties, DBCs are currently applied in purification of biomaterials,[35-36] DNA detection,[37] templated synthesis[38] and in nanoelectronics[39].

All classes of DNA nanomaterials described above have in common that the size and shape are very well defined, probably better than in any other bottom-up fabricated material. This feature has dramatic consequences for

applications in the field of biomedicine where multifunctional nanoparticles start to play an increasingly important role, especially in the areas of drug delivery and bioimaging. The DNA nanoobjects act as a shape persistent scaffold allowing precise positioning of various moieties like targeting units or drug payloads. On the other hand all the different types of DNA assemblies exhibit distinctive properties. While the functionality of a pristine DNA scaffold is relatively limited, in the case of DNA hybrid materials extra functions are implemented via the non-nucleic acid components.

Although the use of DNA nanoobjects in biomedicine is still in its early stages, promising examples have been provided that demonstrate the applicability and benefits of using DNA-based nanomaterials over other systems like liposomes, polymeric micelles and polymersomes[40-43]. The most obvious use of oligonucleotide nanostructures in the medical field is the delivery of siRNA, antisense RNA or genes. However, several excellent reviews on this topic have been published recently[44-47]. The same holds true for DNA nanoobjects employed in the context of cellular and *in-vivo* bioimaging[48-49]. Therefore, both topics will not be covered in this manuscript. Here we will summarize the use of pristine DNA nanoobjects and DNA hybrid materials as carriers in the field of therapeutic delivery and vaccination. For the different classes of DNA nanomaterials we start with describing the preparation methods followed by the stability in biological environments and cell uptake behavior. Finally, we discuss controlled release or performance of the nanostructures *in-vitro* and *in-vivo*.

1.2 Delivery with pristine DNA scaffolds

1.2.1 DNA tetrahedral

While the field of DNA nanotechnology aimed for increasing the structural complexity, which is often associated to the utilization of a large number of DNA strands per nanoobject, the demands for DNA-based carrier systems poses different requirements on the design. Since for *in-vitro* and *in-vivo* experiments usually larger quantities of materials are needed, the number of

strands per DNA nanostructure with different sequence composition should be kept at a minimum due to cost issues. For the same reason the lengths of the sequences should be limited. One example of such a structure consisting of a small number of sequences is the DNA tetrahedron[50] and it was even demonstrated that this nanoobject can be prepared from a single DNA strand of 286 nucleotides (nt)[16]. While this approach requires the synthesis of DNA by rolling circle amplification or *in-vivo* replication, the same object can be realized from four chemically synthesized single strands of 55 nt. The resulting structures exhibit edges being composed of 17 base pairs (bp) of ds DNA which equals 5.8 nm considering a length of 0.34 nm per bp (See Fig. 1.4A)[50]. An object of the same geometry was realized by assembly of DNA tiles[51]. Seven strands were converted into a tile and four of these units form a tetrahedral structure. At the middle of each strut of the tetrahedron one ss overhang was incorporated that allows the implementation of a triangular feature within each plane of the object (See Fig. 1.4B). By the addition of interfering strands these inserts can be removed allowing the change of porosity of the tetrahedron's surface, which might be important for the trapping and release of cargo.

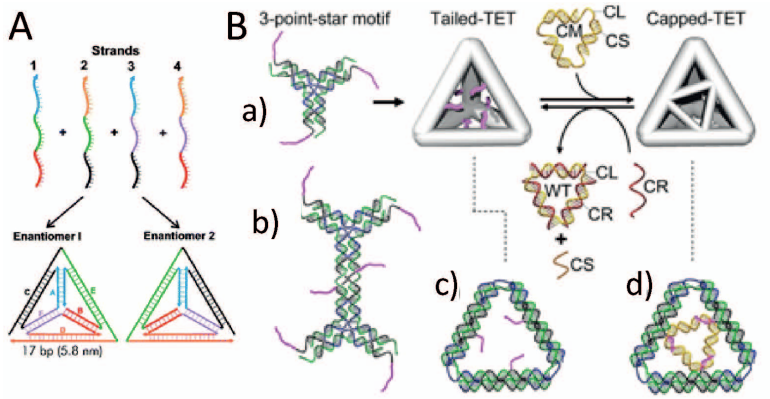

Figure 1.4 (A) Synthetic scheme for a tetrahedron composed of four DNA strands[50]. (B) Schematic design of the DNA tetrahedron with controllable porosity[51]. (a) Four 3-point-star tiles are used to construct a DNA tetrahedron with extended ss tails near the middle of the struts, offering the binding sites for the capping motif (CM), which is formed through hybridization of a longer circular DNA strand (CL) with three copies of shorter strands (CS). CM can be removed by addition of a cap-removal strand (CR) that is fully complementary to CL. (b) Details of dimer formation between two 3-point-star motifs. (c, d) Face structures of a uncapped and capped tetrahedron, respectively.

Initial experiments for the cell uptake of a tetrahedral DNA nanostructure were performed without any cargo[52]. For that purpose cultured human embryonic kidney cells were incubated with fluorescently labeled DNA cages. The uptake was investigated by confocal microscopy and flow cytometry. Significant internalization of the tetrahedron was detected for pristine nanoobjects and for ones treated with a transfection reagent. Subcellular localization revealed presence of the cages in the cytosol. Stability experiments were carried out employing Förster resonance energy transfer (FRET) experiments indicating structural integrity of the DNA cages for at least 48 h. The same cages were equipped with CpG motifs to induce immunostimulation[53]. CpG motifs are short oligonucleotides where a 2'-deoxycytidine is connected by a phosphodiester bond to 2'-deoxyguanosine. When these nucleotides are unmethylated as in natural viral and bacterial DNA they have immunostimulatory activity[54]. This CpG motif occurs very rarely in vertebrate genomes and is therefore considered a pathogen-associated molecular pattern indicating invasion of pathogens[55]. In this context the first step of eliciting an immune response is binding of CpG ODNs to Toll-like receptor 9 (TLR9) present in B cells and plasmacytoid dendritic cells (pDCs), which is followed by a signaling cascade[56]. In a therapeutic context, CpG ODNs can be applied as an agonist of TLR9 to boost the immune response which is favourable during the treatment of cancer and allergic diseases[57]. For that reason CpG-derived ODNs were investigated and tested in preclinical studies as vaccine adjuvants[58-59].

When the CpG motifs were appended to the tetrahedron, the nanoobjects were resistant to nuclease degradation and remained intact in fetal bovine serum and in cells for at least several hours. More important, they entered macrophage-like RAW264.7 cells without transfection agents and their CpG motif was recognized by TLR9. As a result of that binding event immunoregulatory downstream pathways were activated. Various pro-inflammatory cytokines including tumor necrosis factor (TNF)-α, interleukin (IL)-6 and IL-12 were up-regulated. Due to the fact that the tetrahedral nanostructures are mechanically stable several CPG motifs attached to the surfaces were accessible for TLR9 which resulted in a multivalency effect of enhanced immunostimulation (See Fig. 1.5)[60].

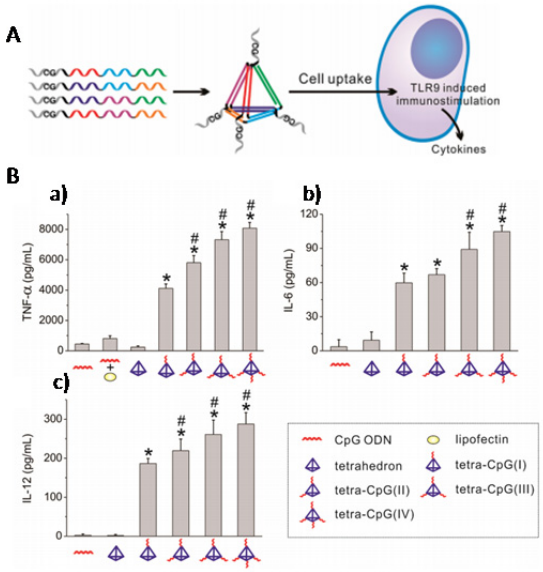

Figure 1.5 (A) Assembly of CpG grafted DNA tetrahedron delivery systems for eliciting an immune response[60]. (B) Release levels of cytokines TNF-α (a), IL-6 (b) and IL-12 (c) from RAW264.7 cells using different immunostimulatory nanoobjects.

After these successful *in-vitro* experiments, DNA tetrahedra equipped with CpG motifs were employed *in-vivo* for vaccination (See Fig. 1.6A)[61]. Therefore, streptavidin (STV) was incorporated into the DNA nanocages to form an antigen-adjuvant complex. The immunogenicity of this complex was assessed in a BALB/c mouse model by measuring the anti-STV antibody response and compared to an unassembled mixture of STV and CpG ODN or STV alone. It was found that mice immunized with the STV-CpG ODN-tetrahedron developed a much higher level of anti-STV IgGs than the above mentioned controls after a period of 70 days. To substantiate this outcome antibody secreting cells (ASCs) that originate from STV-specific memory B cells present in spleen cells were quantified (See Fig. 1.6B). Significantly elevated levels of specific ASCs were determined for mice immunized with the tetrahedron-CpG ODN-STV complexes compared to those immunized with free CpG + STV and STV only. These results indicate that the fully loaded tetrahedron induces a strong and long-term immunity against the antigen due in part to the generation of STV-specific

memory B cells. Further experiments proved the safety of the DNA carrier because no immune response against the carrier, i.e. a ds DNA tetrahedron, was developed, which could result in tissue damage or trigger autoimmunity[61]. This work shows the great potential of scaffolds generated by DNA nanotechnology to serve as a general platform for vaccine development. A major part of the DNA tetrahedron's potency in the biomedical field is derived from its rigid 3D scaffold allowing specific multivalent interactions with cellular components.

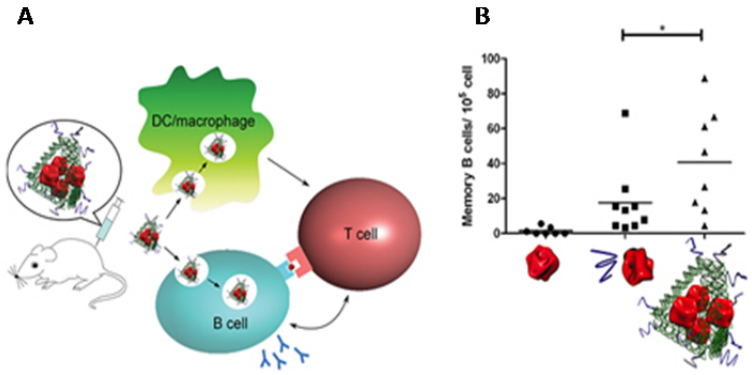

Figure 1.6 (A) Schematic drawing of the DNA tetrahedron vaccine complex containing the antigen streptavidin (red) and CpG ODNs (purple)[61]. (B) ELISPOT assay of specific memory B cell response in mice stimulated by STV, STV+CpG and CpG-STV DNA tetrahedron, respectively.

However, DNA tetrahedra with a flexible unit were generated as well[62]. One of the struts of the tetrahedron was constructed from a ss RNA aptamer recognizing ATP. When this assembly was internalized into HeLa cells ATP levels within living cells could be measured indicating that the construction of intracellular logic sensors is feasible.

1.2.2 Branched DNA nanostructures and polypods

The DNA tetrahedron represents a simple shape persistent scaffold allowing to present four units at each vertex like the CpG motif or cell surface recognizing aptamers. Equally simple regarding the design but of more structural flexibility are branched structures or polypods. The simplest assembly of this type is Y-shaped and can be constructed from three ODN strands (See Fig. 1.7A)[63]. Already in 2008 such a DNA nanostructure was equipped with several immunostimulatory CpG motifs[64]. Cytokine production (TNF-α and IL-6) after addition of the Y-structure to RAW264.7 cells was measured. It was found that the ds Y-shape is effective in inducing greater amounts of TNF-α and IL-6 in macrophage like TLR9-positive cells than conventional ss ODNs or ds ODNs containing the same amounts of CpG motifs. This high immunostimulatory activity of Y-ODN is at least partly associated with increased uptake by the TLR9-positive cells but not with stabilization through the DNA nanostructure. Other factors like higher affinity of Y-ODN to the TLR9 receptor or intracellular localization may also contribute to the increased immunostimulation.

In a follow up study the same authors fabricated dendritic DNA nanostructures by ligating Y-shaped DNA monomers[65]. In this manner, the second and third dendrimer generation were fabricated with 12 and 24 CpG motifs located at the periphery of the DNA nanostructures, respectively (See Fig. 1.7B). The dendritic DNA architectures induced greater amounts of TNF-α and IL-6 from RAW264.7 cells than a mixture of Y-shaped DNA encoding the same CPG motifs as present in the dendrimers. The dendritic DNA was internalized six to 15 times more efficiently by the macrophage-like cells than Y-DNA, which resulted in the secretion of much greater (100-fold or more) amounts of cytokines. These results suggest that a dendritic architecture with multiple CpG motifs at the rim is a viable design for a DNA nanostructure to increase the immunostimulatory activity without any chemical modification of the natural phosphodiester DNA backbone.

In addition to the trigonal Y-shaped unit, polypods with a higher degree of branching were evaluated regarding their immunostimulatory potential[66].

For that purpose a tri-, tetra-, hexa- and octapod consisting of three, four, six and eight ODNs, respectively, were assembled (See Fig. 1.7 C). Again at the end of the branches CpG motifs were established yielding assemblies consisting of DNA in the B-form with a diameter of around 10 nm. The melting temperature of the nanoobjects decreased with increasing the degree of branching. Each polypod DNA induced the secretion of TNF-α and IL-6 from macrophage-like RAW264.7 cells to a greater extent than ss or ds non-branched CpG containing DNA. Evenly important, the highly branched architectures, i.e. hexa- and octapod, were more effective in stimulating cytokine production than the structures with a lower branching degree, i.e. tri- and tetrapod. Other properties that are dependent on the degree of branching are the uptake and the stability in serum. The more branched the polypods are the better they are taken up in TLR9-positive cells but the less stable they are. From these results it could be concluded that the CpG-containing polypods with hexagonal and octagonal symmetry are promising biodegradable nanoobjects with high immunostimulatory activity.

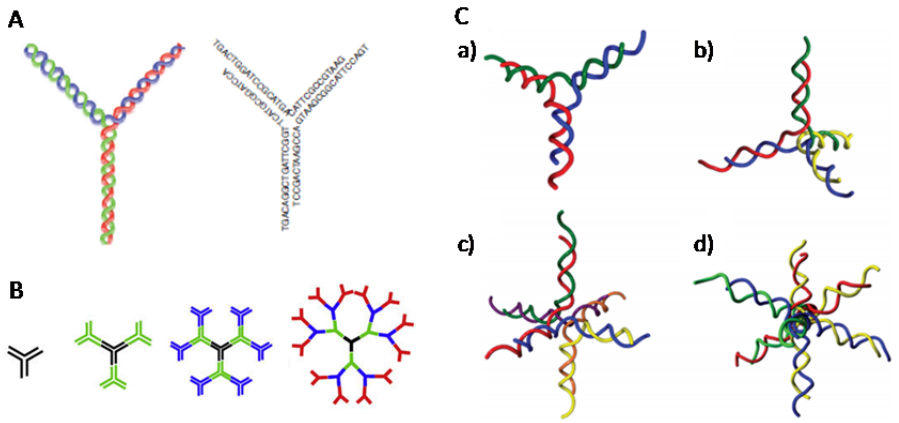

Figure 1.7 (A) Schematic representation of Y shaped ODNs[63]. (B) Schematic design of dendrimer-like DNA (DL-DNA), from left to right: Y-DNA; first generation DL-DNA, second generation DL-DNA, and third generation DL-DNA[65]. (C) Schematic representation of models of polypods: a) tripod-DNA, b) tetrapod-DNA, c) hexapod-DNA and d) octapod-DNA[66].

1.2.3 DNA icosahedra

In addition to directly using branched DNA structures for immunostimulation, more complex polyhedra can be fabricated from those building blocks. The resulting assemblies contain a triangular tensegrity motif and were employed for drug delivery purposes[67]. From six individual DNA single strands, six-point-star motifs were formed (See Fig. 1.8A) that via sticky end cohesion self-assemble into an icosahedron (See Fig. 1.8B). In one of the six strands an aptamer sequence was incorporated that protrudes from the icosahedron surface and is responsible for MUC 1 recognition. This protein belongs to an important class of tumor surface markers which are uniquely expressed on a broad range of epithelial cancer cells with high abundance[68-69]. The final step of the carrier fabrication consisted of loading of Doxorubicin (Dox) by intercalation (See Fig. 1.8C). This anthracycline derivative is frequently employed in chemotherapeutic anticancer treatment[70-72]. The potency of the icosahedral carrier system was assessed by *in-vitro* cell culture experiments employing flow cytometry, confocal fluorescence microscopy and cytotoxicity tests. In co-culture experiments it could be demonstrated that the DNA nanocarrier was efficiently taken up by the human breast cancer cell line MCF-7 that is MUC1 positive while no internalization was observed in Chinese hamster ovary cells (CHO-K1) that do not express MUC1. Besides this superb targeting function the Dox-loaded carrier exhibited a greater cytotoxicity in MCF-7 cells than free Dox indicating specific and efficient delivery of anticancer drugs and suggesting the potential use of DNA icosahedra for use in targeted cancer therapy[67].

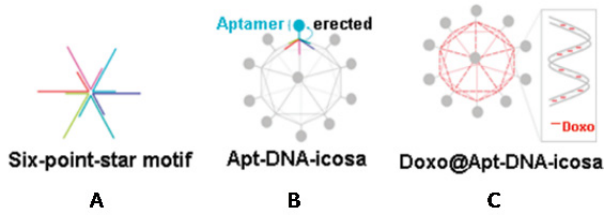

Figure 1.8 Schematic representation of (A) the six-point-star motif, (B) the DNA icosahedron and (C) the DNA icosahedron containing intercalated Dox for targeted delivery[67].

Another function that was realized with icosahedral DNA nanostructures is *in-vivo* imaging[73]. Therefore, fluorescein isothiocyanate (FITC)-labeled dextran (FD10) with a molecular weight of 10 kDa was encapsulated in an icosahedral DNA cage. The encapsulation procedure starts with the formation of two icosahedral halves from five-way junctions similar as described above (See Fig. 1.9A)[19]. These two assemblies were incubated with FD10 and subsequently joined by hybridization resulting in a full DNA icosahedron containing two FD10 units within their interior (See Fig. 1.9B). These host guest complexes were microinjected into *Caenorhabditis elegans*. This organism is a nematode that contains scavenger cells, called coelomocytes, which endocytose fluid from the pseudocoleom. After introducing the loaded icosahedra, these nanoobjects were specifically internalized by the coelomocytes due to interactions with anionic ligand-binding receptors and subsequent receptor-mediated endocytosis. In stark contrast, the pristine FD10 lacks negative surface charges and was therefore taken up by fluid phase endocytosis resulting in its non-specific distribution throughout the pseudocoleom after microinjection. After proving the complete alteration of endocytotic uptake pathways due to different molecular interactions the functionality of the cargo was examined *in-vivo*. Due to their pH sensitivity, FITC on Dextran was employed as pH sensor to measure the proton concentration in organelles, inside cells and whole organisms[74-75]. When encapsulated in the DNA nanocage this function remains unchanged and the host guest complexes were employed to map the pH changes during endosomal maturation along the ALBR pathway in coelomocytes in living worms. This work represented the first demonstration of functionality and emergent behavior of a cargo-loaded DNA nanostructure *in-vivo*[73].

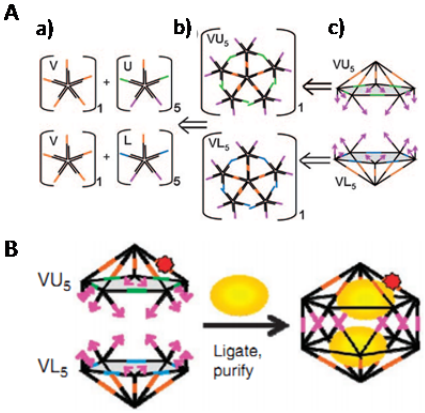

Figure 1.9 (A) Synthetic strategy for constructing the DNA icosahedron, (B) Encapsulation of (FITC)-Dextran into DNA icosahedron[73].

1.2.4 DNA origami

As introduced above, the DNA origami technique deals with folding a ss long DNA strand into almost any 2D or 3D shape with the help of many different "staple" strands[8, 76]. These strands bind to the long one at different positions to define the overall structure and they can be utilized to site specifically introduce additional functionalities by hybridization.

Before the DNA origami structures were introduced for biomedical purposes their stability in cell lysates was investigated[77]. Four assemblies were fabricated for that purpose: a 2D rectangular origami (90 x 60 nm)[10], a 2D equilateral triangle (120 nm long with 30 nm wide sides) with an open central triangular cavity of 60 nm per side, a 3D multilayer rectangular parallelepiped structure (16 x 16 x 30 nm) and a 2D rectangular structure with staple strands bearing overhangs allowing hybridization (See Fig. 1.10)[10]. These DNA architectures were incubated with cell lysate from which nuclear DNA and cell membrane debris were removed. After incubation times of 1 and 12 h the origami structures were investigated by non-denaturing gel electrophoresis and by direct visualization employing AFM as well as transmission electron microscopy. Taking into account all three methods it can be concluded that all the origami assemblies are stable at 25°C with the cell lysates tested, i.e. metaplastic human esophageal epithelial cell line,[78] End1/E6E7 cells, MCF-10A cells and cancerous HeLa

and MDA-MB-231 cells. In contrast, ss M13mp18 viral DNA and ds λ DNA that acted as control showed alterations already after 1 h incubation with the cell lysates. Finally, it was demonstrated that ss DNA features protruding from the origami structures remained intact and could be successfully used for detection of mRNA from the lysate. These results suggest that DNA origami scaffolds have the potential to serve as an *in-vitro* diagnostic platform and might be of importance for single cell proteomic analysis when integrated into microfluidic chips.

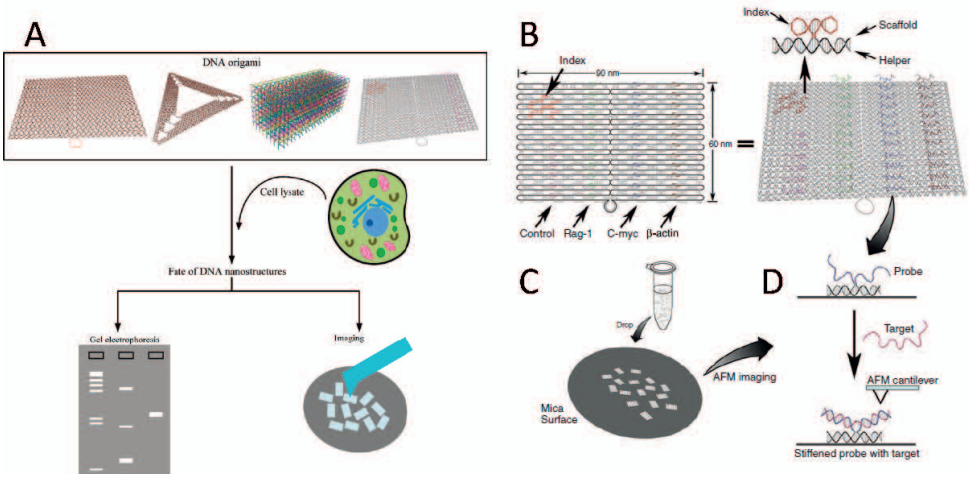

Figure 1.10 (A) DNA origami structures used for testing the stability in cell lysate, from left to right: 2D rectangle, 2D equilateral triangle, 3D multilayer rectangular structure and a 2D rectangle with staple strands bearing ss overhangs[77]. (B) (Left) Schematic representation of DNA origami structure for nucleic acid detection (Rag-1, C-myc, β-actin and control). The DNA square was composed of circular single-stranded M13 viral DNA (black) and >200 staple strands[10]. Through incorporation of helper strands ss overhangs were formed allowing for hybridization with the target sequence. (Right) 3D illustration of the DNA origami. (C) Representation of target detection using DNA origami structures. (D) (Top) ss helper strands on top of the tile and (bottom) detection of target sequence using atomic force microscopy (AFM).

The same results also confirm the stability of DNA origami objects inside cellular environments and therefore their application as delivery vehicle will be discussed in the following paragraph. As shown above many DNA nanostructures were tested regarding their immunostimulatory potency when equipped with CpG motifs. For the same purpose structurally complex DNA

origami scaffolds were successfully utilized as well. Freshly isolated spleen cells were incubated with a hollow 30-helix origami tube (approximately 80 x 20 nm) with 62 binding sites for hybridization of CpG motifs distributed over the surface. This DNA origami scaffold that was constructed from M13mp18 DNA (8634 nt) and 227 staple ODNs was taken up into endosomes and triggered a strong immune response indicated by cytokine secretion, which was entirely dependent on TLR9 stimulation. As controls for the DNA origami tubes, CpG ODNs complexed with Lipofectamine, a standard transfection agent, were employed which showed lower immunostimulation when applied at equal amounts. Tubes without hybridized CpG motifs induced a low amount of cytokine production that was not related to TLR9 recognition. In contrast to the cationic carrier Lipofectamine, the DNA tubes exhibited no detectable cytotoxicity for splenocytes and therefore qualify themselves as an efficient and non-toxic immunostimulans.

Similar tubes as generated for immunostimulation were harnessed for cancer therapy[79]. In this study, two types of DNA origami tubes were employed that were smaller than the one applied for immunostimulation. The first type exhibited a straight nanotube structure using a conventional number of 10.5 bases per helical turn to determine crossover positions between neighboring helices. This S-Nano design relied on a scaffold strand containing 7560 nt, exhibited a length of 138 nm and a diameter of 13 nm. As a second design, a twisted version (called T-Nano) with similar dimensions was constructed (See Fig. 1.11). It is based on a 8634 nt long scaffold and during hybridization of staples every seventh nt an insertion was introduced similar as reported before[80]. The accommodation of 12 bp per turn resulted in a global right handed twist to partially relief the stress induced by imposing an unnatural twist density on the DNA. Subsequently, an anticancer drug was loaded into the DNA origami tubes by intercalation. The T-Nano design was able to accommodate 33% more Dox than the S-Nano structure although T-Nano contains only 14% more base pairs than the straight tube. The difference in loading capacity might be explained by the higher affinity of Dox to the 12 bp/turn helix. After loading, the release from the tubes was studied. The T-Nano design retains the drug to a larger extend than S-Nano resulting in a slower release profile. The release kinetics of T-Nano indicated

that 50% of the drug could be retained for more than several hours which was translated into a higher toxicity of this system towards three different breast cancer cell lines (MDA-MB-231, MDA-MB-468 and MCF-7) compared to free Dox. The S-Nano/Dox system and ds DNA loaded with Dox were less potent in similar experiments. These findings and the non-toxic nature of the T-Nano origami structure itself suggest that twisted DNA origami designs are a suitable delivery platform for targeted cancer therapy.

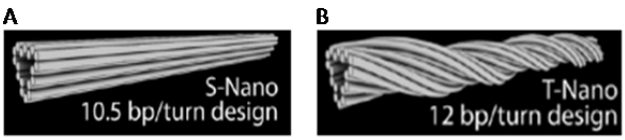

Figure 1.11 3D models of (A) straight nanotube (S-Nano), using 10.5bp per turn twist density and (B) twisted nanotube (T-Nano), having 12bp/turn[79].

In a different study it could even been shown that DNA origami carriers have the potential to overcome drug resistance[81]. A DNA origami tube and a triangle were loaded with Dox, similar as described above, and were administered to drug sensitive (reg) and drug resistant (res) MCF7 human breast adenocarcinoma cells (See Fig. 1.12). Free Dox and Dox-loaded origami assemblies were both active in killing the reg-MCF7 cell line. In contrast, free Dox and ds DNA with intercalated Dox moieties were not effective in inducing cell death in res-MCF7 cells. However, when the same cells were incubated with the origami structures containing the same amount of Dox as the above controls cell death was induced. This is a strong hint that DNA origami structures have the potential to overcome Dox resistance. In the next step, the reason for this characteristic of the origami carrier was investigated. The origins of cultured cancer cells becoming resistant against cytotoxic anticancer drugs can be manifold[82-83]. One of the most common reasons is decreased drug concentrations inside cells as e.g. induced by efflux pumps in the membrane that eject drugs or decrease drug uptake. In this regard, it was demonstrated that the folded DNA nanostructures increase the uptake of the anticancer drug in res-MCF7 cells. Another reason for the development of multidrug resistance is related to intracellular pH, both in the cytoplasm and in acidic organelles[84]. In tumor cells with a resistant

phenotype the anticancer drugs are predominantly localized in acidic compartments like the lysosomes and are therefore not able to reach the site of action, i.e. the cytosol or nucleus[85]. Therefore, the co-administration of agents liberating the drugs from these compartments was carried out allowing redistribution of the drug to the active sites[86-87]. In this study, it was revealed that treatment of res-MCF7 cells with Dox-loaded origami objects resulted in elevated pH indicating the inhibition of acidification of lysosomal compartments. Taken together, overcoming drug resistance by the origami assemblies can be explained by a combination of two features. Firstly, the origami scaffold increases Dox uptake and, secondly, induces a change of pH in lysosomes leading to a redistribution of the drug to the target sites.

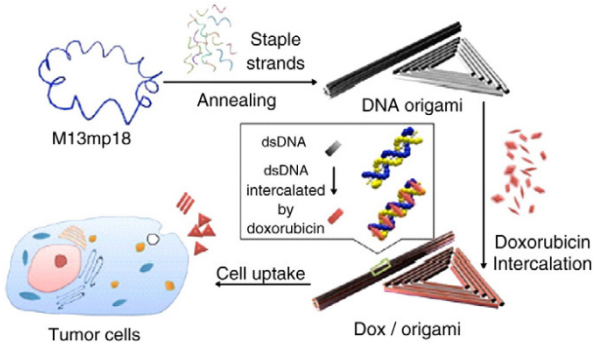

Figure 1.12 Schematic representation of DNA origami systems, DNA tube and DNA triangle, for Dox delivery[81].

A more complex vehicle regarding functionality was based on an origami design consisting of a hexagonal barrel with dimensions of 35 nm x 35 nm x 45 nm (See Fig. 1.13)[88]. This called logic-gated nanorobot was constructed in such a way that the two domains forming the barrel were covalently connected at the rear and were non-covalently fastened twice at the opposite site. These two non-covalent connections were designed as DNA aptamer-based locks that open in response to antigen keys. In the closed state the lock consists of an aptamer-complement duplex that after binding of the molecular "key" dissociates or opens to form an aptamer-target complex. Due to the presence of two aptamer locks at the front side a logic gate-type

behavior can be implemented into the origami structure. When the locks are equipped with sequences recognizing different targets opening of the barrel only occurs when both antigen keys are present emulating an AND-gate behavior. Inside the DNA barrel 12 attachment sites were placed for the incorporation of cargo molecules by hybridization. Au nanoparticles and Fab antibody fragments covalently connected to ODNs served as payload. After locking and loading the functionality of the nanorobot was tested. It was demonstrated that when the proper combination of antigen keys was present the nanorobot opens its barrel structure and binds to a cell surface which was measured by flow cytometry due to the presence of a fluorescent label that was attached to the payload antibodies. Finally, the nanorobots were investigated in regard to their ability to get activated and interfaced to cells to interfere with signaling pathways. Thereby it was demonstrated that after specific unlocking the nanorobots induced growth arrest in leukemic cells in a dose dependent manner. In addition to the inhibition task, various methods of signaling pathway activation were demonstrated. It was shown that nanorobots could collect flagellin from solution and induce T cell activation. All the experiments prove that the origami robots can induce a variety of tunable changes in cell behavior. Moreover, bioactive molecules may be introduced indirectly via interactions with loaded antibody fragments, enabling applications in which the robot fulfills a scavenging task before targeted payload delivery.

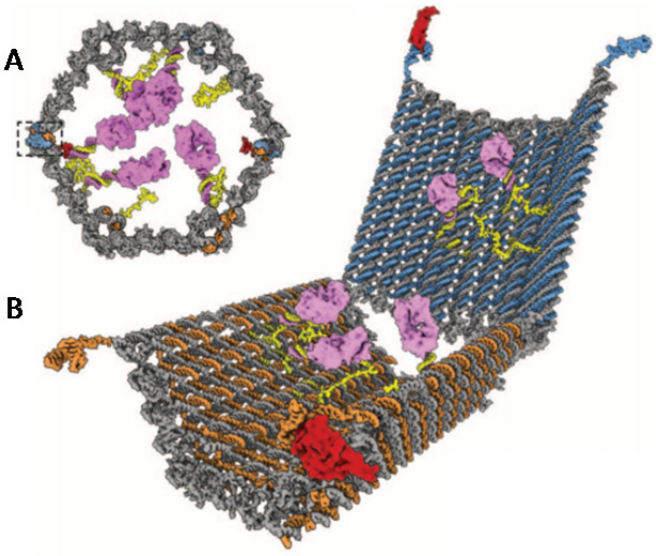

Figure 1.13 (A) Schematic front orthographic view of DNA nanorobot in the closed state with a protein payload attached inside. (B) 3D view of DNA nanorobot in the open state[88].

While all the origami structures in this paragraph consist of many different units, especially a high number of staple strands, efforts to reduce the quantity of building blocks are necessary for cost efficiency and practical applications. One such alternative to the origami method to produce tube structures is the utilization of rolling circle amplification (RCA). RCA is an enzymatic method that allows the fabrication of long, ss DNA of periodic sequence from cyclic templates. The resulting RCA products were employed to construct long tracks of proteins[89] and nanoparticles[90]. For the assembly of nanotubes, a circular ss DNA was combined with a primer strand and DNA polymerase Phi29 producing the periodic ss DNA **Guide** (See Fig. 1.14)[91]. This long DNA strand coding alternatingly binding regions (**BR**) and spacer regions (**SR**) was hybridized with spacer strand **1a** to form **1**. The ss BR was then hybridized with triangular rung **2** to result in an open nanotube **RCA-NT$_o$**. This extended structure was transformed in the closed tube **RCA-NT**. The dimensions of such triangular tubes could be controlled by the length of the RCA product ranging from around 0.7 to 1.2 μm. Similar as the origami tubes, the RCA-derived assemblies were more

resistant towards the digest by nucleases compared to conventional ds DNA and they were internalized in human cervical cancer cells (HeLa). With the same cell line, uptake of ds DNA was negligible. Combined with their proven uptake and release behavior these DNA-economic nanotubes are a potentially unique platform for drug delivery and bioimaging[92].

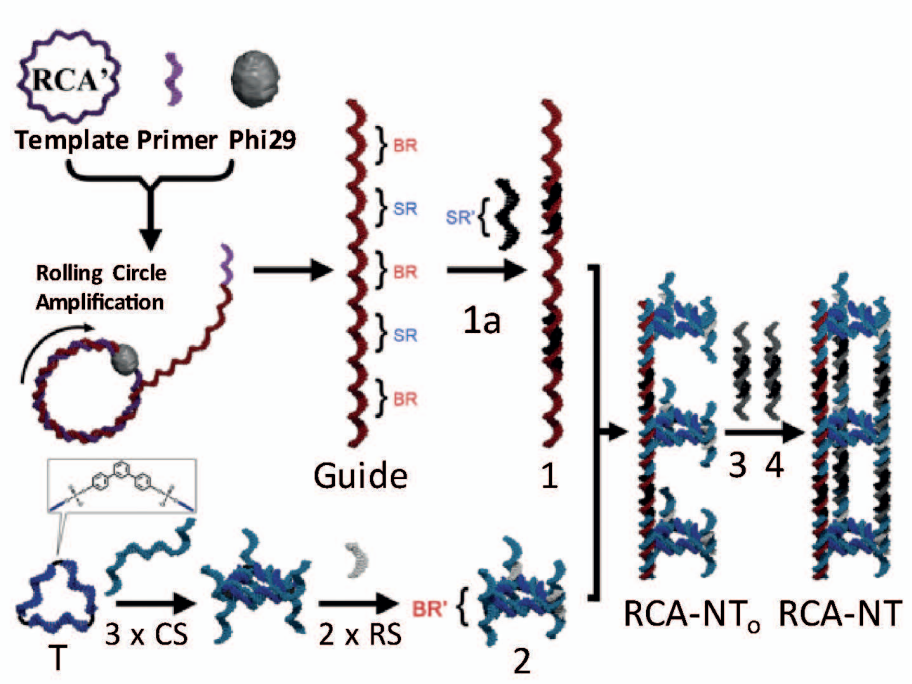

Figure 1.14 Design of RCA nanotubes[91]. The backbone strand 1 with alternating segments of BR and SR is prepared by RCA. On each vertex of triangular rung 2, two well oriented ss DNA sequences extend longitudinally for hybridization with 1 to construct the open nanotube RCA-NTo. Double-stranded linkers 3 and 4 are used to form the full nanotube RCA-NT.

An even more reductionist approach regarding sequence efficiency is the use of a single DNA strand that governs the ability to self-assemble into a tube[93]. This 52 nt long strand is divided into four segments which exhibit a length of 10, 16, 16 and 10 bases, respectively, and are all self-complementary. Due to that particular design they assemble into tubes with a length of up to 60 µm and varying diameters in the range of several tenths of

nanometers. Initial steps towards employing these DNA tubes for targeted cancer therapy have been undertaken. The 52 nt DNA strands were conjugated to folic acid, a targeting unit, and Cy3, a fluorescence imaging agent. Subsequently, cancerous KB cells that overexpress the folate receptor were incubated with the dually labeled nanotubes. The 1D nanostructures were strongly adsorbed on the cell surface and parts of them effectively internalized. At the same time, like for other DNA tube constructs, they showed no obvious toxicity.

1.3 Delivery with scaffolds consisting of nucleic acids combined with other materials

There are several differences between the DNA nanostructures described above and the hybrid materials discussed in this paragraph. The dominant motif in all pristine nucleic acid assemblies is the DNA double helix forming a rigid and to a great extent shape persistent scaffold. In DNA nanostructures derived from DNA hybrid materials both single- and double-stranded nucleic acids are found. In those materials the orientation of the DNA is dictated by the attachment to the core not by hybridization. While pristine DNA assemblies almost exclusively rely on Watson-Crick base pairing, nanostructures from DNA hybrid materials are formed by covalent bonds either to an inorganic core or to a hydrophobic polymer. Various core structures are known that served as anchoring points like Au,[94] Ag,[95] Fe_3O_4,[96] CdSe,[97] or hydrophobic polymers[98-100].

1.3.1 DNA nanoparticles with an inorganic core

1.3.1.1 DNA-Au NPs

The most important inorganic core material in the context of drug delivery is Au. DNA-Au NPs were fabricated by mixing ODNs containing a terminal sulfhydryl group with citrate-stabilized colloidal Au NPs. The ODNs replace the small ligand and cover the surface.[21] To increase the density of DNA a

method called salt-aging was developed. High salt concentrations (> 0.15 M) were applied to screen the negative charges of the DNA backbone allowing the assembly of a densely packed ODN corona[101]. Via these methods DNA NPs are accessible with core diameters ranging from 2 to 250 nm[102-103]. Important in the context of biomedical applications and the long-term toxicity of inorganic NPs[104-106] is the fact that the Au core can also be completely removed. For that purpose the ODN was attached via a propargyl ether-modified terminal nucleotide on an Au NP template and cross-linked. Finally, the core was removed by oxidative dissolution[107].

As for the pristine DNA nanoobjects a major threat for the *in-vitro* and *in-vivo* applications of Au NPs is the digestion by nucleases. Detailed studies have been performed for these materials and the findings might be of importance for the pristine DNA assemblies as well. By incubation of DNA-Au NPs with DNAse I it was demonstrated that ds nucleic acids are more stable when bound to a core compared to pristine ds DNA[27]. The same stability was observed in an intracellular environment (C166 cells). The reason for the enhanced integrity of DNA bound to the Au NPs was investigated[108]. It turned out that not steric inhibition of binding of the nuclease was responsible for the increased stability but the high local ion concentration associated to the densely packed DNA. Pristine DNA and DNA-Au NPs exhibited comparable enzymatic digestion rates under conditions where salt concentrations do not affect the enzyme's activity. In contrast, at high salinities the degradation rate of NP-bound DNA was drastically reduced relative to unbound one. From these results it was concluded that the high local sodium ion concentration is the dominating factor for the origin of enhanced stability of DNA. In serum the stabilizing effect is further increased due to absorption of serum proteins on the surface of DNA-Au NPs and associated therewith the reduced access by nucleases.

Even more surprising than the improved integrity of DNA on the NPs was the finding that DNA-Au NPs were able to enter a large variety of cell types. Usually, transfection reagents[109-110] are required to deliver ODNs or genes to cells due to the fact that the cell surface is negatively charged and represents a strong barrier for the negatively charged polyelectrolyte DNA due to electrostatic repulsion. Up to now it was shown that DNA-Au NPs are

taken up by more than 30 cell lines, primary cells and neurons without the need for a positively charged transfection agent.[94] In view of these remarkable results with uptake of millions of NPs per cell the mechanism of this process was studied in more detail. A key requirement for pronounced uptake is a dense DNA surface layer on the particles since cellular internalization of bare citrate particles or particles passivated with BSA is orders of magnitude lower[111-112]. The influence of the core for uptake is minor since both DNA-coated iron oxide NPs as well as spherical nucleic acids (DNA NPs after core removal) exhibit high cellular uptake. The universal uptake behavior is promoted in part by membrane-bound scavenger receptors[113] which recognize specific polyanionic ligands including ODNs[114] or phosphorthioated ODNs[115] and induce receptor-mediated endocytosis. A possible uptake mechanism may look like that: First, serum proteins such as BSA adsorb to the ODN shell of the Au NPs which slightly inhibits uptake. Subsequently, the scavenger receptors bind to the DNA-Au NPs and initiate endocytosis while the serum proteins are replaced from the NP surface. A strong hint supporting this mechanism is the reduced uptake after these receptors were inhibited by their natural agonists such as poly-inosine and fucoidan[116].

Due to this favorable property profile, DNA-Au NPs were exploited for drug delivery purposes. In this context their ability for targeting was assessed first[117]. Therefore, a monoclonal antibody (mAb) recognizing human epithelium growth factor receptor 2 (HER2) was conjugated to an ODN. HER2 is part of the ErbB protein family that is involved in signaling pathways leading to increased cell proliferation and differentiation[118-119]. The mAb conjugate was hybridized with DNA-Au NPs to be connected via non-covalent bonds. The resulting DNA-Au NPs were taken up by HER2-positive cells (SKOV-3) to a much greater extent and at a faster initial rate relative to HER2-negative cells documenting the targeting effect and cell type selectivity of the conjugated mAb.

Besides equipping the DNA-Au NPs with Ab they were loaded with anticancer drugs[120]. As a starting point served DNA-Au NPs that were functionalized with an ODN carrying a terminal amine at the rim of the NP. This terminal group was functionalized with a Pt(IV) complex. Cisplatin is a

well-established anticancer drug[121-122] and Pt (IV) complexes act as an attractive alternative to Pt (II) species. Pt(IV) compounds are more inert and cause less side effects relative to Pt(II)-based anticancer drugs that exhibit higher reactivity and thus lower biological stability. The Pt(IV)-loaded DNA-Au NPs were successfully internalized by cells and reduced to liberate cisplatin. This active species entered the cell nucleus and formed 1,2-d(GpG) intrastrand cross-links with genomic DNA. The effectiveness of the Pt DNA-Au NPs was superior to cisplatin in killing several kinds of cancerous cell lines. Another anticancer drug, Paclitaxel, was incorporated into DNA-Au NPs[123]. This potent chemotherapeutic agent is characterized by a low solubility in aqueous media which can limit its effectiveness. Moreover, treatment regimens with this drug were limited by eventual acquirement of resistance of the cancer cells. Similar as described in the context of the Pt-loaded NPs, Paclitaxel was covalently connected to the surface of DNA-Au NPs. Through the conjugation to NPs the hydrophylicity and stability of the drug was significantly increased compared to free Paclitaxel. The NP-based drug delivery system was more effective in inducing apoptosis *in-vitro* across several cell lines and concentrations than the free active. Notably, cell death was even induced in Paclitaxel-resistant MES-SA/Dx5 cells underlining the potency of DNA-Au NP systems for drug delivery.

Besides loading anticancer drugs by covalent connections to the DNA-Au NPs the chemotherapeutic agents were introduced by non-covalent bonds into the NP system[124]. Dox and actinomycin D (actD) were intercalated in pre-designed binding sites of two respective types of ds DNA-Au NPs (core diameter 15 nm)[125-126]. Regarding the liberation of the drugs from the carrier it was found for Dox that the rate constant for release was four orders of magnitude smaller than for Dox-loaded duplex DNA in solution. In stark contrast, for actD a similar rate constant for release was found for NP-loaded drug and drug bound to ds DNA. Cytotoxicity measurements employing neuroblastoma cells revealed no obvious toxicity of the unloaded DNA carriers. When loaded with the chemotherapeutic agents both vehicles showed higher toxicity at low drug concentrations but were less cytotoxic at higher concentrations compared to the freely administered actives.

In extension to intercalating Dox molecules into the nucleic acid shell of Au NPs, the carriers were equipped with a targeting function[127]. For that purpose served an aptamer that targets prostate cancer cells by recognizing prostate-specific membrane antigen (PSMA)(See Fig. 1.15)[128]. The targeted nucleic acid NPs were internalized in LNCaP cells that express PSMA three times more efficiently than PC3 cells that are PSMA-negative. In addition to histological detection of NP uptake and quantification by inductively coupled plasma atomic emission spectroscopy, computed tomography was carried out *in-vitro* to prove the targeting of the NP system. At the same time these experiments document the utility of this delivery vehicle to fulfill also a bioimaging function.

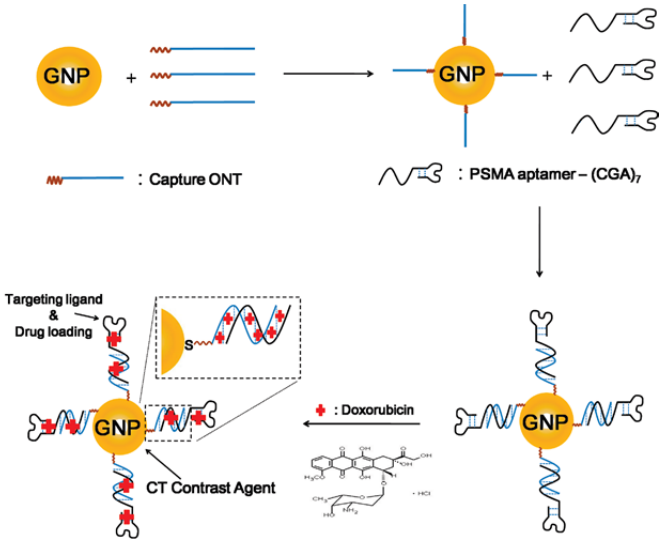

Figure 1.15 Schematic representation of the assembly of targeting Dox-loaded Au NPs using the PSMA aptamer[127].

Besides employing the gold core for imaging purposes, it was exploited for the stimulus-induced release of anticancer drugs[129]. The shape of the core was chosen to be rod-like (50 nm x 10 nm). The DNA shell on top was loaded with Dox and the surface was decorated with folic acid targeting units by hybridization. The modular assembly of this multifunctional carrier is illustrated in Fig. 1.16. Compared to spherical Au NPs their rod-like

counterparts exhibit a plasmon band at higher wavelength in the near infrared (NIR) region (650-900 nm). Since NIR light can deeply penetrate tissue[130] and can be effectively converted into heat after absorption by the Au nanorods (NRs), the light-induced liberation of Dox from the DNA coated rods was successfully realized *in-vitro* and *in-vivo*. Due to the drug release, tumor growth in BALB/c nude mice was efficiently inhibited. This work represents an example of a combination of three kinds of therapy, i.e. NIR-based thermotherapy, triggered chemotherapy and targeted delivery. Although the NRs were intratumorally injected this work is the basis for further developments achieving optimal biodistribution for systematic administration. Such an optimization process is greatly facilitated by the modular assembly platform which might be easily transferred to treatments of other human diseases.

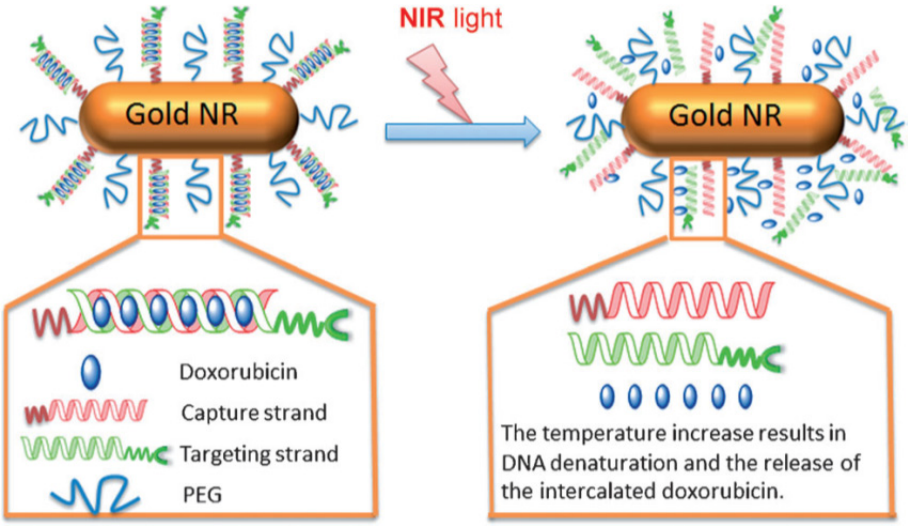

Figure 1.16 Schematic representation of Au NRs for targeted Dox delivery functionalized using folic acid targeting strands[129]. Upon irradiation with NIR light the NR is heated and induces dehybridization of the targeting and capture strand, resulting in release of the loaded drug.

As described for the pristine DNA nanoobjects, DNA-Au NPs were employed for immunostimulation as well[131]. For that purpose the inorganic core was functionalized with CpG motifs. Strikingly, the CpG Au NPs were

more than one order of magnitude more effective in inducing TNF-α secretion compared to naked ss CpG ODNs. These experiments suggested that CpG Au NPs can act as proinflammatori stimuli *in-vitro* and might be a promising therapeutic tool in animals.

1.3.1.2 NPs composed of silica and DNA

Aside from DNA-Au nanomaterials, mesoporous silica nanoparticle (MSN) conjugates offer great opportunities for drug delivery. These structures are highly porous and thus have a high drug loading capacity. Furthermore, their pore size can be easily tailored, they are biocompatible and exhibit high thermal stability. The synthesis of MSNs proceeds through growth of triethyl orthosilicate under basic conditions onto micellar rod scaffolds that act as a template and typically are made of *n*-cetyltrimethylammonium bromide (CTAB)[132]. Afterwards the surfactant is removed under acidic conditions to yield MSNs with a diameter of around 100 – 200 nm and pores with sizes of 2 – 10 nm. Functionalized MSN can be prepared through co-condensation with functional oligosilicates such as chlorinated or amino-modified trimethoxysilanes[133-134]. Herein the position of the functional group is controlled by the time point at which the modifiers are added. When supplementing them early in the growth process functionalities will be incorporated in the core, whereas addition at the end of the synthesis yields surface-modified MSNs.

Due to their channel architecture various types of release mechanisms for MSNs were developed. Most of these mechanisms rely on external stimuli to trigger the liberation of drugs like the presence of small molecules[135] or enzymes[136], changes in the redox potential[137] or pH[138] and photoirradiation[139]. A key role in the release process play different kinds of capping agents that include organic molecules, gold nanoparticles, polymers, antibodies and DNA. When using ODNs as gate of the channels, the most straight-forward method to block the pores is by functionalization of MSNs with two complementary strands of ss DNA at the pore mouths. Hybridization results in ds DNA that effectively closes the pores and yields a nanocontainer that is responsive to both temperature changes and presence of nuclease (See Fig. 1.17A). This simple approach was successfully used

for the delivery of the hydrophobic anticancer drug camptothecin to human liver cancer cells (HepG2) and showed improved drug uptake over the free drug while the MSN itself showed no cytotoxicity[140].

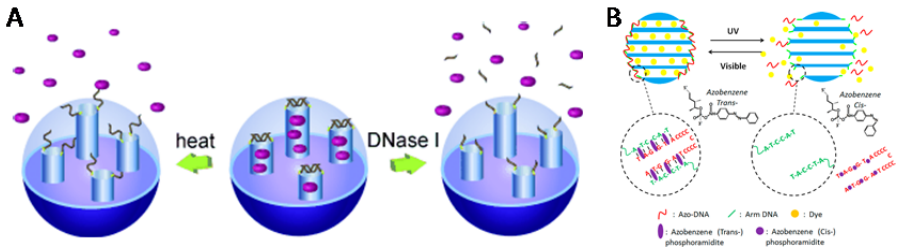

Figure 1.17 (A) MSN loaded with dye and capped using ds DNA[140]. These architectures can be employed for delivery employing temperature (left) or enzyme induced (right) release. (B) A similar approach for capping MSN that uses modified ODNs[141]. Upon irradiation with UV light the azobenzene modification undergoes a conformational change thereby interfering with hybridization.

When using modified ODNs as capping moieties other stimuli could be employed to release payloads. One such example is the photo-induced release of Dox that was achieved through incorporation of photoswitchable azobenzenes in the capping DNA (See Fig. 1.17B)[141]. In the absence of light these moieties are in a *trans*-configuration and therefore allow for hybridization of two DNA strands. However, under irradiation with UV light the azobenzene undergoes isomerization into the *cis*-configuration, which interferes with hybridization. As a result, the two DNA strands separate and Dox was released. This process is reversible. Upon irradiation with visible light the pores of the MSN were closed again after sufficient drug had been released. *In-vitro* studies using this method were performed on CEM and A549 cells and revealed that these MSNs do not exhibit obvious cytotoxicity before irradiation with UV light. However, after irradiation cell viability dropped to only 10% showing an efficient drug release.

In an approach that used a more complex nucleic acid architecture, the DNA i-motif was employed to facilitate pH responsive release of a model compound (See Fig. 1.18A)[142]. This special secondary structure of DNA is comprised of a single strand that folds into a quadruplex through multiple

cytidines that are protonated at acidic pH[143-144]. In the quadruplex state the pores of the MSN were blocked. However, at basic pH the cytidines were deprotonated and the secondary structure was lost within minutes to facilitate release of the payload. By fabrication of NHS-activated MSNs the ss DNA coding for the i-motif was coupled to the nanoparticles. After loading of the DNA-functionalized MSNs with the model compound rhodamine B, the pH was lowered in order to close the pores. Using this simple preparation procedure loaded MSNs were obtained that showed complete release of the dye at basic pH within 24 h while less than 5% leakage was observed in the same period at acidic pH. Furthermore, partial release was shown by changing the pH after the desired amount of payload was liberated.

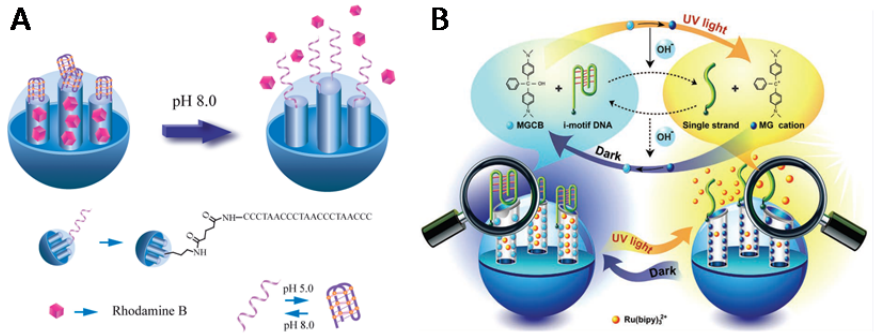

Figure 1.18 (A) Loaded MSN capped with i-motif DNA[142]. Increase of the pH results in disaggregation of the quadruplex and opening of the pores. (B) Malachite green carbinol-modified MSN for light-induced pH increase and dye release[145].

Besides utilizing changes in pH as stimulus for release, light-triggered liberation of the loaded compound was achieved using the i-motif again (See Fig. 1.18B)[145]. For this purpose malachite green carbinol (MGCB) was immobilized on the surface of the NP after introducing the i-motif. MGCB functions as a light inducible hydroxide emitter as it dissociates into malachite green cations and OH^- upon irradiation with UV light (365 nm). The photochemical transformation creates a local increase in pH and hence induces the unfolding of the i-motif and subsequent release of the cargo. When the light is turned off, the process is reversed and the stable

quadruplex is formed again to close the pores of the MSNs. Using this approach a controlled pH increase from 4.9 to 10.1 was achieved when irradiating the nanocarriers. Upon removal of the light source the initial pH value was regained after 20 min. The release of the loaded model compound ($Ru(bipy)_3^{2+}$) proved to be strongly dependent on the light conditions. Under light irradiation as much as 85% of the payload was released while in the dark only 5% leakage was observed. In addition, this approach allowed partial drug release by removing the light source after the desired amount of cargo was released.

Other DNA structures functioning as gate keepers were realized as well. To this end metal ion binding stem loop sequences were formed through hybridization to DNA functionalized MSN allowing for Zn^{2+} and Mg^{2+} mediated release of model compounds methylene blue (MB^{2+}) and thionine (Th^{+})[146]. Addition of the metal ions resulted in the formation of a catalytically active complex, called DNAzyme, that cleaves one of the strands and thereby opens the pores. Using different DNAzymes metal specific release was achieved and in a mixture of NPs controlled liberation of payloads was demonstrated. Additionally, incorporation of an aptamer in the loop sequence resulted in capped MSNs requiring two promoters to trigger release. Most importantly, release of the more relevant DOX was shown employing a Mg^{2+} and ATP dependent DNAzyme. As cancerous cells have a high metabolic activity, large amounts of ATP are present rendering this approach promising for future tumor treatment.

Apart from using the structural properties of DNA to cap the pores of MSNs, ODNs were used as anchor to attach different capping groups by employing the unique self-recognition properties of DNA. It was shown that avidin was able to function as capping agent when MSNs were functionalized with biotin modified ds DNA at the pore mouths[147]. Upon heating above the melting temperature the double strands dehybridize and avidin is removed, resulting in release of the loaded compound from the MSN. Furthermore, it was shown that the release temperature can easily be altered by changing the length of the connecting DNA. Aside from heating the whole sample, release by localized heating was also demonstrated. To this end, superparamagnetic iron oxide nanocrystals were employed that can be heated by a rapidly

alternating magnetic field[148]. Hybridization of DNA functionalized MSNs with iron oxide NPs that are equipped with the complementary sequence results in loaded nanoparticles capped by DNA anchored iron oxide NPs. Additionally, the iron oxide nanoparticles do not only serve as capping agents, but also can be employed as contrast enhancing agents in magnetic resonance imaging. Important to note is that this method provides an elegant manner for liberation without the need of an invasive stimulus.

1.3.2 Amphiphilic DNA block copolymers

In addition to DNA NPs with an inorganic core, nanosized objects with a DNA corona and a soft interior part can be generated by employing polymeric materials. In general, amphiphilic block copolymers have been utilized frequently for drug delivery purposes[149]. Thereby, a hydrophobic polymer segment is covalently connected to a hydrophilic one. Upon microphase separation, mostly spherical aggregates are formed that exhibit a hydrophobic interior and a hydrophilic shell[150]. The core is usually exploited to load hydrophobic drugs or for encapsulation of toxic actives to prevent them from harming healthy tissue. The shell is often composed of polyethylene glycol because of its resistance towards protein adsorption and the prevention of immunogenicity[151]. Alternatively, stimulus responsive water soluble polymer segments are found in the corona of the micelles allowing the particles to react towards changes in their environment to improve the performance of the carrier system.

Another way to introduce function into these micellar systems is the utilization of DNA as a constituent part of the amphiphilic block copolymer. Several ways have been established to synthesize DNA block copolymers. Early methods to access linear DNA block copolymers (DBCs) relied on coupling the ODN segment to the hydrophobic polymer in solution which did not result in good coupling yields[32]. A more efficient approach relied on attaching the nucleic acid segment to the DNA unit on the solid phase. Therefore, the ODN was synthesized by conventional phosphoramidite chemistry on controlled porous glass or a polymeric support[152]. Afterwards, a phosphoramidite polymer, which was obtained by phosphitylation of its

terminal hydroxyl group, was coupled to the detritylated end of the ODN that was still attached to the solid phase. After removal of the protective groups and cleavage from the support amphiphilic DBCs were obtained in good yields.[38] Other ways for the fabrication of DBCs rely on molecular biology methods employing different enzymes[36, 153-155].

After detailing their preparation methods, the self-assembly of amphiphilic DBCs will be discussed. When these materials are introduced into buffer they form spherical micelles. The size of these nanoobjects can be easily controlled by adjusting the lengths of the different polymer blocks. Just to give an example, a DBC consisting of a ODN 22mer connected to a poly(propylene oxide) (PPO) segment of weight average molecular weight (M_w) of 6800 g/mol results in micelles with a hydrodynamic radius of 10 nm. When the DNA block is extended to 84 nucleotides a diameter of 23 nm is obtained[155]. The geometry of the spherical aggregates could be switched into rod-like objects by a simple hybridization procedure[156]. Therefore, the ss DNA-*b*-PPO micelles were mixed with long DNA templates that encode several times the complementary sequence of the micelle corona inducing a transformation into rod-like micelles. Watson-Crick base pairing aligned the hydrophobic polymer segments along the DNA double helix, which resulted in selective dimer formation (See Fig. 1.19). Even the length of the resulting nanostructures could be precisely adjusted by the number of nucleotides of the templates. Rod-like particles with lengths between 30 and 37 nm were generated. This study demonstrated that structurally well-defined DNA nanoobjects can not only be produced by Watson-Crick base paring as described in the context of pristine DNA assemblies but also by interactions of hydrophobic polymers. The use of hydrophobic interactions represents a new principle for DNA nanoconstruction.

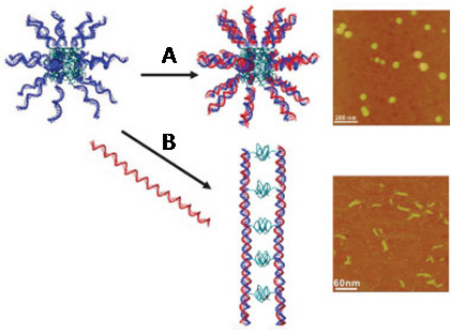

Figure 1.19 Preparation of soft DNA nanoparticles with different shapes and the corresponding AFM pictures of the nanoobjects[156]. (A) Base pairing of ss DNA-b-PPO micelles with a short complementary sequence yields micelles with a ds corona maintaining the overall spherical shape of the aggregates. (B) Hybridization with long DNA templates results in rod-like micelles consisting of two parallel aligned double helices.

The spherical and rod-like DBC nanostructures were investigated in regard to their interaction with cells. Uptake studies into the cancerous Caco 2 cell line revealed an internalization behavior that is strongly dependent on the geometry of the nanostructures[157]. It turned out that the rod-like aggregates were taken up to a much greater extent than ss and ds spherical micelles. In the context of drug delivery this is an important finding because it suggests that shape is an important design criterion for drug carriers. It is noteworthy that all the DNA aggregates were taken up much better than the ss and ds DNA controls. The same finding that nanoparticles with a high nucleic acid density are efficiently incorporated into cells was previously observed for DNA-Au NPs and was later seen for pristine DNA nanoobjects as well (vide supra).

After investigating the non-directed uptake of DBC aggregates, these systems were employed for targeted chemotherapeutic drug delivery[158]. For that purpose ODN-modified targeting units (folic acid) were “clicked” into the spherical micelle corona by hybridization, allowing perfect control of surface functionalities of the nanoparticle system. When folate is conjugated to the 5’-end of the ODN it is present at the surface of the micelles (See Fig 1.20, a). If the targeting moiety is connected to the 3’-end it is located at the inside of the DBC aggregates. In addition, different stoichiometries of ODN-folate conjugates to micelles allowed control of number of targeting unit per

micelle. The aggregation number of this DNA-*b*-PPO system was determined to be 25 resulting in an average of 25 folate units on the surface of the DBC vehicles when fully hybridized with 5'-functionlized ODNs. Cell culture experiments with Caco 2 cells revealed that cellular uptake strongly depends on the density of targeting units on the surface of the carriers. Receptor-mediated uptake is most efficient for the design with the maximum number of folate groups on the surface. As convenient the DBC aggregates are equipped with surface functionalities, as simple the drug loading can be carried out. By just mixing the hydrophobic anticancer drug Dox with the micelles, the cargo accumulates in the core of the DBC aggregates (See Fig. 1.20, b). When the DBC particles that were most efficient in targeting were administered with the cytotoxic payload to cancer cells *in-vitro* the Caco 2 cells were efficiently killed, whereas the NPs themselves did not show any toxicity.

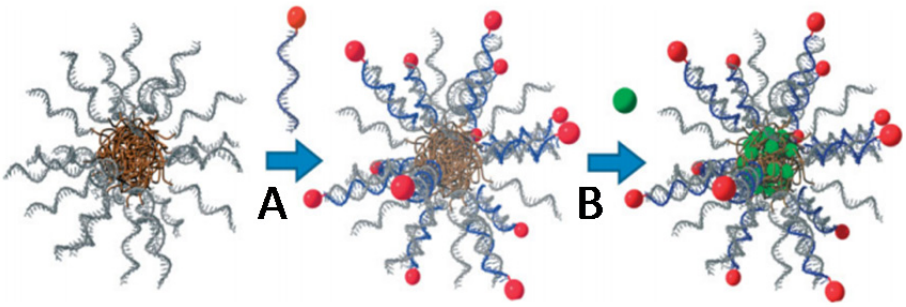

Figure 1.20 Schematic representation of the drug delivery system based on DNA block copolymers[158]. (A) Targeting units (red dots) that are connected to the complementary sequence of the micelles are hybridized to equip the nanoparticle surface with folate moieties. (B) The anticancer drug (green dots) is loaded into the core of the micelles. Due to hydrophobic interactions of Doxorubicin with PPO the drug accumulates in the interior of the block copolymer aggregates.

These experiments qualify the amphiphilic DBCs as delivery system with high future potential. The hydrophobic polymer organizes the ss ODN moieties to form a dense ss DNA corona that can be easily equipped with many different functionalities by hybridization as proven for targeting and bioimaging agents. Moreover, the core of the DNA nanoparticles can be exploited for the loading with hydrophobic cargo. In this way a

combinatorial testing of different compositions of DBC-based drug delivery systems becomes feasible. Similarly to the DBC micelle system, aptamers recognizing Ramos cells were assembled into micelles through implementation of a hydrophobic moiety at one end of the ODN. Interestingly, due to the multimerization of the aptamer sequence an increased binding of the micelles compared to the pristine nucleic acid sequence was achieved[159].

In future experiments, especially during *in-vivo* applications, the DBC aggregates, like any other micelle system, might disaggregate due to dilution upon administration. For that reason we stabilized DBC aggregates by adding a hydrophobic cross-linker to the core that was photo-polymerized[160]. At the same time the DNA-*b*-PPO system was blended with Pluronic, a triblock copolymer with a PEG-*b*-PPO-*b*-PEG architecture. As a result, the corona of the micelle corona consists of ODN and PEG units. It was proven that the PEG moieties at the surface of the aggregates did not interfere with hybridization. In this way, a stable DNA nanoparticle system was generated combining a PEG-stealth function with all the favorable properties of pristine DBC micelles.

A second way of stabilizing DBC aggregates is encapsulation of the whole nanoobject. This goal was successfully realized with virus capsids. Micelles of amphiphilic DBCs acted as efficient template for the formation of virus-like particles of the Cowpea Chlorotic Mottle Virus (CCMV)[161]. Under neutral pH CCMV coat protein dimers self-assemble into T = 1 and T = 2 particles consisting of 90 and 120 proteins, respectively. The resulting nanoobjects exhibit a diameter of approximately 20 nm. The incorporation of hydrophilic and hydrophobic payloads was achieved in a very simple manner similar as described earlier for the DBC drug delivery system (See Fig. 1.21). Hydrophobic compounds, like pyrene, were accumulated in the core of the micelles during preparation of DBC micelles. Subsequently, the loaded micelles were incorporated into CCMV particles. For the loading of hydrophilic compounds the cargo was conjugated to complementary ODNs to that of DBC particles prior to the encapsidation process. The encapsulation was verified by several techniques including TEM, FPLC, UV/Vis and fluorescence spectroscopy.

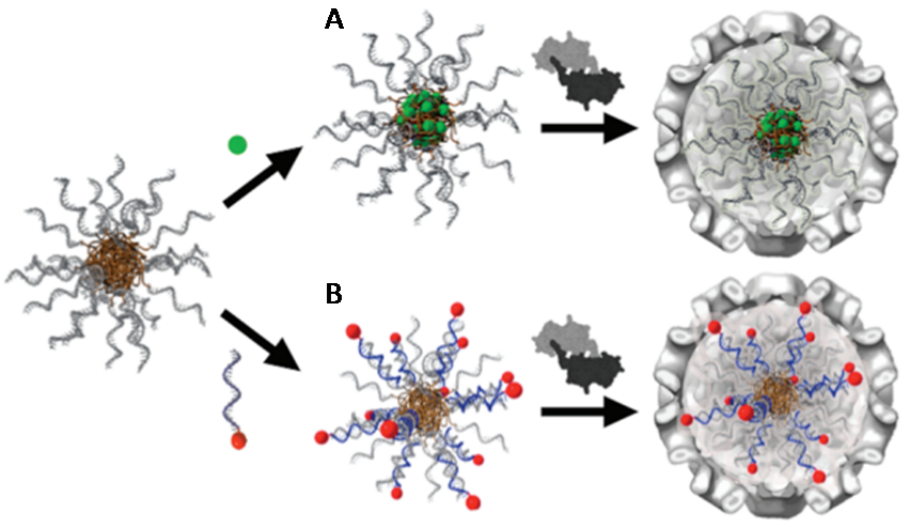

Figure 1.21 DNA micelle-templated virus capsid formation[161]. (A) Loading of hydrophobic molecules (green) into the core. (B) Hydrophilic moieties (red) are attached to the DNA NP by hybridization. Subsequently, coat proteins encapsulate the micelle by a simple mixing process at neutral pH.

While amphiphilic DBCs are superb materials for the preparation of functionalized micelles they were also employed in the context of vesicle systems. DNA-*b*-PPO was stably incorporated into the phospholipid membrane of vesicles (See Fig. 1.22)[162]. In this way, the containers are encoded with sequence information. The ODNs present on the surface were used for anchoring a photosensitizer by hybridization. Upon light irradiation the PPO was oxidized leading to leakage in the membrane and cargo release. It was even demonstrated that in mixtures of vesicles payload is only released when sequence specific hybridization takes place. Liposomes lacking the code for photo-sensitizer hybridization remain unaffected.

When vesicles were functionalized with an aptamer recognizing cancerous cells, targeted liposomes could be successfully delivered[163]. In the same work the binding of the aptamer to the cell surface could be instantaneously inhibited and disrupted by addition of the complement of the aptamer sequence.

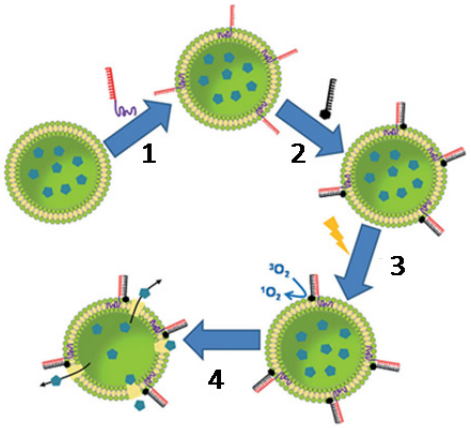

Figure 1.22 Illustration of selective cargo release from DBC-decorated phospholipid vesicles[162]. 1) DBCs are stably anchored in unilamellar lipid vesicles; 2) DBC-decorated vesicles are functionalized with conjugated ODN-photosensitizers by hybridization; 3) singlet oxygen is generated by light irradiation; and 4) selective cargo release is induced by the oxidative effect of singlet oxygen.

While in DBC micelles and DBC encoded vesicles the polymer was employed to organize a ss DNA moiety by hydrophobic interactions the opposite allocation of functions was realized. A DNA cube with ss regions was employed as a scaffold to place DBCs in a predefined manner in space (See Fig. 1.23)[164]. In this way, upon hybridization of DBCs, synthetic polymer units could be placed at various corners of the cube indicating that with the help of DNA nanotechnology synthetic macromolecules can be programmably positioned in 3D on a DNA scaffold. Moreover, the decoration of the cube with polymer units increased the nuclease resistance compared to non-polymer containing DNA cages. These hybrid structures like many of the above mentioned DBC systems represent promising precision materials for biomedical and drug delivery applications.

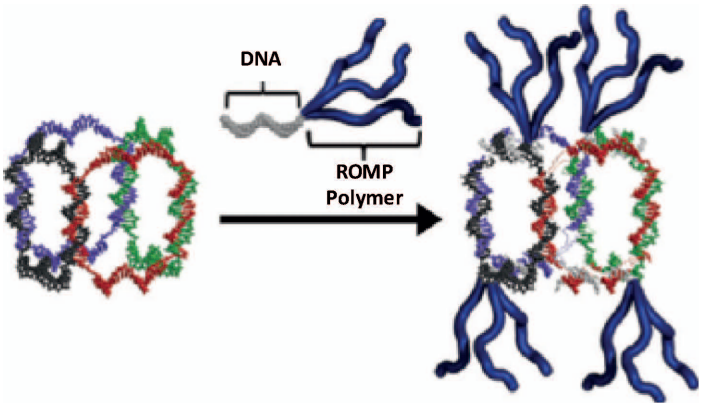

Figure 1.23 Schematic design of a polymer-conjugated DNA cube[164]. The cube is designed to hybridize with four DNA polymer conjugates, two on both the top and bottom face. In each face the polymers are directed perpendicular to each other through site-specific hybridization in order to minimize steric hindrance.

1.4 Conclusion

DNA nanotechnology has developed into an independent field of research in the recent years. Dramatic improvements have been booked regarding the accessibility of possible structures. One can firmly state that nowadays almost any 2D or 3D shaped nanoobject is achievable with DNA as a building block. In contrast to many other self-assembling systems the geometry and size of DNA nanoarchitectures can be designed very accurately due to the well-known self-recognition properties of DNA and the knowledge of the exact structure of the double helix on the atomic level. Without any doubt, the DNA origami technique is nowadays the one giving the highest degree of flexibility regarding the structural variety. Although DNA nanostructures being composed of nucleic acid hybrid materials allow less structural control and variability they give the opportunity for the implementation of extra functionality.

Both types of materials, pristine DNA nanoobjects and DNA hybrid structures, were exploited in the context of biomedical applications. DNA nanoobjects were employed as scaffolds to act as a drug carrier or to display functionalities that induce immunostimulation. Why are nucleic acid

nanostructures so appealing for those potential applications? There are several answers to this question. An obvious one is that the DNA nanostructures can be decorated with a multitude of functionalities including drugs, targeting moieties and stealth units. With the help of the DNA scaffold these entities can be positioned with a similar accuracy as the DNA itself. The great need for multifunctional carriers in the context of drug delivery vehicles does not need to be further explained here. Another striking feature of the DNA nanoobjects is their modular fabrication relying on self-assembly. Only a few or a large number of building blocks are mixed together in a single step resulting in the formation of the desired nanostructure. In this way, variations of the design or the decoration of the carrier can be easily achieved. In stark contrast, other carrier scaffolds like dendrimers mostly require cumbersome multistep synthesis which does not allow testing of many designs and structural variations. It needs to be mentioned here that the DNA sequences need to be synthesized as well, but their fabrication relies on well-established automated synthesis methods and ODNs are available from commercial suppliers. Moreover, via the self-assembly process with DNA a large size range is covered ranging from only a few nanometer like the DNA tetrahedron to structures in the micrometer scale like the extended DNA tubes. Another striking feature suggesting the use of DNA-based carrier systems is that they are taken up by cells without the need for a transfection agent. This was first discovered for DNA-Au NPs and seems to be true for many other DNA nanostructures as well that are composed of high density DNA like DBC micelles, DNA polyhedra and DNA origami tubes. An equally important characteristic for their biomedical application is their low immunogenicity. Several examples demonstrate that once the DNA is tightly compressed in a dense DNA scaffold immunogenicity is low like shown for some pristine DNA and DNA-Au NPs. Moreover, for all DNA-based materials presented here no or only a low toxicity was found in the absence of the payload or stimulans, while they greatly improve the performance of the active compounds.

While DNA nanostructures from pristine nucleic acids and from DNA hybrid material have several common features they also exhibit differences. Pristine DNA nanostructures mostly allow more structural control if one thinks e.g. of the DNA origami method compared to DNA-Au NPs or DBC

micelles. On the other hand DNA-Au NPs and DBC aggregates allow much higher densities of surface units compared to pristine nucleic acid structures. For the former ones ss DNA is arranged in space by an Au- or a hydrophobic polymer core while for the latter ones overhangs of ss DNA can be introduced into double helical structures with lower frequency.

Another good reason for testing DNA nanostructures for the purpose of drug delivery is the large flexibility of how drugs can be loaded into the DNA carrier. As demonstrated for chemotherapeutics like Dox intercalation into the double helix is a valuable method. But drugs can also be chemically attached to the surface of the nanocarriers which at the same time helps increasing the solubility of a drug. Alternatively, hydrophobic actives might be incorporated into the lipophilic core of DBC aggregates. Another loading strategy consists of hybridizing drug-ODN conjugates onto single stranded sites of the DNA carrier.

While DNA nanoobjects offer several possibilities for drug incorporation they allow unprecedented control over release as well. Due to the specific hydrogen bonds formed between adenine and thymine and guanosine and cytosine the melting temperature between two complementary DNA strands can be precisely controlled. This feature can be exploited for the temperature-controlled release of compounds that are attached to the strands or that are intercalated. Likewise, the hydrogen bonding in DNA can be exploited for sequence specific release with the help of DNA or RNA input strands. In this case one of the strands needs to contain a toehold overhang that allows strand exchange and therewith release. Other DNA-mediated release mechanisms rely on specific DNA sequences. The i-motif is switching in response to pH between a compact quadruplex structure and an extended single stranded conformation. This allowed controlled release when those structures are introduced as valves at the tip of silica channels. Light as a stimulus for drug release is another option. In case of silica particles a photobase induces local pH changes and switching of the i-motif. On the surface of liposomes photosensitizer units can be hybridized and exploited for sequence-specific release of cargo.

Class	*DNA nanoobject*	*Lit.*	*Immunostimulatory effect*
Pristine DNA	Tetrahedron	60	Tetrahedra functionalized with 4 CpG motifs increase TNF-α and IL-6 concentrations by a factor of 13 and 35, respectively, compared to ds CpG motifs.
		61	Doubled antibody response and significantly higher levels of memory B cells were found when using the NP enhanced vaccines compared to the unassembled individual components.
	Dendrimers	64	Y shaped structures cause a 1.5- to 3-fold increase in release of TNF-α and IL-6, respectively, compared to ds CpG.
		65	2^{nd} and 3^{rd} dendrimer generations strongly increase TNF-α levels by a factor of 7 and 22, respectively, compared to ds CpG. IL-6 concentrations were approx. increased by a factor of 3 (G2) and 5 (G3).
	Polypods	66	With increasing branching of the pods an enhanced stimulation was found for both TNF-α and IL-6. For the prior cytokine a 5-fold to 400-fold increase was observed compared to ds DNA. For IL-6 release induced by ds DNA the values were below the detection limit.
	DNA tubes	53	TLR9 specific immune responses were triggered using CpG decorated nanotubes with a fivefold increase in IL-6 concentrations compared to undecorated tubes.
DNA hybrids	DNA-Au NPs	131	Strongly stimulated cytokine release in comparison with non-NP CpG motifs. In relation to ss CpG, a 16- and 10-fold increase in TNF-α and IL-6 concentrations was observed, respectively.

Table 1.1. Overview of DNA nanostructures equipped with CpG motifs for immunostimulation.

The summary above shows that pristine DNA nanostructures and nanoobjects composed of DNA hybrid materials offer unprecedented control over structure and functionality in a biological or cellular environment. Several *in-vitro* studies have shown the exciting properties of nano-sized nucleic acid-based carrier materials. However, the scope of these investigations is still limited. The focus has been on two main areas, i.e. usage of DNA-based carriers for cancer treatment and as immunostimulans exploiting the multimerization of the CpG motif (See Table 1.1). Further *in-vitro* experiments might extend the applications of this carrier family to other indications and diseases. Even more important for the demonstration of the great potency of DNA nanomaterials in the biomedicine arena is the establishment of these vehicles *in-vivo*. Such experiments are still scarce but one can imagine that more successful examples will be presented soon due to the fact that the field of DNA-based carriers has gained great momentum in the very recent years. In the near future it is expected that the scope and limitations of such delivery vehicles regarding indications, targeting-ability, toxicity, immunogenicity, pharmacokinetics and pharmacological efficacy (local pharmacological effects, toxicity in non-target tissue, and overall effect on disease progression) will be shown. This preclinical validation calls for fabrication of DNA nanomaterials of pharmaceutical grade and at larger scales. For pristine nucleic acids and DNA block copolymers these requirements can be met with established techniques such as solid-phase synthesis and automated HPLC. One example thereof is the commercially available anti-VEGF nucleic acid aptamer used for treatment of wet age related macular degeneration[31]. In regard to inorganic DNA hybrids, probably more effort is necessary to achieve the homogeneity and scale established in pharmaceutical industry. These considerations help to realize the long-term goal of this branch of nanomedicine research which is to identify promising nucleic acid-based carrier systems and bring them into the clinic. However, the latter endeavour is beyond a short time frame.

1.5 Thesis motivation and overview

The field of DNA nanotechnology has made enormous progress in the last decades and already has had a high impact in other fields. To date, the formation of almost any 2D or 3D structure with a large variety of functionalities is possible, which is even more impressive when one realizes that all is made possible through the specific interaction of only four building blocks. Simple Watson-Crick base pairing of adenine with thymine and cytosine with guanine governs the assembly process, with one possible structural outcome. Functionality can be incorporated through the use of specific oligonucleotides such as aptamers that allow for targeting. When additional features are desired DNA hybrid structures can be employed. These can contain simple organic fluorophores that serve for imaging purposes or gold NPs that allow for local heating. On the other hand, when coupling a hydrophobic moiety to the DNA, such as a polymer or an alkyl chain, amphiphiles are formed that self-assemble into micellar objects through microphase separation. This thesis focuses on the synthesis and characterization of such amphiphiles and their application in the field of medicine. In order to fully exploit the many appealing features of DNA, oligonucleotides are used for the assembly of the NPs as well as for incorporation of functionality. Using the complete set of available tools described above NPs can easily be tailored to a specific goal and represent a modular drug delivery platform.

In **Chapter 1** the use of DNA based nanostructures for drug delivery was presented and differentiation was made between NPs made of pristine nucleic acids and those comprised of DNA hybrid materials. For the latter structures a distinction was made between carriers with an inorganic core composed of gold or silica and amphiphilic DNA block copolymers that exhibit a soft hydrophobic interior. Despite the many examples presented, the use of DNA nanotechnology in medicine is still limited and many more intriguing applications are awaiting to be explored.

For the synthesis of hybrid oligonucleotides a large variety of conjugation strategies is available that can be divided into two major classes; solution based coupling and solid phase synthesis (SPS). After performing synthesis, purification of the obtained product is necessary. For many organic and

biological molecules reversed phase high performance liquid chromatography (RPC HPLC) is the current gold standard to obtain high purity materials. However, for synthesis of more complicated hybrids, such as DNA block copolymers (DBCs), purification using gel electrophoresis is often chosen as it is more predictable. In **Chapter 2** synthesis, RPC HPLC purification and characterization of several different amphiphilic DNA poly(propylene oxide) (PPO) di- and tri-block copolymers is presented. Afterwards, the influence of the appended polymer block on hybridization will be investigated. Therefore, the melting temperature (T_m) for a number of di- and triblock copolymer designs was measured. These experiments give information about the suitability of these amphiphilic DBCs for use as carrier materials since their ability of base pairing is of paramount importance for carrier loading.

In the next chapter, similar soft mater DNA nanoparticles are tested in the context of ophthalmic drug delivery. To date, treatment of most eye related disease is performed using eye drops. However, therapy is hindered due to the low availability of the drug, as most of the active ingredient is washed away due to blinking and tearing upon installation. In order to find a suitable carrier that allows drug delivery to the eye, in **Chapter 3** different lipid-modified DNA nanoparticles were synthesized and their adsorption to the cornea for prolonged drug action was investigated. To impart a hydrophobic character an alkyl chain was conjugated to the nucleobase, thereby creating an amphiphile able to form nanoparticles (NPs). These carriers exhibit a hydrophobic interior and a corona of single stranded DNA and can easily be functionalized through hybridization. Several different NPs were synthesized by altering the amount of modified and total number of nucleotides. It will be demonstrated how these structural parameters influence adsorption to the cornea.

After selection of the best adhering NP the translation into a drug delivery platform was pursued. For incorporation of the active compound several loading strategies are available. Hydrophobic drugs can easily be retained in the interior of the nanoobject, whereas covalent attachment to the carrier is a more appropriate strategy for hydrophilic compounds. However, all of these loading methods are limited to certain drugs, require chemical modification

of the active pharmaceutical ingredient or do not offer control over the release. To develop a truly modular delivery platform a novel loading strategy is presented in **Chapter 4** that is based on the use of aptamers that are hybridized on the NP. Such small RNA or DNA strands selectively bind the compound of interest and can be developed for virtually any molecule. Using this loading strategy, two antibiotics containing lipid DNA NPs will be presented. Moreover, their performance in animal experiments and even with human tissue will be illustrated.

For successful development of the NPs into a drug delivery platform the stability of the vehicle and its toxicity play an important role. In the past, several promising nanoparticles used for drug delivery have failed due to inherent toxicity of the carrier or instability. As such, preliminary screening of these properties is performed in **Chapter 5**. First, the NP adhering best to the cornea was selected and its toxicity profile with three ocular cell lines was investigated. Afterwards, the pristine NPs and one antibiotic-loaded carrier were further tested for induction of apoptosis *in-vivo*. Finally, the stability of the vehicles was elucidated. To this end the pristine and loaded NPs were stored under different conditions. Subsequently, they were analyzed by gel electrophoresis and RPC HPLC to detect possible degradation products.

1.6 References

[1] J. D. Watson, F. H. C. Crick, *Cold Spring Harb. Sym.* **1953**, *18*, 123-131.
[2] L. M. Smith, *Nature* **2006**, *440*, 283-284.
[3] N. C. Seeman, *J. Theor. Biol.* **1982**, *99*, 237-247.
[4] N. C. Seeman, *Nature* **2003**, *421*, 427-431.
[5] J. Chen, N. C. Seeman, *Nature* **1991**, *350*, 631-633.
[6] E. Winfree, F. R. Liu, L. A. Wenzler, N. C. Seeman, *Nature* **1998**, *394*, 539-544.
[7] A. Kuzuya, R. S. Wang, R. J. Sha, N. C. Seeman, *Nano Lett.* **2007**, *7*, 1757-1763.
[8] P. W. K. Rothemund, *Nature* **2006**, *440*, 297-302.
[9] E. S. Andersen, M. Dong, M. M. Nielsen, K. Jahn, R. Subramani, W. Mamdouh, M. M. Golas, B. Sander, H. Stark, C. L. Oliveira, J. S. Pedersen,

V. Birkedal, F. Besenbacher, K. V. Gothelf, J. Kjems, *Nature* **2009**, *459*, 73-76.

[10] Y. Ke, S. Lindsay, Y. Chang, Y. Liu, H. Yan, *Science* **2008**, *319*, 180-183.

[11] S. Rinker, Y. Ke, Y. Liu, R. Chhabra, H. Yan, *Nat. Nanotechnol.* **2008**, *3*, 418-422.

[12] A. V. Pinheiro, D. R. Han, W. M. Shih, H. Yan, *Nat. Nanotechnol.* **2011**, *6*, 763-772.

[13] C. Zhang, M. Su, Y. He, X. Zhao, P. A. Fang, A. E. Ribbe, W. Jiang, C. D. Mao, *P. Natl. Acad. Sci. USA* **2008**, *105*, 10665-10669.

[14] D. E. Ingber, *Annu. Rev. Physiol.* **1997**, *59*, 575-599.

[15] D. Liu, M. S. Wang, Z. X. Deng, R. Walulu, C. D. Mao, *J. Am. Chem. Soc.* **2004**, *126*, 2324-2325.

[16] Z. Li, B. Wei, J. Nangreave, C. Lin, Y. Liu, Y. Mi, H. Yan, **2009**, *131*, 13093-13098.

[17] R. P. Goodman, I. A. T. Schaap, C. F. Tardin, C. M. Erben, R. M. Berry, C. F. Schmidt, A. J. Turberfield, *Science* **2005**, *310*, 1661-1665.

[18] W. M. Shih, J. D. Quispe, G. F. Joyce, *Nature* **2004**, *427*, 618-621.

[19] D. Bhatia, S. Mehtab, R. Krishnan, S. S. Indi, A. Basu, Y. Krishnan, *Angew. Chem. Int. Ed.* **2009**, *48*, 4134-4137.

[20] Y. He, T. Ye, M. Su, C. Zhang, A. E. Ribbe, W. Jiang, C. D. Mao, *Nature* **2008**, *452*, 198-141.

[21] C. A. Mirkin, R. L. Letsinger, R. C. Mucic, J. J. Storhoff, *Nature* **1996**, *382*, 607-609.

[22] D. Nykypanchuk, M. M. Maye, D. van der Lelie, O. Gang, *Nature* **2008**, *451*, 549-552.

[23] R. J. Macfarlane, B. Lee, M. R. Jones, N. Harris, G. C. Schatz, C. A. Mirkin, *Science* **2011**, *334*, 204-208.

[24] J. I. Cutler, E. Auyeung, C. A. Mirkin, *J. Am. Chem. Soc.* **2012**, *134*, 1376-1391.

[25] J. J. Storhoff, R. Elghanian, R. C. Mucic, C. A. Mirkin, R. L. Letsinger, *J. Am. Chem. Soc.* **1998**, *120*, 1959-1964.

[26] D. S. Seferos, D. A. Giljohann, H. D. Hill, A. E. Prigodich, C. A. Mirkin, **2007**, *129*, 15477-15479.

[27] N. L. Rosi, *Science* **2006**, *312*, 1027-1030.

[28] J. Dobson, *Gene Ther.* **2006**, *13*, 283-287.

[29] M. Lemaitre, B. Bayard, B. Lebleu, *P. Natl. Acad. Sci. USA* **1987**, *84*, 648-652.

[30] J. P. Leonetti, G. Degols, P. Milhaud, C. Gagnor, M. Lemaitre, B. Lebleu, *Nucleos. Nucleot.* **1989**, *8*, 825-828.

[31] *Retina* **2002**, *22*, 143-152.

[32] J. H. Jeong, T. G. Park, *Bioconjug. Chem.* **2001**, *12*, 917-923.

[33] Z. Y. Zhao, L. Y. Wang, Y. Liu, Z. Q. Yang, Y. M. He, Z. B. Li, Q. H. Fan, D. S. Liu, *Chem. Commun.* **2012**, *48*, 9753-9755.

[34] M. P. Chien, A. M. Rush, M. P. Thompson, N. C. Gianneschi, *Angew. Chem. Int. Ed.* **2010**, *49*, 5076-5080.
[35] M. D. Costioli, I. Fisch, F. Garret-Flaudy, F. Hilbrig, R. Freitag, *Biotechnol. Bioeng.* **2003**, *81*, 535-545.
[36] M. Safak, F. E. Alemdaroglu, Y. Li, E. Ergen, A. Herrmann, *Adv. Mater.* **2007**, *19*, 1499-1505.
[37] G. Tong, J. M. Lawlor, G. W. Tregear, J. Haralambidis, *J. Org. Chem.* **1993**, *58*, 2223-2231.
[38] F. E. Alemdaroglu, K. Ding, R. Berger, A. Herrmann, *Angew. Chem. Int. Ed.* **2006**, *45*, 4206-4210.
[39] M. Kwak, J. Gao, D. K. Prusty, A. J. Musser, V. A. Markov, N. Tombros, M. C. A. Stuart, W. R. Browne, E. J. Boekema, G. ten Brinke, H. T. Jonkman, B. J. van Wees, M. A. Loi, A. Herrmann, *Angew. Chem. Int. Ed.* **2011**, *50*, 3206-3210.
[40] R. Duncan, *Nat. Rev. Drug Discov.* **2003**, *2*, 347-360.
[41] P. Tanner, P. Baumann, R. Enea, O. Onaca, C. Palivan, W. Meier, *Accounts Chem. Res.* **2011**, *44*, 1039-1049.
[42] Y. Kakizawa, K. Kataoka, *Adv. Drug Deliver. Rev.* **2002**, *54*, 203-222.
[43] S. Ganta, H. Devalapally, A. Shahiwala, M. Amiji, *J. Control. Release* **2008**, *126*, 187-204.
[44] M. J. Campolongo, S. J. Tan, J. F. Xu, D. Luo, *Adv. Drug. Deliver. Rev.* **2010**, *62*, 606-616.
[45] J.-W. Keum, J.-H. Ahn, H. Bermudez, *Small* **2011**, *7*, 3529-3535.
[46] K. A. Whitehead, R. Langer, D. G. Anderson, *Nat. Rev. Drug Discov.* **2009**, *8*, 129-138.
[47] P. Guo, O. Coban, N. M. Snead, J. Trebley, S. Hoeprich, S. Guo, Y. Shu, *Adv. Drug Deliv. Rev.* **2010**, *62*, 650-666.
[48] M. J. Campolongo, S. J. Tan, J. Xu, D. Luo, *Adv. Drug. Deliv. Rev.* **2010**, *62*, 606-616.
[49] E. Katz, I. Willner, *Angew. Chem. Int. Ed.* **2004**, *43*, 6042-6108.
[50] R. P. Goodman, R. M. Berry, A. J. Turberfield, *Chem. Commun.* **2004**, 1372-1373.
[51] C. Zhang, C. Tian, X. Li, H. Qian, C. Hao, W. Jiang, C. Mao, *J. Am. Chem. Soc.* **2012**, *134*, 11998-12001.
[52] A. S. Walsh, H. Yin, C. M. Erben, M. J. A. Wood, A. J. Turberfield, *ACS Nano* **2011**, *5*, 5427-5432.
[53] V. J. Schuller, S. Heidegger, N. Sandholzer, P. C. Nickels, N. A. Suhartha, S. Endres, C. Bourquin, T. Liedl, *ACS Nano* **2011**, *5*, 9696-9702.
[54] G. J. Weiner, H. M. Liu, J. E. Wooldridge, C. E. Dahle, A. M. Krieg, *P. Natl. Acad. Sci. USA* **1997**, *94*, 10833-10837.
[55] S. Bauer, H. Wagner, *Curr. Top. Microbiol. Immunol.* **2002**, *270*, 145-154.
[56] S. Rothenfusser, E. Tuma, S. Endres, G. Hartmann, *Hum. Immunol.* **2002**, *63*, 1111-1119.

[57] D. E. Fonseca, J. N. Kline, *Adv. Drug. Deliver. Rev.* **2009**, *61*, 256-262.
[58] J. Vollmer, A. M. Krieg, *Adv. Drug Deliver. Rev.* **2009**, *61*, 195-204.
[59] D. M. Klinman, *Nat. Rev. Immunol.* **2004**, *4*, 248-257.
[60] J. Li, H. Pei, B. Zhu, L. Liang, M. Wei, Y. He, N. Chen, D. Li, Q. Huang, C. Fan, *ACS Nano* **2011**, *5*, 8783-8789.
[61] X. Liu, Y. Xu, T. Yu, C. Clifford, Y. Liu, H. Yan, Y. Chang, *Nano Lett.* **2012**, *12*, 4254-4259.
[62] H. Pei, L. Liang, G. Yao, J. Li, Q. Huang, C. Fan, *Angew. Chem. Int. Ed.* **2012**, *51*, 9020-9024.
[63] Y. G. Li, Y. D. Tseng, S. Y. Kwon, L. D'Espaux, J. S. Bunch, P. L. Mceuen, D. Luo, *Nat. Mater.* **2004**, *3*, 38-42.
[64] M. Nishikawa, M. Matono, S. Rattanakiat, N. Matsuoka, Y. Takakura, *Immunology* **2008**, *124*, 247-255.
[65] S. Rattanakiat, M. Nishikawa, H. Funabashi, D. Luo, Y. Takakura, *Biomaterials* **2009**, *30*, 5701-5706.
[66] K. Mohri, M. Nishikawa, N. Takahashi, T. Shiomi, N. Matsuoka, K. Ogawa, M. Endo, K. Hidaka, H. Sugiyama, Y. Takahashi, Y. Takakura, *ACS Nano* **2012**, *6*, 5931-5940.
[67] M. Chang, C. S. Yang, D. M. Huang, *ACS Nano* **2011**, *5*, 6156-6163.
[68] M. Brayman, A. Thathiah, D. D. Carson, *Reprod. Biol. Endocrinol.* **2004**, *2*, 4.
[69] S. J. Gendler, *J. Mammary Gland. Biol.* **2001**, *6*, 339-353.
[70] N. L. Bartlett, G. R. Petroni, B. A. Parker, N. D. Wagner, J. P. Gockerman, G. A. Omura, G. P. Canellos, M. Robert, J. L. Johnson, B. A. Peterson, *Cancer* **2001**, *92*, 207-217.
[71] J. H. Edmonson, I. A. Petersen, T. C. Shives, M. R. Mahoney, M. G. Rock, M. G. Haddock, F. H. Sim, W. J. Maples, M. I. O'Connor, L. L. Gunderson, M. L. Foo, D. J. Pritchard, J. C. Buckner, S. L. Stafford, *Cancer* **2002**, *94*, 786-792.
[72] Y. Mishima, E. Nagasaki, Y. Terui, T. Irie, S. Takahashi, Y. Ito, M. Oguchi, K. Kawabata, S. Kamata, K. Hatake, *Cancer* **2004**, *101*, 1437-1444.
[73] D. Bhatia, S. Surana, S. Chakraborty, S. P. Koushika, Y. Krishnan, *Nat. Commun.* **2011**, *2*, 339.
[74] J. A. Thomas, R. N. Buchsbaum, A. Zimniak, E. Racker, *Biochemistry* **1979**, *18*, 2210-2218.
[75] G. R. Martin, R. K. Jain, *Cancer Res.* **1994**, *54*, 5670-5674.
[76] Y. G. Ke, L. L. Ong, W. M. Shih, P. Yin, *Science* **2012**, *338*, 1177-1183.
[77] Q. A. Mei, X. X. Wei, F. Y. Su, Y. Liu, C. Youngbull, R. Johnson, S. Lindsay, H. Yan, D. Meldrum, *Nano Lett.* **2011**, *11*, 1477-1482.
[78] M. C. Palanca-Wessels, M. T. Barrett, P. C. Galipeau, K. L. Rohrer, B. J. Reid, P. S. Rabinovitch, *Gastroenterology* **1998**, *114*, 295-304.

[79] Y. X. Zhao, A. Shaw, X. Zeng, E. Benson, A. M. Nystrom, B. Hogberg, *ACS Nano* **2012**, *6*, 8684-8691.
[80] H. Dietz, S. M. Douglas, W. M. Shih, *Science* **2009**, *325*, 725-730.
[81] Q. Jiang, C. Song, J. Nangreave, X. Liu, L. Lin, D. Qiu, Z. G. Wang, G. Zou, X. Liang, H. Yan, B. Ding, *J. Am. Chem. Soc.* **2012**, *134*, 13396-13403.
[82] I. Pastan, M. M. Gottesman, *Annu. Rev. Med.* **1991**, *42*, 277-286.
[83] M. M. Gottesman, *Annu. Rev. Med.* **2002**, *53*, 615-627.
[84] M. Schindler, S. Grabski, E. Hoff, S. M. Simon, *Biochemistry* **1996**, *35*, 2811-2817.
[85] J. Z. Fuks, S. Wadler, P. H. Wiernik, *J. Clin. Pharmacol.* **1987**, *27*, 357-365.
[86] N. Altan, Y. Chen, M. Schindler, S. M. Simon, *P. Natl. Acad. Sci. USA* **1999**, *96*, 4432-4437.
[87] S. J. Hurwitz, M. Terashima, N. Mizunuma, C. A. Slapak, *Blood* **1997**, *89*, 3745-3754.
[88] S. M. Douglas, I. Bachelet, G. M. Church, *Science* **2012**, *335*, 831-834.
[89] S. Beyer, P. Nickels, F. C. Simmel, *Nano Lett.* **2005**, *5*, 719-722.
[90] Z. X. Deng, Y. Tian, S. H. Lee, A. E. Ribbe, C. D. Mao, *Angew. Chem. Int. Ed.* **2005**, *44*, 3582-3585.
[91] G. D. Hamblin, K. M. Carneiro, J. F. Fakhoury, K. E. Bujold, H. F. Sleiman, *J. Am. Chem. Soc.* **2012**, *134*, 2888-2891.
[92] P. K. Lo, P. Karam, F. A. Aldaye, C. K. McLaughlin, G. D. Hamblin, G. Cosa, H. F. Sleiman, *Nat. Chem.* **2010**, *2*, 319-328.
[93] H. P. Liu, Y. Chen, Y. He, A. E. Ribbe, C. D. Mao, *Angew. Chem. Int. Ed.* **2006**, *45*, 1942-1945.
[94] D. A. Giljohann, D. S. Seferos, L. D. Weston, M. D. Massich, P. C. Patel, C. A. Mirkin, *Angew. Chem. Int. Ed.* **2010**, *49*, 3280-3294.
[95] J. S. Lee, A. K. R. Lytton-Jean, S. J. Hurst, C. A. Mirkin, *Nano Lett.* **2007**, *7*, 2112-2115.
[96] J. I. Cutler, D. Zheng, X. Y. Xu, D. A. Giljohann, C. A. Mirkin, *Nano Lett.* **2010**, *10*, 1477-1480.
[97] G. P. Mitchell, C. A. Mirkin, R. L. Letsinger, *J. Am. Chem. Soc.* **1999**, *121*, 8122-8123.
[98] M. Kwak, A. Herrmann, *Angew. Chem. Int. Ed.* **2010**, *49*, 8574-8587.
[99] F. E. Alemdaroglu, A. Herrmann, *Org. Biomol. Chem.* **2007**, *5*, 1311-1320.
[100] M. Kwak, A. Herrmann, *Chem. Soc. Rev.* **2011**, *40*, 5745-5755.
[101] R. Elghanian, J. J. Storhoff, R. C. Mucic, R. L. Letsinger, C. A. Mirkin, *Science* **1997**, *277*, 1078-1081.
[102] J. S. Lee, D. S. Seferos, D. A. Giljohann, C. A. Mirkin, *J. Am. Chem. Soc.* **2008**, *130*, 5430-5431.
[103] S. J. Hurst, A. K. R. Lytton-Jean, C. A. Mirkin, *Anal. Chem.* **2006**, *78*, 8313-8318.

[104] G. Bhabra, A. Sood, B. Fisher, L. Cartwright, M. Saunders, W. H. Evans, A. Surprenant, G. Lopez-Castejon, S. Mann, S. A. Davis, L. A. Hails, E. Ingham, P. Verkade, J. Lane, K. Heesom, R. Newson, C. P. Case, *Nat. Nanotechnol.* **2009**, *4*, 876-883.

[105] A. Nel, T. Xia, L. Madler, N. Li, *Science* **2006**, *311*, 622-627.

[106] Y. Pan, S. Neuss, A. Leifert, M. Fischler, F. Wen, U. Simon, G. Schmid, W. Brandau, W. Jahnen-Dechent, *Small* **2007**, *3*, 1941-1949.

[107] J. I. Cutler, K. Zhang, D. Zheng, E. Auyeung, A. E. Prigodich, C. A. Mirkin, *J. Am. Chem. Soc.* **2011**, *133*, 9254-9257.

[108] D. S. Seferos, A. E. Prigodich, D. A. Giljohann, P. C. Patel, C. A. Mirkin, *Nano Lett.* **2009**, *9*, 308-311.

[109] J. P. Behr, *Accounts Chem. Res.* **1993**, *26*, 274-278.

[110] D. Luo, W. M. Saltzman, *Nat. Biotechnol.* **2000**, *18*, 33-37.

[111] D. A. Giljohann, D. S. Seferos, P. C. Patel, J. E. Millstone, N. L. Rosi, C. A. Mirkin, *Nano Lett.* **2007**, *7*, 3818-3821.

[112] B. D. Chithrani, A. A. Ghazani, W. C. W. Chan, *Nano Lett.* **2006**, *6*, 662-668.

[113] A. Matsumoto, M. Naito, H. Itakura, S. Ikemoto, H. Asaoka, I. Hayakawa, H. Kanamori, H. Aburatani, F. Takaku, H. Suzuki, Y. Kobari, T. Miyai, K. Takahashi, E. H. Cohen, R. Wydro, D. E. Housman, T. Kodama, *P. Natl. Acad. Sci. USA* **1990**, *87*, 9133-9137.

[114] D. R. Greaves, S. Gordon, *J. Lipid Res.* **2005**, *46*, 11-20.

[115] M. K. Bijsterbosch, M. Manoharan, E. T. Rump, R. L. A. De Vrueh, R. van Veghel, K. L. Tivel, E. A. L. Biessen, C. F. Bennett, P. D. Cook, T. J. C. van Berkel, *Nucleic Acids Res.* **1997**, *25*, 3290-3296.

[116] N. Liu, M. Hentschel, T. Weiss, A. P. Alivisatos, H. Giessen, *Science* **2011**, *332*, 1407-1410.

[117] K. Zhang, L. L. Hao, S. J. Hurst, C. A. Mirkin, *J. Am. Chem. Soc.* **2012**, *134*, 16488-16491.

[118] N. E. Hynes, H. A. Lane, *Nat. Rev. Cancer* **2005**, *5*, 341-354.

[119] J. Baselga, S. M. Swain, *Nat. Rev. Cancer* **2009**, *9*, 463-475.

[120] S. Dhar, W. L. Daniel, D. A. Giljohann, C. A. Mirkin, S. J. Lippard, *J. Am. Chem. Soc.* **2009**, *131*, 14652-14653.

[121] E. R. Jamieson, S. J. Lippard, *Chem. Rev.* **1999**, *99*, 2467-2498.

[122] Rosenber.B, L. Vancamp, J. E. Trosko, V. H. Mansour, *Nature* **1969**, *222*, 385-386.

[123] X. Q. Zhang, X. Xu, R. Lam, D. Giljohann, D. Ho, C. A. Mirkin, *ACS Nano* **2011**, *5*, 6962-6970.

[124] C. M. Alexander, J. C. Dabrowiak, M. M. Maye, *Bioconjugate Chem.* **2012**, *23*, 2061-2070.

[125] J. B. Chaires, J. E. Herrera, M. J. Waring, *Biochemistry* **1990**, *29*, 6145-6153.

[126] F. Sha, F. M. Chen, *Biophys. J.* **2000**, *79*, 2095-2104.

[127] D. Kim, Y. Y. Jeong, S. Jon, *ACS Nano* **2010**, *4*, 3689-3696.
[128] V. Bagalkot, O. C. Farokhzad, R. Langer, S. Jon, *Angew. Chem. Int. Ed.* **2006**, *45*, 8149-8152.
[129] Z. Xiao, C. Ji, J. Shi, E. M. Pridgen, J. Frieder, J. Wu, O. C. Farokhzad, *Angew. Chem. Int. Ed.* **2012**, *51*, 11853-11857.
[130] V. Ntziachristos, J. Ripoll, L. H. V. Wang, R. Weissleder, *Nat. Biotechnol.* **2005**, *23*, 313-320.
[131] M. Wei, N. Chen, J. Li, M. Yin, L. Liang, Y. He, H. Y. Song, C. H. Fan, Q. Huang, *Angew. Chem. Int. Ed.* **2012**, *51*, 1202-1206.
[132] B. G. Trewyn, J. A. Nieweg, Y. Zhao, V. S. Y. Lin, *Chem. Eng. J.* **2008**, *137*, 23-29.
[133] J. Kecht, A. Schlossbauer, T. Bein, *Chem. Mater.* **2008**, *20*, 7207-7214.
[134] V. Cauda, A. Schlossbauer, J. Kecht, A. Zurner, T. Bein, *J. Am. Chem. Soc.* **2009**, *131*, 11361-11370.
[135] E. Climent, A. Bernardos, R. Martinez-Manez, A. Maquieira, M. D. Marcos, N. Pastor-Navarro, R. Puchades, F. Sancenon, J. Soto, P. Amoros, *J. Am. Chem. Soc.* **2009**, *131*, 14075-14080.
[136] K. Patel, S. Angelos, W. R. Dichtel, A. Coskun, Y. W. Yang, J. I. Zink, J. F. Stoddart, *J. Am. Chem. Soc.* **2008**, *130*, 2382-2383.
[137] T. D. Nguyen, H. R. Tseng, P. C. Celestre, A. H. Flood, Y. Liu, J. F. Stoddart, J. I. Zink, *P. Natl. Acad. Sci. USA* **2005**, *102*, 10029-10034.
[138] C. B. Gao, H. Q. Zheng, L. Xing, M. H. Shu, S. N. Che, *Chem. Mater.* **2010**, *22*, 5437-5444.
[139] N. G. Liu, D. R. Dunphy, P. Atanassov, S. D. Bunge, Z. Chen, G. P. Lopez, T. J. Boyle, C. J. Brinker, *Nano Lett.* **2004**, *4*, 551-554.
[140] C. E. Chen, J. Geng, F. Pu, X. J. Yang, J. S. Ren, X. G. Qu, *Angew. Chem. Int. Ed.* **2011**, *50*, 882-886.
[141] Q. Yuan, Y. Zhang, T. Chen, D. Lu, Z. Zhao, X. Zhang, Z. Li, C. H. Yan, W. Tan, *ACS Nano* **2012**, *6*, 6337-6344.
[142] C. Chen, F. Pu, Z. Huang, Z. Liu, J. Ren, X. Qu, *Nucleic Acids Res.* **2011**, *39*, 1638-1644.
[143] K. Gehring, J. L. Leroy, M. Gueron, *Nature* **1993**, *363*, 561-565.
[144] M. Gueron, J. L. Leroy, *Curr. Opin. Struc. Biol.* **2000**, *10*, 326-331.
[145] D. G. He, X. X. He, K. M. Wang, J. Cao, Y. X. Zhao, *Adv. Funct. Mater.* **2012**, *22*, 4704-4710.
[146] Z. Zhang, D. Balogh, F. Wang, I. Willner, *J. Am. Chem. Soc.* **2013**, *135*, 1934-1940.
[147] A. Schlossbauer, S. Warncke, P. M. E. Gramlich, J. Kecht, A. Manetto, T. Carell, T. Bein, *Angew. Chem. Int. Ed.* **2010**, *49*, 4734-4737.
[148] E. Ruiz-Hernandez, A. Baeza, M. Vallet-Regi, *ACS Nano* **2011**, *5*, 1259-1266.
[149] A. Rosler, G. W. M. Vandermeulen, H. A. Klok, *Adv. Drug Deliver. Rev.* **2012**, *64*, 270-279.

[150] M. Moffitt, K. Khougaz, A. Eisenberg, *Accounts Chem. Res.* **1996**, *29*, 95-102.
[151] F. M. Veronese, G. Pasut, *Drug. Discov. Today* **2005**, *10*, 1451-1458.
[152] M. H. Caruthers, *Accounts Chem. Res.* **1991**, *24*, 278-284.
[153] F. E. Alemdaroglu, W. Zhuang, L. Zophel, J. Wang, R. Berger, J. P. Rabe, A. Herrmann, *Nano Lett.* **2009**, *9*, 3658-3662.
[154] M. S. Ayaz, M. Kwak, F. E. Alemdaroglu, J. Wang, R. Berger, A. Herrmann, *Chem. Commun.* **2011**, *47*, 2243-2245.
[155] F. E. Alemdaroglu, J. Wang, M. Borsch, R. Berger, A. Herrmann, *Angew. Chem. Int. Ed.* **2008**, *47*, 974-976.
[156] K. Ding, F. E. Alemdaroglu, M. Boersch, R. Berger, A. Herrmann, *Angew. Chem. Int. Ed.* **2007**, *46*, 1172-1175.
[157] F. E. Alemdaroglu, N. C. Alemdaroglu, P. Langguth, A. Herrmann, *Macromol. Rapid Comm.* **2008**, *29*, 326-329.
[158] F. E. Alemdaroglu, N. C. Alemdaroglu, P. Langguth, A. Herrmann, *Adv. Mater.* **2008**, *20*, 899-902.
[159] Y. Wu, K. Sefah, H. Liu, R. Wang, W. Tan, *P. Natl. Acad. Sci. USA* **2009**, *107*, 5-10.
[160] M. Kwak, A. J. Musser, J. Lee, A. Herrmann, *Chem. Commun.* **2010**, *46*, 4935-4937.
[161] M. Kwak, I. J. Minten, D.-M. Anaya, A. J. Musser, M. Brasch, R. J. M. Nolte, K. Mullen, J. J. L. M. Cornelissen, A. Herrmann, *J. Am. Chem. Soc.* **2010**, *132*, 7834-7835.
[162] A. Rodriguez-Pulido, A. I. Kondrachuk, D. K. Prusty, J. Gao, M. A. Loi, A. Herrmann, *Angew. Chem. Int. Ed.* **2013**, *52*, 1008-1012.
[163] Z. Cao, R. Tong, A. Mishra, W. Xu, G. C. Wong, J. Cheng, Y. Lu, *Angew. Chem. Int. Ed.* **2009**, *48*, 6494-6498.
[164] C. K. McLaughlin, G. D. Hamblin, K. D. Hanni, J. W. Conway, M. K. Nayak, K. M. Carneiro, H. S. Bazzi, H. F. Sleiman, *J. Am. Chem. Soc.* **2012**, *134*, 4280-5286.

2. Synthesis and characterization of DNA block copolymers revisited

2.1 Introduction

Block copolymers have found their way into daily-life applications due to the properties originating from their self-assembly behavior[1-2]. In these materials, formation of ordered domains is observed as a result of microphase separation which occurs due to repulsion between the two dissimilar polymer blocks that are covalently connected. The strength of this repelling force determines the morphology of the formed super structures and it depends on the used monomers, the length of the individual polymer units and the block length ratio[3]. By altering these parameters the properties of the material can precisely be tuned to fit the desired application. As a result a large number of block copolymers are currently used in a commercial setting. In order to further expand their functionality; researchers have become increasingly interested in block copolymers that include biomacromolecules such as peptides or oligonucleotides (ODNs). These hybrids benefit from the properties of both the natural and organic components and therefore have several advantages compared to

conventional synthetic polymers. For example, in biomedicine conjugation of polyethylene glycol with therapeutic peptides is used to improve circulation times in the body and decrease the immune response[4-6]. Whereas proteins and peptides are often functionalized with polymers to improve stability[7] and catalytic properties[8], DNA block copolymers (DBCs) are used in a different context. In such structures, the DNA can be used as a building block for precise assembly due to its unique self-recognition properties through Watson-Crick base pairing. In this regard, DBCs have been utilized for sequence specific assembly of nanometer sized objects[9-12], directed functionalization of nanoparticles[13-14], sequence controlled release of loaded compounds[15] and targeted drug delivery[16]. In contrast to peptide conjugates, when DNA is incorporated into bioorganic hybrids the nucleic acid part always remains charged and hydrophilic which bears challenges for synthesis, purification and characterization. As such, these processes still need optimization to further exploit the unique properties of DBC materials.

Similar to other bioconjugation protocols, the fabrication of DBCs can be divided into two major classes; solution based coupling and solid phase synthesis[17]. For the former method several reactions can be employed to perform conjugation of the two blocks, depending on the functional groups on the DNA and the polymer. In Fig. 2.1 different synthetic strategies of solution coupling are summarized and R_1 represents the functionalized polymer while R_2 indicates the modified ODN. Of note is that the reactive groups are interchangeable in most cases.

One of the most widely used solution phase coupling strategies is based on the formation of an amide bond through reaction of an amino modified ODN with a carboxylic acid terminated polymer (see Fig. 2.1A)[18-22]. This coupling reaction is mediated by *N*-hydroxy succinimide (NHS) and *N*,*N*'-dicyclohexylcarbodiimide (DCC), which form the activated ester of the polymer moiety, which then reacts with the amine-modified DNA. An important feature of this method is that the activated intermediate does not need to be purified and can be used for coupling immediately because the starting materials do not interfere with the conjugation reaction.

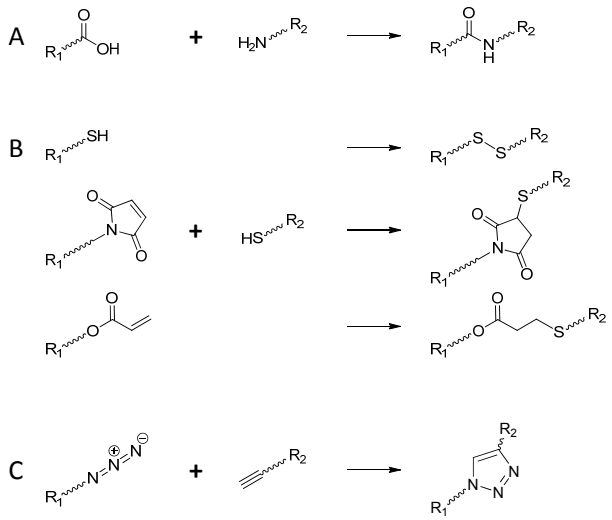

Figure 2.1. DBC formation through solution phase coupling. (A) Via amide bond formation, (B) using disulfide bond formation (top) or Michael addition (bottom two) or (C) through a 1,3-dipolar cycloaddition.

Additionally, the reaction is fast and high yields are obtained when coupling molecules with low molecular weights. In a second strategy, a sulfhydryl-modified ODN is used for conjugation through disulfide bond formation with a thiol functionalized polymer (See Fig. 2.1B)[23]. Alternatively, the same ODN can be used for conjugation through a Michael addition reaction when a maleimide- or acrylate-modified polymer is employed[24-25]. As a last solution phase coupling method the Huisgen 1,3-dipolar cycloaddition can be used for hybrid formation. This reaction has become increasingly popular due to the development of DNA compatible click catalysts ensuring high specificity and limited cross-reactivity (See Fig. 2.1C)[26]. Although commonly used for small molecule modifications, solution phase coupling strategies have also been employed for hydrophilic and slightly hydrophobic polymers as both can be solubilized in an aqueous environment.

Alternatively, coupling can be performed using solid phase synthesis (SPS). The SPS approach was first developed by Merrifield. He successfully demonstrated fabrication of a peptide through repeated coupling of amino acids to the growing chain that is immobilized on a polymer resin bead[27].

This revolutionary method laid the foundation for automated oligonucleotide synthesis which facilitates the fabrication of ODNs in large scales with high fidelity at an affordable price. This has made DNA accessible to a wide scientific community and allowed introduction of non-natural building blocks and modifications. For synthesis of DBCs this approach has several advantages over solution based coupling as it is fully automated and compatible with hydrophobic polymers. For coupling the hydroxyl terminated polymer is first activated as β-cyanoethylphosphoramidite (See Fig. 2.2) and afterwards attached to the terminal hydroxyl group on the growing DNA chain. After deprotection and cleavage from the solid support, the DBC can be isolated from the crude reaction mixture using various purification techniques.

To date, high performance liquid chromatography (HPLC) is the gold standard for DNA and RNA purification and characterization due to its high reproducibility, speed and scalability[28]. ODNs are readily purified by anion exchange (AEX) or reversed phase (RPC) HPLC depending on the

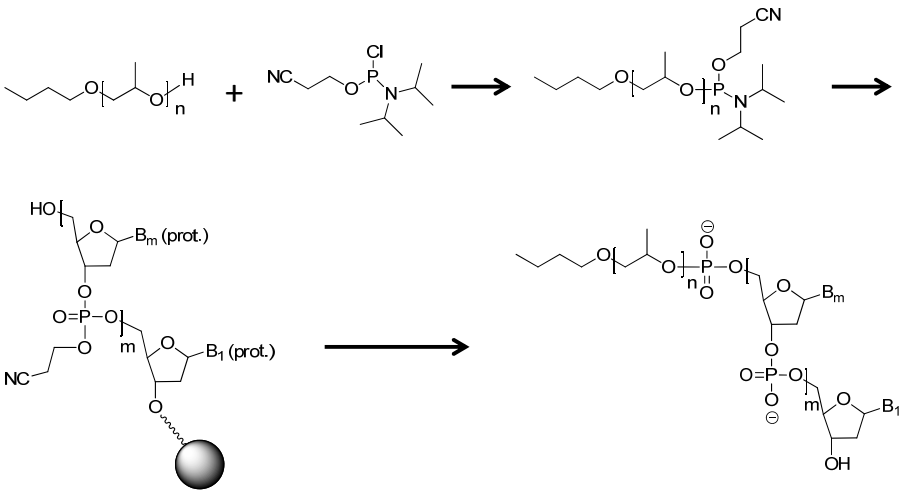

Figure 2.2. DBC formation using solid phase synthesis approach, exemplified by poly(propylene oxide)-*block*-DNA fabrication. Firstly the polymeramidite is formed through reaction of 2-cyanoethyl *N,N*-diispropylchlorophosphoramidite with the terminal hydroxyl group on the polymer. The amidite is then coupled as last modification to the growing DNA chain. Finally, the product is deprotected and cleaved from the solid support.

modification and final use of the product. In the former technique, separation of the products relies on a difference in negative charges. As the full product contains the most phosphate groups it will bind stronger to the column and therefore elute at higher salt concentrations. This approach is especially suitable for workup of more complex DNA and RNA sequences that have secondary interactions since it allows for a variety of denaturating methods such as addition of chaotropic agents, elevated temperatures or increased pH without the loss of resolution. However, a downside is the need of an additional desalting step to obtain the final product salt-free and without afore mentioned additives. The other technique, RPC HPLC, is based on separation of the product by a difference in hydrophobicity. To obtain good resolution, native DNA sequences can be synthesized with the last hydrophobic 5' hydroxyl protective group (DMT) remaining on the full-length product, thereby separating it from by-products. Afterwards, the DMT group can easily be removed under slight acidic conditions, obtaining the pure product after precipitation. On the other hand, functionalized ODNs are separated from truncated sequences due to the hydrophobic character of the modification. An advantage of this technique over AEX chromatography is the use of volatile buffers, which avoids the need for additional desalting and allows a direct coupling of the HPLC with mass spectrometers. As a result this approach is generally preferred for standard DNA purification. For DBCs, especially amphiphilic ones, HPLC purification has not been explored yet. To date, they have only been purified using AEX HPLC and polyacrylamide gel electrophoresis (PAGE), where separation is based on the molecular weight and charge of the ODN. This yields good resolution and high purity DBCs, but the latter technique is elaborate, time consuming and results in low yields. Additionally, it is hard to purify larger quantities as it is difficult to scale up polyacrylamide gel electrophoresis. Another drawback is the toxic nature of acrylamide. Therefore, it is desirable to replace this technique by HPLC where possible.

In this chapter, solid phase synthesis of several different DNA-poly(propylene oxide) (DNA-PPO) block copolymers will be pursued. Additionally, we show for the first time that the obtained products can be purified by RPC HPLC. Finally, the influence of the polymer on the melting temperature (T_m) will be investigated.

2.2 Results and discussion

2.2.1 DBC synthesis and characterization

To explore HPLC purification of DBCs, three DNA diblock and one DNA triblock copolymer were synthesized (See Table 2.1). Of the three diblock copolymers, 22-PPO is composed of a 22mer oligonucleotide bearing the PPO polymer at the 5' terminus. The sequence of the DNA was designed such that it does not exhibit self-complementarity or other secondary structures. The other two diblock copolymers, c22-PPO and cr22-PPO, consist of a sequence complementary to the 22mer to which the polymer is coupled at the 5' or 3' end, respectively. Finally, a triblock copolymer was synthesized through reaction of a PPO diamidite and therefore contains two 22mer sequences linked at the 5' end to the polymer block.

Name	Sequence
22mer	5'-CCTCGCTCTGCTAATCCTGTTA-3'
22-PPO	**PPO**-5'-CCTCGCTCTGCTAATCCTGTTA-3'
c22mer	5'-TAACAGGATTAGCAGAGCGAGG-3'
c22-PPO	**PPO**-5'-TAACAGGATTAGCAGAGCGAGG-3'
cr22-PPO	5'-TAACAGGATTAGCAGAGCGAGG-3'-**PPO**
22-PPO-22	ATTGTCCTAATCGTCTCGCTCC-5'-**PPO**-5'-CCTCGCTCTGCTAATCCTGTTA-3'

Table 2.1. Sequences of used DBCs and their native DNA counterpart.

For synthesis of the DNA diblock copolymers the polymeramidite was formed through reaction of chlorophosphoramidite with the free hydroxyl group of PPO monobutyl ether (weight average molecular weight (M_w) ~1000 g/mol). For the triblock architectures PPO (M_w ~1000 g/mol) containing two terminal hydroxyl groups was used to obtain the active amidite. Afterwards, the solution was transferred to the automated DNA synthesizer and the DBCs were synthesized using a modified coupling method for the polymer to ensure conjugation. After synthesis of the DBCs the product was deprotected, cleaved from the solid support and purification by HPLC was pursued. As the PPO polymer is hydrophobic the crude mixtures were analyzed on an ÄKTA Explorer using a RPC column. Since

the DBCs merely differ in sequence and position of the polymer block, the resulting chromatograms are very similar and as such the one of 22-PPO is shown as example (See Fig. 2.3).

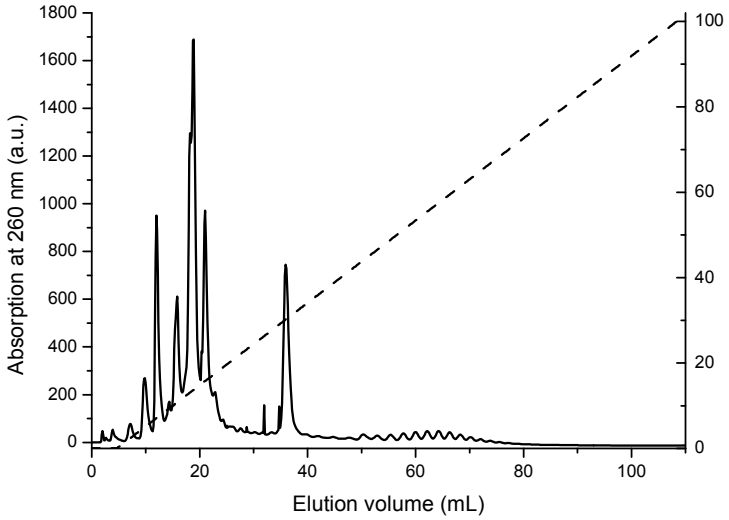

Figure 2.3. Analytical RPC HPLC elugram of crude mixture of 22-PPO synthesis. Dotted line indicates percentage of buffer B. Buffers are A: 100 mM triethylammonium acetate (TEAAc) and 2.5% acetonitrile, B: 100 mM TEAAc and 65% acetonitrile.

The elugram of the crude reaction mixture shows a large number of peaks, most of them observed below elution volumes of 40 ml. These presumably correspond to unmodified DNA or side products such as failed sequences that have been capped during synthesis. At larger elution volumes (50 - 80 ml) several smaller peaks are observed that elute at higher concentrations of acetonitrile. It was hypothesized that, as the DNA polymer conjugate was expected to be the most hydrophobic component in the reaction mixture, the observed peak array represents the DBC product. The conjugate was expected not to elute as a single peak due to the polydispersity of the PPO block and as such every single peak should represent a copolymer with a specific number of propylene oxide units. For purification the gradient was optimized in order to elute the DBCs together. It must be noted that for the purification of the triblock copolymer AEX HPLC was performed afterwards in order to separate the diblock copolymer from the triblock copolymer.

After purification, the products were characterized by denaturating PAGE (See Fig. 2.4).

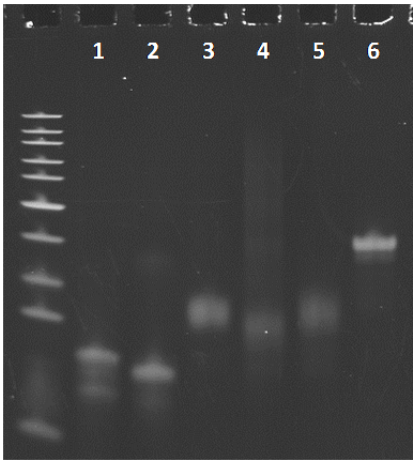

Figure 2.4. Denaturating PAGE characterization of HPLC purified DBCs (15% TBE-Urea, 120 V, 90 min). Lane 1: 22mer, lane 2: c22mer, lane 3: 22-PPO, lane 4: c22-PPO, lane 5: cr22-PPO, lane 6: 22-PPO-22

The electrophoretic analysis of the obtained product shows that the diblock copolymers (lanes 3 – 5) have a lower electrophoretic mobility than the pristine DNA (lanes 1 – 2). Compared to the other DBCs, the triblock architecture exhibits an even lower mobility due to its increased size. These findings are in good agreement with earlier PAGE results obtained for similar conjugates[16, 29].

To further characterize the products they were also analyzed by RPC HPLC on a Shimadzu VP series HPLC (See Fig. 2.5). As can be seen from the chromatograms, the DBCs are obtained with reasonable purity after RPC

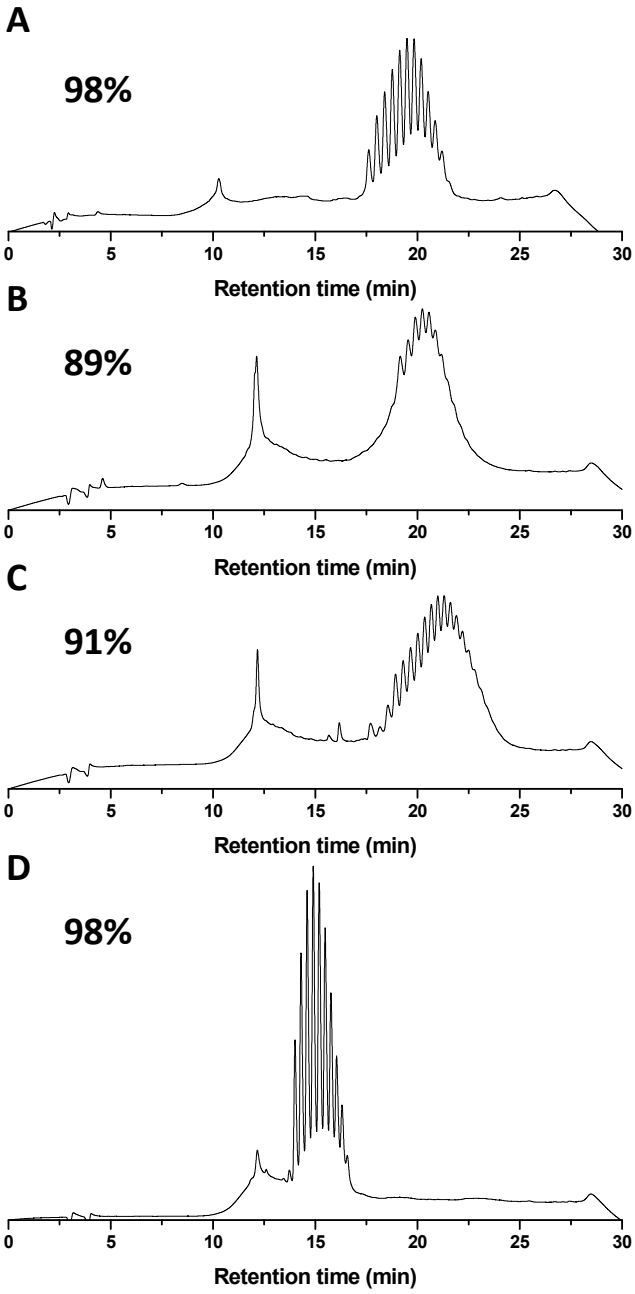

Figure 2.5. RPC HPLC characterization of purified PPO diblock and triblock copolymers. (A) Elugram of 22-PPO (purity 98%). (B) Elugram of c22-PPO (purity 89%). (C) Elugram of cr22-PPO (purity 91%). (D) Elugram of 22-PPO-22 (purity 98%).

purification. The purity of the obtained products corresponds well to results that were obtained for RPC purification of ODNs with a small molecule modification[28]. The sharp peak at 10 or 12 minutes elution time, corresponds to the unmodified 22mer or c22mer that was injected as control (data not shown). The obtained DBCs elute later as a broad peak with several sub-peaks visible that correspond to the individual conjugates. When comparing the different DBCs with each other the triblock copolymer shows a lower retention time than the diblock copolymers, indicating its less hydrophobic character. This is expected since this conjugate contains 2 hydrophilic DNA chains that are connected to a single PPO block.

For final confirmation of the identity of the DBCs their mass was measured by MALDI-TOF mass spectrometry (See Table 2.2 and Fig. 2.9). Again, as the spectra are very similar, only the one of 22-PPO is shown (See Fig. 2.6).

DBC	M_w Calculated	M_w Found
22-PPO	7733	7723
c22-PPO	7979	7910
cr22-PPO	7979	7992
22-PPO-22	14350	14277

Table 2.2. Molecular weight analysis of DBCs by MALDI-TOF mass spectrometry. Molecular weights were calculated using the M_w of the PPO polymer. Measured molecular weights correspond to the M_w found by MALDI-TOF measurements.

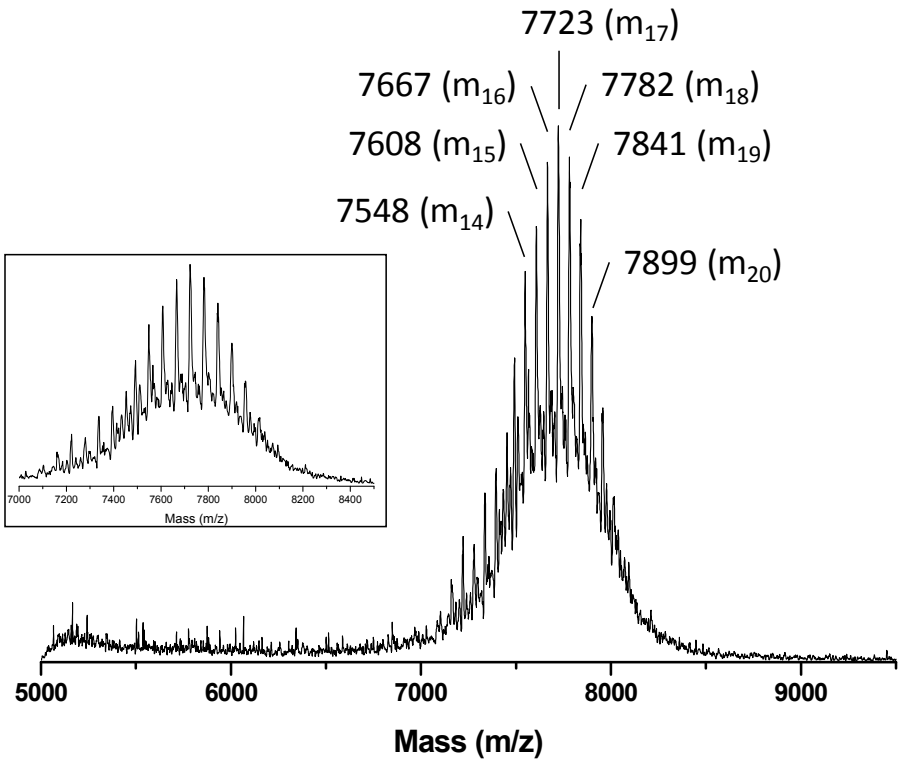

Figure 2.6. MALDI-TOF mass spectrum of 22-PPO with molecular weights indicated. Inset shows the zoomed mass spectrum from 7000 to 9500 g/mol. Numbers in brackets indicate number of monomer units in the PPO polymer.

The molecular weights of all DBCs correspond to the calculated values with differences of less than 70 g/mol (~1%), giving the final confirmation of the identity of the DBCs. As can be seen for the exemple spectrum, also during MALDI-TOF analysis several peaks are found. The mass difference between the individual peaks is 58 units, which resembles the molecular weight of the PPO repeating unit. As such, the exact number of monomers in the polymer block of DBCs can be calculated (See Fig. 2.6). The mass spectrometry results also confirm the hypothesis made on the identity of the array of peaks earlier observed during purification by RPC HPLC.

2.2.2 Investigation of polymer influence on the melting temperature

After characterization, the influence of polymer-DNA and polymer-polymer interactions on the T_m was studied. The temperature at which the two strands dehybridize is determined by a number of factors including the sequence, salt concentration and nature of the nucleic acid. However, also modification of the DNA has resulted in altered melting points. For example, replacing the ribose moieties by a peptide backbone (PNA) results in a greatly increased T_m due to the lack of negative charges[30]. Less drastic changes at the terminus of the oligonucleotide have proven to T_m. Conjugation of gold NPs to DNA increased the T_m due to cooperative effects which depend on the particle size, DNA surface density and interparticle distance[31]. As such, when conjugating oligonucleotides with larger moieties alterations of the T_m

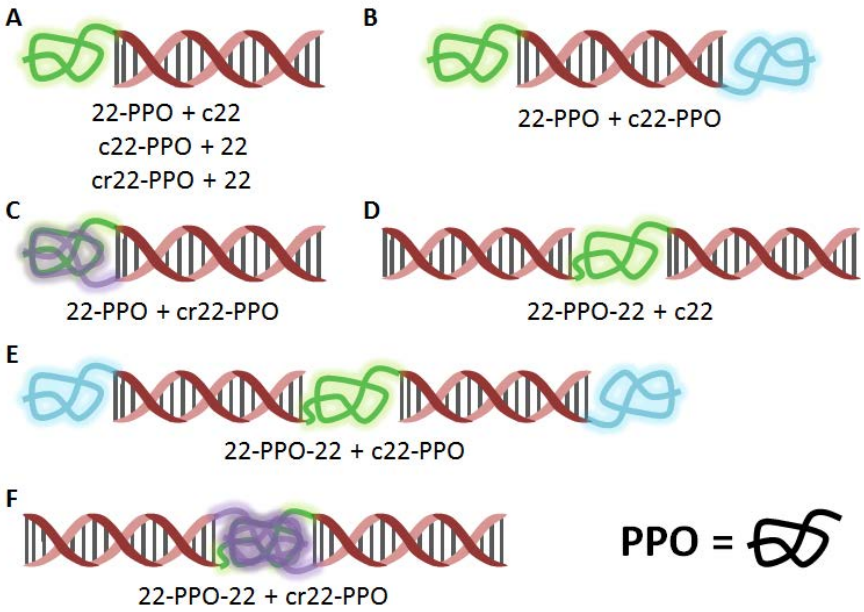

Figure 2.7. Designed ds DBC architectures obtained through hybridization of DNA-PPO diblock and triblock copolymers with corresponding complementary DNAs. (A) DBC resulting from hybridization of 22-PPO with c22mer, c22-PPO with 22mer or cr22-PPO with 22mer. (B) DBC resulting from hybridization of 22-PPO with c22-PPO. (C) DBC resulting from hybridization of 22-PPO with cr22-PPO. (D) DBC resulting from hybridization of 22-PPO-22 with c22mer. (E) DBC resulting from hybridization of 22-PPO-22 with c22-PPO. (F) DBC resulting from hybridization of 22-PPO-22 with cr22-PPO.

can be expected. To investigate such changes for DBCs, several architectures were designed that can be obtained through hybridization of the DNA conjugates with pristine complementary DNA (c22mer or 22mer) or one of the synthesized DBCs. For the diblock copolymers, the resulting constructs exhibit a single polymer block (See Fig. 2.7A), a double polymer block on either side (See Fig. 2.7B) or at the same side of the double stranded DNA segment (See Fig. 2.7C). In case of the triblock copolymer structures with two double stranded (ds) DNAs attached to the same polymer (See Fig. 2.7D), alternatingly PPO-DNA-PPO-DNA-PPO blocks (See Fig. 2.7E) or three polymer blocks confined by two DNA strands (See Fig. 2.7F) can be obtained. The formation of these architectures through hybridization was confirmed by native PAGE analysis (See Fig. 2.8).

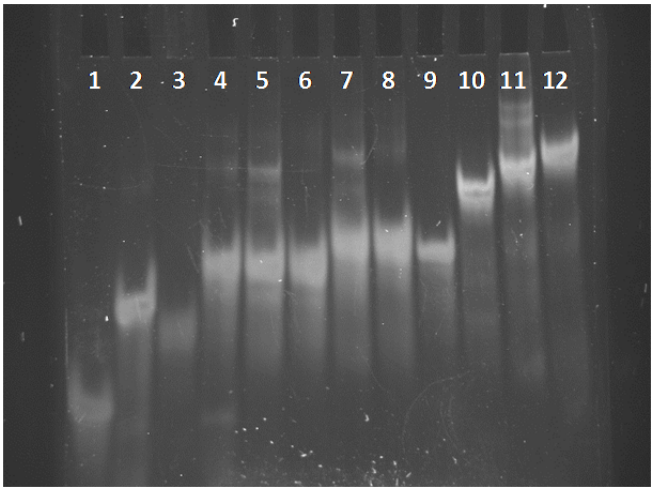

Figure 2.8. Native PAGE characterization of ds DBC architectures (15% TBE, 120 V, 105 min). Lane 1: ss 22mer, lane 2: ds 22mer, lane 3: ss 22-PPO, lane 4: 22-PPO + c22mer, lane 5: c22-PPO + 22mer, lane 6: cr22-PPO + 22mer, lane 7: 22-PPO + c22-PPO, lane 8: 22-PPO + cr22-PPO, lane 9: ss 22-PPO-22, lane 10: 22-PPO-22 + c22mer, lane 11: 22-PPO-22 + c22-PPO, lane 12: 22-PPO-22 + cr22-PPO.

When looking at the results from the PAGE analysis, a lower electrophoretic mobility of the hybridized DBCs is observed compared to the ss controls, indicating successful Watson-Crick basepairing. Additionally, when comparing the ds samples containing one DBC (lanes 3-5 and 10) with the

samples containing two DBCs (lanes 7, 8, 11 and 12) a further decrease in electrophoretic mobility is found due to the presence of an additional polymer block.

After confirming hybridization, the T_m of the DBC architectures was determined. To this end, the solutions were heated at 0.5 °C/min while measuring the absorption at 260 nm[32-33]. Afterwards the slope was calculated and T_m was taken at the maximum slope. (See Table 2.3). The complete absorption spectra and the slope as function of the temperature are given in the experimental section (See Fig. 2.10).

Sample	Complement	Graphical representation	Tm (°C)
22mer	c22mer		70
22-PPO	c22mer		70
	c22-PPO		69
	cr22-PPO		70
c22-PPO	22mer		68
cr22-PPO	22mer		69
22-PPO-22	c22mer		69
	c22-PPO		68
	cr22-PPO		71

Table 2.3. Calculated T_m values for hybridized DBCs. All melting temperatures were determined in duplo.

When comparing the T_m values of the different DBCs with the ones of the pristine DNA duplex one observes a difference of only 3 °C, which lies very close to the error of the measurement (2 °C). This finding indicates that the synthetic polymer has no influence on the T_m.

2.3 Conclusion

In conclusion, this study presented the synthesis of three DNA diblock and one triblock copolymers. The latter one was fabricated for the first time, while DBC diblock architectures containing a PPO segment have been reported before. Moreover, the first attempt of purification using RPC HPLC was successfully demonstrated. The RPC HPLC purification of DBCs containing PPO units offers the possibility to separate individual components out of the polydisperse mixture, which is impossible for anion exchange chromatography or gel electrophoresis. PAGE characterization of the products showed similar electrophoretic retentions as found in published results on DBCs. Additionally, MALDI-TOF analysis proved the identity of the products and confirmed that the peaks observed in the RPC HPLC analysis correspond to the individual DNA-PPO conjugates with specific number of repeat units. Lastly, it was shown that the polymer unit does not influence the melting temperature and ability for hybridization, despite its large molecular weight and hydrophobic nature. This is an important finding as the vast majority of today's DNA hybrid architectures are functionalized through hybridization. Hence, alteration of these properties might have large consequences on the broad use of these structures.

2.4 Experimental

2.4.1 Materials

All chemicals and reagents were purchased from commercial suppliers and were used without further purification, unless otherwise noted. The poly(propylene oxide) polymers and 2-cyanoethyl *N*,*N*-diisopropylchlorophosphoramidite were purchased from Sigma-Aldrich and were used as received. All solvents and reagents for oligonucleotide synthesis were acquired from Novabiochem (Merck, UK) and SAFC (Sigma-Aldrich, Netherlands). Solid supports (Primer Support^{TM}, 200 μmol/g) from GE Healthcare were used for the synthesis of DNA. The concentrations of the DNA were measured on a Jasco V-630 UV-VIS spectrometer (JASCO Benelux BV) using 1 cm light-path quartz cuvette.

Unmodified oligonucleotides were purchased from Biomers.net in HPLC purification grade. NMR spectra were recorded on a Varian Mercury (400 MHz) NMR spectrometer at 25 °C.

2.4.2 Synthesis of poly(propylene oxide) amidite

Prior to DNA synthesis the PPO was activated as β-cyanoethylphosphoramidite. Therefore, PPO (1.80 g, M_w ~1000 g/mol) was dissolved in freshly distilled dichloromethane (10 ml) under inert conditions. To this solution 1.5 equivalents of freshly distilled diisopropylethylamine and 1.5 equivalents of 2-cyanoethyl N,N-diisopropylchlorophosphoramidite were added drop wise. The solution was allowed to stir for 12 hours. Afterwards, the solution was poured into dichloromethane (30 ml), washed with 1 M NH_4Cl (15 ml) and dried over $MgSO_4$. Solvents were removed under vacuum and the product was redissolved in anhydrous dichloromethane to a final concentration of 0.15 M and characterized by NMR (P^{31} NMR, 400 MHz: 147.8 ppm). For synthesis of the diblock copolymers 22-PPO, c22-PPO and cr22-PPO, mono n-butyl terminated PPO was used. For synthesis of the triblock copolymer 22-PPO-22, a PPO polymer containing two hydroxyl groups at the termini was used.

2.4.3 DNA block copolymer synthesis and purification

All DNA block copolymers were synthesized using standard automated solid-phase phosphoramidite coupling methods on an ÄKTA oligopilot plus (GE Healthcare) DNA synthesizer. For coupling of conventional amidites 5.0 equivalents were used with a coupling time of 4 minutes. For attachment of the polymer 10 coupling cycles were performed with 1.1 equivalents and a recycling time of 15 minutes. In between the coupling cycles, no oxidation and capping steps were performed. To obtain cr22-PPO reversed amidites were used that exhibit the active amidite at the 5' hydroxyl group and contain a DMT-protected 3' OH group. The products were cleaved from the solid support in concentrated ammonia at 60 °C for 6 h.

DBCs were purified by reverse-phase high performance liquid chromatography (HPLC) using a C15 RESOURCE RPC^{TM} 1 ml reverse phase column (GE Healthcare) through custom gradients using elution buffers A: 100 mM triethylammonium acetate (TEAAc) and 2.5% acetonitrile, B: 100 mM TEAAc and 65% acetonitrile. For diblock copolymers a single RPC HPLC purification proved sufficient to obtain the products in high purity. For the 22-PPO-22 triblock copolymer AEX HPLC purification was performed in addition using a HiTrap Q HP 5 mL column (GE Healthcare) and a custom gradient with elution buffers A: 25 mM Tris-HCl and B: 25 mM Tris-HCl and 1 M NaCl. After purification the triblock copolymer was desalted using a HiTrap Desalting column with 20% ethanol as elution buffer.

2.4.4 Characterization of DBCs

Gel electrophoresis of the products and hybridized architectures was performed using a 15% TBE self-cast polyacrylamide gel. The samples were run at 120 V for 90 min after which staining of the bands was performed using SYBR Gold (Life Technologies Europe BV).

RPC HPLC analysis of the products was carried out on a Shimadzu VP series HPLC equipped with a PDA detector and using a Symmetry C8 3.5 μm column 3 x 150 mm (Waters). A linear gradient 0 – 90% B in 20 min was applied at 30 °C using buffer A: 100 mM triethylammonium acetate (TEAAc) and 5% acetonitrile and buffer B: 5% buffer A and 95% CH_3CN. The DNA was monitored at a wavelength of 260 nm.

DBCs were characterized by MALDI-TOF mass spectrometry using a 3-hydroxypicolinic acid matrix. Spectra were recorded on an ABI Voyager DE-PRO MALDI TOF (linear reflector) Biospectrometry Workstation mass spectrometer.

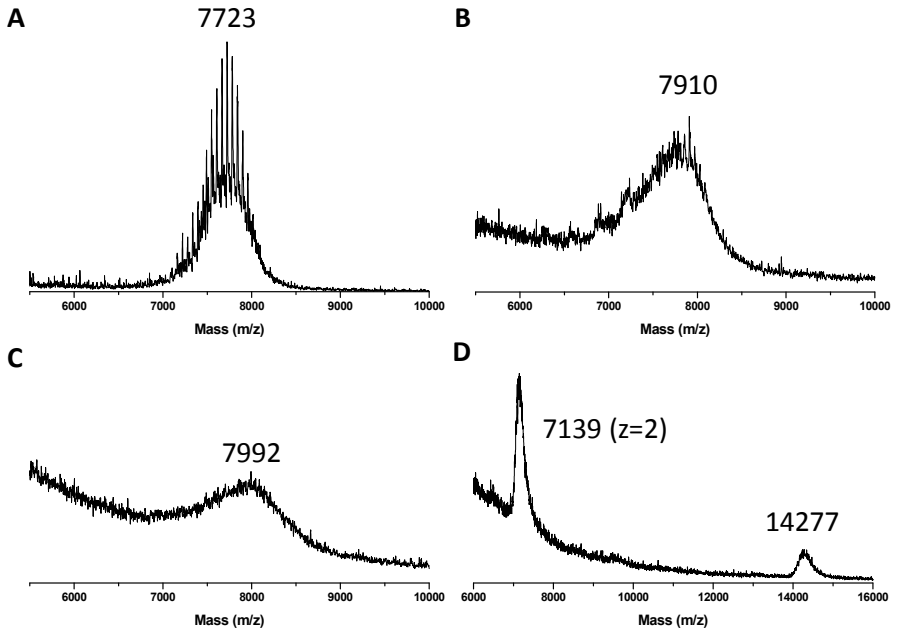

Figure 2.9. MALDI-TOF mass spectra of synthesized PPO DBCs with molecular weights indicated. (A) Spectrum of 22-PPO. (B) Spectrum of c22-PPO. (C) Spectrum of cr22-PPO. (D) Spectrum of 22-PPO-22.

2.4.4 Melting temperature determination

For T_m determination 500 µL of ds DBC sample was prepared in 1x hybridization buffer (25 mM Tris-HCl pH = 7.5, 50 mM NaCl, 12 mM $MgCl_2$) at a final concentration of 1 and 2 µM. Subsequently the samples were hybridized using a thermal gradient (90 °C, 30 min; -1 °C/2 min until RT). Afterwards DBC solutions were transferred to a quartz cuvette with a path length of 10 mm and the cuvette was closed. Melting curves were then collected on a Jasco V-630 spectrophotometer (JASCO Benelux BV) equipped with the thermal control module (Jasco ETCS-761). The denaturation curve was measured for both samples at 260 nm at a heating rate of 0.5 °C/min, measuring the absorption every 1 °C. For determination of the T_m the slope of the measured spectrum was calculated (See Fig. 10). The melting temperatures were determined in duplicate and did not vary more than 2 °C.

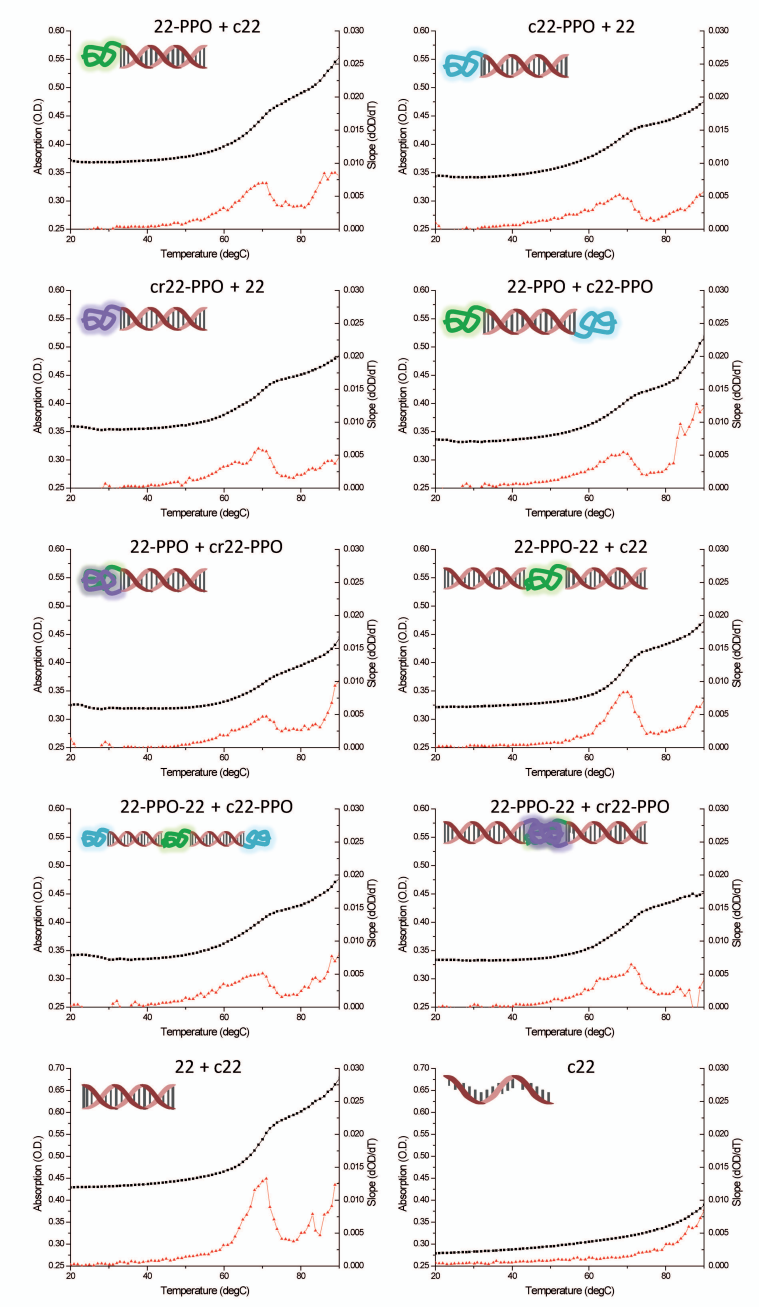

Figure 2.10. Melting curves of measured DBC architectures (squares, left Y-axis) and calculated slope for corresponding sample (triangle, right Y-axis)

2.5 Acknowledgement

For the help with the RPC HPLC analysis I would like to acknowledge the efforts of Agnieszka Gruszka.

2.6 References

[1] F. S. Bates, G. H. Fredrickson, *Phys. Today* **1999**, *52*, 32-38.
[2] S. Förster, M. Antonietti, *Adv. Mater.* **1998**, *10*, 195-217.
[3] F. S. Bates, G. H. Fredrickson, *Annu. Rev. Phys. Chem.* **1990**, *41*, 525-557.
[4] G. Pasut, F. M. Veronese, *J. Control. Release* **2012**, *161*, 461-472.
[5] P. Bailon, C. Y. Won, *Expert Opin. Drug. Del.* **2009**, *6*, 1-16.
[6] A. P. Chapman, P. Antoniw, M. Spitali, S. West, S. Stephens, D. J. King, *Nat. Biotechnol.* **1999**, *17*, 780-783.
[7] G. W. M. Vandermeulen, H. A. Klok, *Macromol. Biosci.* **2004**, *4*, 383-398.
[8] H. A. Klok, *Macromolecules* **2009**, *42*, 7990-8000.
[9] Z. Li, Y. Zhang, P. Fullhart, C. A. Mirkin, *Nano Lett.* **2004**, *4*, 1055-1058.
[10] F. E. Alemdaroglu, N. C. Alemdaroglu, P. Langguth, A. Herrmann, *Macromol. Rapid Comm.* **2008**, *29*, 326-329.
[11] T. Mori, M. Maeda, *Polym. J.* **2002**, *34*, 624-628.
[12] T. Zhou, P. Chen, L. Niu, J. Jin, D. Liang, Z. Li, Z. Yang, D. Liu, *Angew. Chem. Int. Ed.* **2012**, *51*, 11271-11274.
[13] T. R. Wilks, J. Bath, J. W. de Vries, J. E. Raymond, A. Herrmann, A. J. Turberfield, R. K. O'Reilly, *ACS Nano* **2013**, *7*, 8561-8572.
[14] M. Kwak, A. J. Musser, J. Lee, A. Herrmann, *Chem. Commun.* **2010**, *46*, 4935.
[15] T. G. Edwardson, K. M. Carneiro, C. K. McLaughlin, C. J. Serpell, H. F. Sleiman, *Nat. Chem.* **2013**, *5*, 868-875.
[16] F. E. Alemdaroglu, N. C. Alemdaroglu, P. Langguth, A. Herrmann, *Adv. Mater.* **2008**, *20*, 899-902.
[17] C. M. Niemeyer, *Bioconjugation protocols : strategies and methods*, 2nd ed., Humana Press, Totowa, N.J., **2011**.
[18] J. H. Jeong, T. G. Park, *Bioconjugate Chem.* **2001**, *12*, 917-923.
[19] J. H. Jeong, S. H. Kim, S. W. Kim, T. G. Park, *Bioconjugate Chem.* **2005**, *16*, 1034-1037.
[20] Y. G. Takei, T. Aoki, K. Sanui, N. Ogata, T. Okano, Y. Sakurai, *Bioconjugate Chem.* **1993**, *4*, 42-46.
[21] R. B. Fong, Z. L. Ding, C. J. Long, A. S. Hoffman, P. S. Stayton, *Bioconjugate Chem.* **1999**, *10*, 720-725.
[22] K. Lee, L. K. Povlich, J. Kim, *Adv. Funct. Mater.* **2007**, *17*, 2580-2587.

[23] M. Oishi, T. Hayama, Y. Akiyama, S. Takae, A. Harada, Y. Yarnasaki, F. Nagatsugi, S. Sasaki, Y. Nagasaki, K. Kataoka, *Biomacromolecules* **2005**, *6*, 2449-2454.

[24] M. Oishi, Y. Nagasaki, K. Itaka, N. Nishiyama, K. Kataoka, *J. Am. Chem. Soc.* **2005**, *127*, 1624-1625.

[25] K. Isoda, N. Kanayama, D. Miyamoto, T. Takarada, M. Maeda, *React. Funct. Polym.* **2011**, *71*, 367-371.

[26] P. M. E. Gramlich, C. T. Wirges, A. Manetto, T. Carell, *Angew. Chem. Int. Edit.* **2008**, *47*, 8350-8358.

[27] R. B. Merrifield, *J. Am. Chem. Soc.* **1963**, *85*, 2149-&.

[28] J. V. Bonilla, G. S. Srivatsa, *Handbook of Analysis of Oligonucleotides and Related Products*, **2011**.

[29] F. E. Alemdaroglu, M. Safak, J. Wang, R. Berger, A. Herrmann, *Chem. Commun.* **2007**, 1358-1359.

[30] M. Egholm, O. Buchardt, L. Christensen, C. Behrens, S. M. Freier, D. A. Driver, R. H. Berg, S. K. Kim, B. Norden, P. E. Nielsen, **1993**, *365*, 566-568.

[31] R. Jin, G. Wu, Z. Li, C. A. Mirkin, G. C. Schatz, *J. Am. Chem. Soc.* **2003**, *125*, 1643-1654.

[32] P. Yakovchuk, E. Protozanova, M. D. Frank-Kamenetskii, *Nucleic Acids Res.* **2006**, *34*, 564-574.

[33] C. Giovannangeli, T. Montenaygarestier, M. Rougee, M. Chassignol, N. T. Thuong, C. Helene, *J. Am. Chem. Soc.* **1991**, *113*, 7775-7777.

3. Ocular adhesion of lipid-DNA nanoparticles

3.1 Introduction

Currently, the vast majority of chronic and acute ophthalmic diseases that are not managed surgically are treated using eye drops - a non-invasive mode of treatment that can be self-administered without medical supervision. However, only a small percentage of the active compound present in eye drops reaches its target tissue as it is rapidly cleared from the eye by tear fluid and eye lid movement[1-2]. As a consequence, frequent administration of highly concentrated eye drops is necessary. Aside from the inefficiency of this dosage form, the requirement of frequent administration leads to poor compliance[3-5]. On the other hand, high concentrations of bioactive compounds produce side-effects that can range from simple irritations to, in extreme cases, a life threatening anaphylactic shock[6-7]. Thus, increasing the half-life of the drug on the eye is an important goal for more efficient treatment of eye diseases with fewer side effects.

To address these challenges nanotechnological approaches have been pursued in the field of ophthalmology[8-9]. Of special interest are polymeric nanoparticles that adhere to the cornea and increase the bioavailability of the released drug. Although satisfactory effectiveness has been demonstrated *in -vitro* and *in-vivo*, these delivery vehicles still face several shortcomings[10-

[12]. The nanoparticles are characterized by a broad size distribution, easily exceed sizes of 100 nm, and their composition needs to be greatly varied to accommodate drugs with different physicochemical properties.

Here we overcome these limitations with the help of a novel carrier system based on DNA nanotechnology. This field has progressed rapidly in the past decades and many strategies have been presented to fabricate nucleic acid nanoarchitectures with well-defined sizes, periodicities and shapes in one-, two- and three dimensions[13-16]. Therefore, it is not surprising that this type of nanostructures has attracted great interest from researchers working in the field of nanomedicine where well-defined multifunctional nanostructures are urgently needed. DNA nanoobjects can be exclusively self-assembled from nucleic acids by Watson-Crick base pairing and functionalization is achieved by hybridization with oligonucleotides. Examples are a DNA icosahedron functionalized with a target cell-recognizing aptamer or a 140 nm-long DNA tube both loaded with anticancer drugs[17-18]. On the other hand, DNA strands can be chemically attached to a nanoscopic inorganic template and easily equipped with targeting units and drug molecules by hybridization with complementary oligonucleotide conjugates[19-20]. A very similar type of nanoparticles for drug delivery was introduced by our group where the inorganic material is replaced by a soft matter core consisting of hydrophobic polymer units that is covalently attached to an oligonucleotide to form a DNA block copolymer[21].

So far, all DNA nanocarriers have been only applied for cancer therapy and proven functionality *in-vivo* is very rare[22]. In this chapter the successful selection of a lipid-modified DNA NPs suitable as ophthalmic drug delivery vehicle is presented. After synthesis and characterization of several different constructs, their *in-vitro* and *in-vivo* adherence properties to the corneal tissue are investigated. For the amphiphile showing the highest affinity the residence time on the eye is elucidated.

3.2 Results and discussion

3.2.1 Nanoparticle design and characteristics

To obtain the desired nanoparticles (NPs), we replaced the hydrophobic polymer unit of our earlier presented DNA block copolymer delivery system by several alkyl-modified 2'-deoxyuridine nucleotides (U) (See Fig. 3.1a). When introduced into an aqueous environment, these DNA amphiphiles self-assemble into micellar nanoparticles(NPs) through microphase separation and thus exhibit a corona of single stranded DNA surrounding a lipid core[23]. For the purpose of imaging we hybridized an oligonucleotide functionalized with a fluorophore (See Fig 3.1b). Previously it was shown that these micelles have a small hydrodynamic diameter of approximately 7 nm, depending on the number of hydrophobically-modified nucleotides and the aggregation number of similar lipid-DNA constructs was around 25[24].

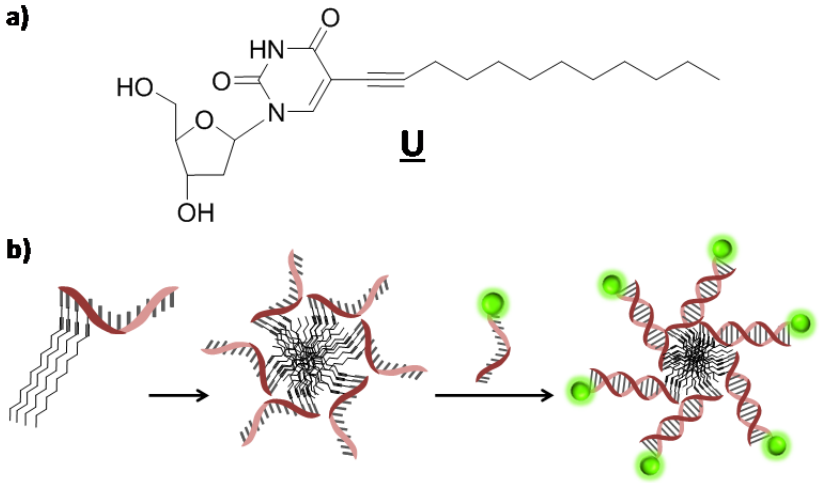

Figure 3.1. Structure of lipid modified nucleotide and functionalization strategy of DNA NPs. (a) Chemical structure of dodecyne-modified deoxyuracil, represented as U in the text. This nucleoside is incorporated into the oligonucleotide chain during DNA synthesis to impart hydrophobic properties. (b) In an aqueous environment, U-modified DNA strands self-assemble to form DNA nanoparticles due to their amphiphilic nature. The nanoparticles can then be functionalized through hybridization with a complementary DNA strand bearing a covalently attached fluorescent dye (green).

Micellar systems are highly dynamic; therefore, it was hypothesized that they can interact with the outermost hydrophobic layer of the cornea. To confirm this assumption and get more insights about the structural requirements for adhesion, several DNA lipid nanoparticles were exposed to corneal epithelium of porcine eyes. The particles were composed of different DNA amphiphiles: U2-12, U4-12, U4-18, U6-12, U6-20 (See Table 3.1). Here, the name of the lipid modified oligonucleotide is annotated as UX-Y, wherein X and Y represent the number of hydrophobic deoxyuridine units and the total number of nucleotides, respectively. For example, U2-12 contains 2 Us at the 5' terminus and in total is composed of 12 nucleotides. The NPs are characterized by CMC values which are ranging from 4 to 27 µM, confirming the micellar nature of the amphiphile aggregates (See Fig. 3.8).

Name	Sequence (5'→3')	Lipid modified bases (# (%))	CMC (µM)
U2T-12	UUTGGCGGATTC	2 (17)	27.4
U4T-12	UUUUGCGGATTC	4 (33)	5.2
U4T-18	UUUUGCGGATTCGTCTGC	4 (22)	4.6
U6T-12	UUUUUUGGATTC	6 (50)	24.3
U6T-20	UUUUUUGCGGATTCGTCTGC	6 (30)	4.2

Table 3.1. Sequences and characteristics of lipid modified oligonucleotides used to formulate NP-containing eye drops.

3.2.2 Determination of best NP binding *in-vitro* and *in-vivo*

To determine the adherence capabilities of the designed NPs to the cornea first *in-vitro* experiments on porcine eyes were performed. Therefore, the eye was incubated with the fluorescently labeled NPs at a concentration of 20 µM for 15 minutes followed by washing in PBS buffer. Cryo sections of the treated eyes were prepared and imaged using a fluorescence microscope (See Fig. 3.2). As control a double stranded (ds) DNA with the same sequence as one of the DNA amphiphiles, but lacking the lipid-modified nucleotide, was also exposed to the cornea in a similar fashion (NoU4-12).

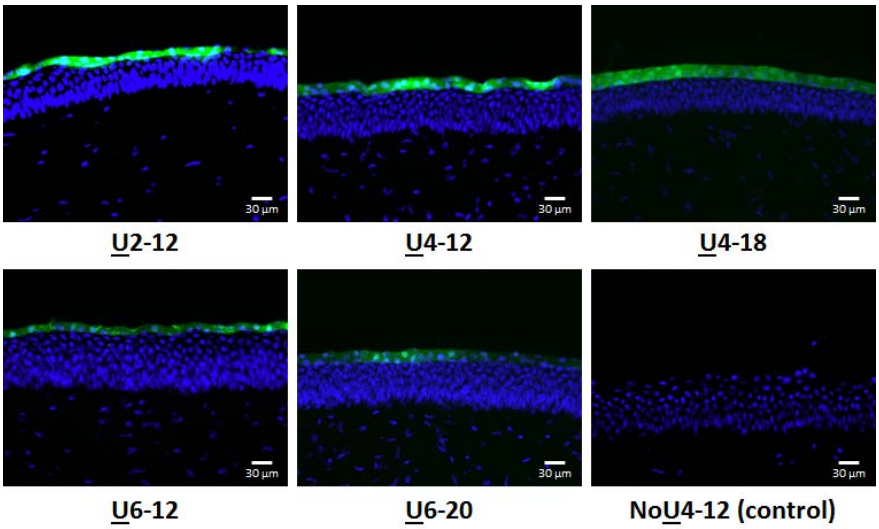

Figure 3.2. Representative fluorescent images of all NPs (green) screened for adherence to porcine cornea (blue).

In the figure above the cornea is visualized through nuclear staining using 4`,6-diamidino-2-phenylindol (DAPI) and therefore is visible in blue. In contrast, the NPs are labeled using a green fluorescent dye. As can be seen, for all the tested NPs good adherence to the porcine cornea is observed while the unmodified control sequence shows no affinity. Among the amphiphiles no clear difference in affinity was notable.

In the next step, the binding capabilities of the different NPs were investigated under realistic conditions by performing *in-vivo* experiments on living rats. The drops containing the DNA amphiphiles at a concentration of 20 µM were administered to conscious rats using a single drop of approximately 30 µL and 30 min, 2 or 24 h after application the animals were sacrificed. Similar as before, cryo sections of the treated eyes were prepared and imaged using fluorescence microscopy. As controls both the single stranded (ss) and ds fluorescently labeled unmodified DNA sequences were also administered. The best delivery system was determined as the NP carrier with the highest percentage of eyes exhibiting the DNA amphiphile and, in the case of similar results, by visual comparison of the cryosections (See Fig. 3.3 and Table 3.2).

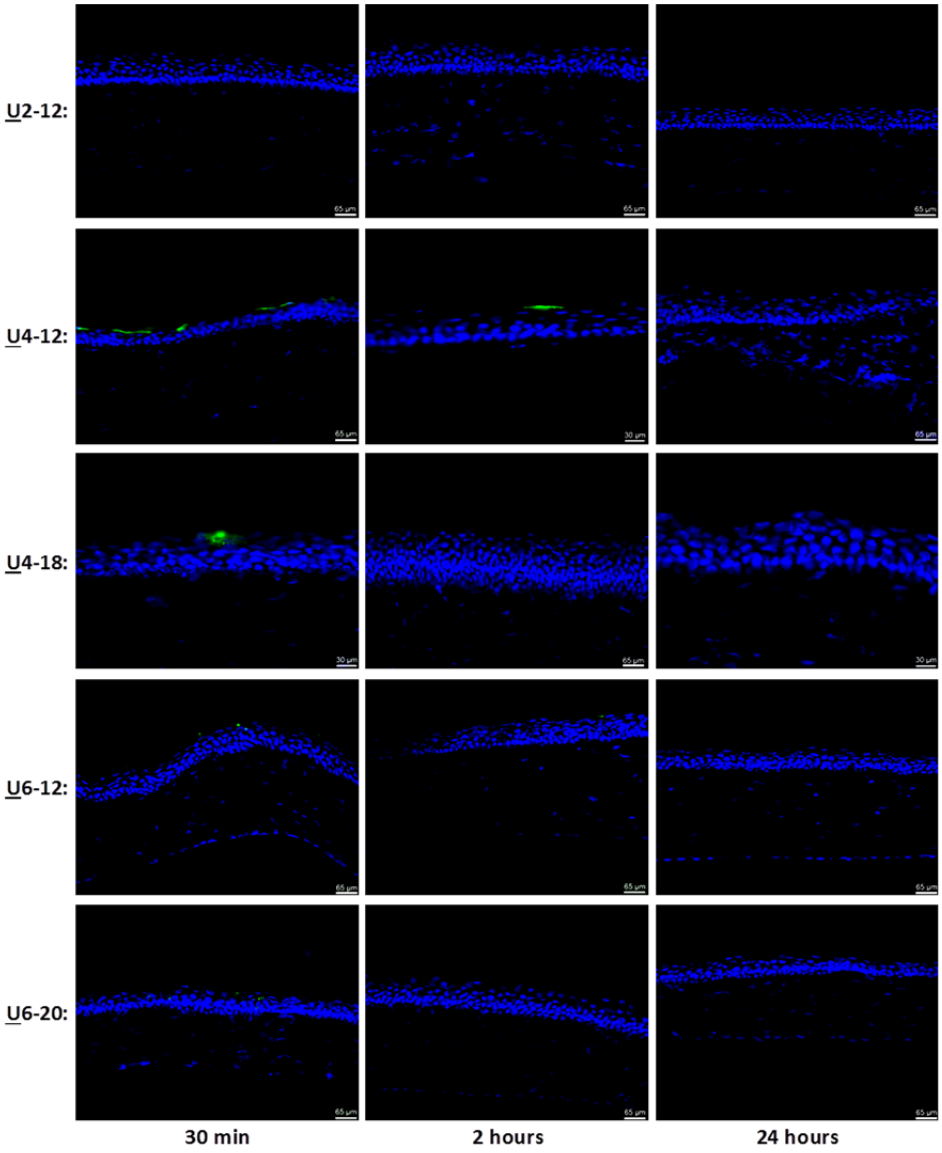

Figure 3.3. Representative fluorescent images of all NPs (green) screened for adherence to the rat cornea (blue).

Time	U2-12	U4-12	U4-18	U6-12	U6-20	cU4-12	NoU4-12
30 min	2/4	6/6	3/5	3/3	4/4	0/2	0/2
2 hours	0/4	4/6	0/4	0/4	2/4	0/2	0/2
24 hours	0/4	0/4	0/4	0/1	0/4	0/2	0/2

Table 3.2. Overview of number of rat eyes tested positive for the presence of NPs out of total number of eyes to which the NPs were administered at various time points.

Among the tested amphiphiles, U4-12 shows the best adherence to the corneal epithelium while both ss and ds 12mer control sequences (NoU4-12 and cU4-12) without any lipid modification do not show any affinity at all. From the results, we can deduce that the optimal ratio between standard and hydrophobic bases that promotes efficient adhesion is around 2:1. NPs composed of ds oligonucleotides with lower (U2-12) or higher (U6-12) ratios exhibit significantly lower affinity. When comparing amphiphiles with a similar percentages of U content (U4-12 and U6-20), strands with a smaller number of nucleotides show better adherence. Therefore, both the number of lipid modifications and the total length of the amphiphile are important parameters determining adhesion to the cornea.

3.2.3 Time dependent adherence of U4-12

Upon identifying U4-12 as the best carrier amphiphile, the adherence time on the cornea was evaluated. To this end, eye drops of the labeled NPs were administrated and the rats were sacrificed after 5, 15, 30 minutes, 1, 2, 4 or 6 hours (See Table 3.3 and Fig. 3.4). Also here, the unmodified ss and ds controls were included at the first time point. As can be observed, the NPs of U4-12 are already visible 5 min after application of the eye drops, thus showing a fast adherence to the cornea. Importantly, neither one of the controls were found at this time period, indicating no interaction of the pristine DNA with the tissue. In contrast, even after a period of four hours the NPs were still present as the distinct green fluorescence of the carrier was clearly visible. This adherence time is significantly longer than of any currently applied ocular medication, thus making these DNA NPs a promising vehicle for ocular drug delivery if equipped with a drug that can be released.

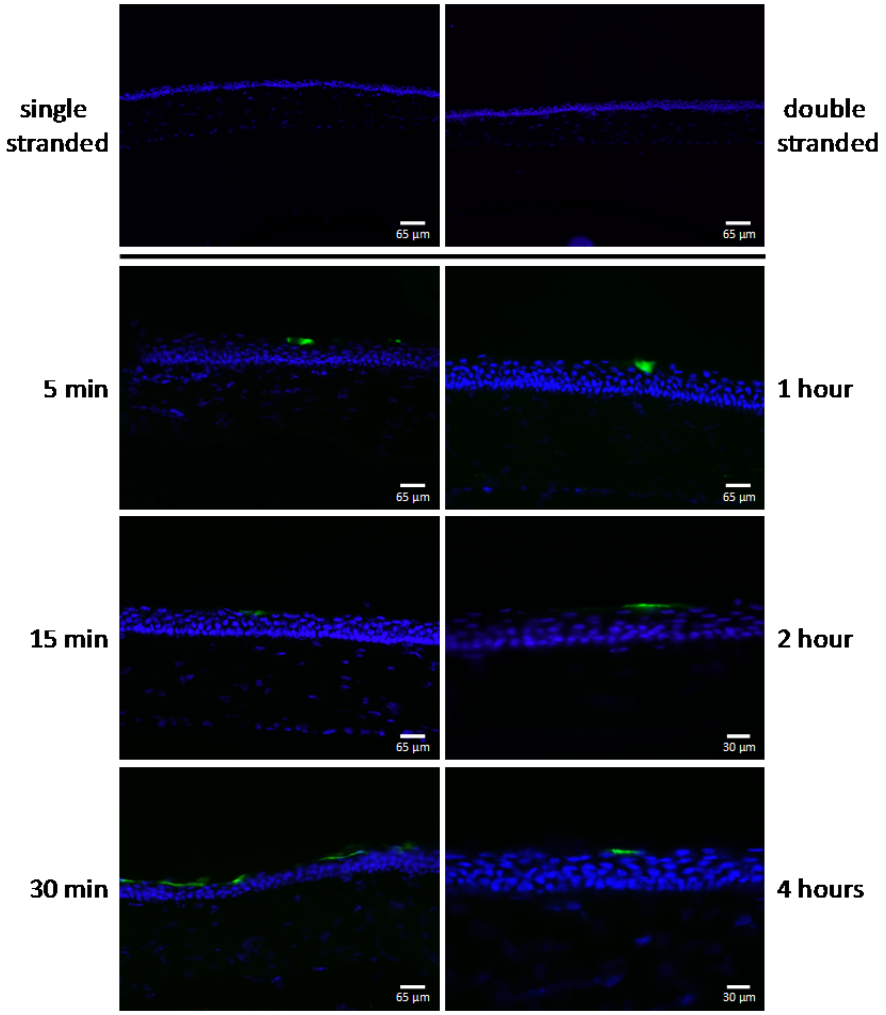

Figure 3.4. Evaluation of the time-dependent NP adhesion for the U4-12 system. Adhesion of U4-12 (green) to the rat cornea (blue) followed by fluorescence microscopy.

Time	U4-12 adherence
5 min	4/4
15 min	4/4
30 min	6/6
1 hour	4/4
2 hours	4/6
4 hours	3/4
6 hours	0/4

Table 3.4. Summary of number of NP positive eyes out of total number of eyes to which the NPs were administered at several time points.

3.3 Conclusion

DNA based nanoparticles have many advantages over NPs composed of other materials. Due to the unique self-recognition properties of DNA the formed architectures are uniform in size and functionality can easily be introduced at any desired place with complete control over the spatial orientation (inside the NP or at the surface of the NP).

Here, we demonstrated for the first time the successful application of DNA nanoparticles in the field of ophthalmology. These nanoparticles are composed of lipid-modified DNA strands which allows for facile modification by simple hybridization. For imaging purposes, fluorescent dye-modified oligonucleotides were attached to the DNA NPs by Watson-Crick base pairing. It was found that through alteration of the lipid content and the total length of the amphiphile the adherence properties of the NPs can be tailored. Furthermore, they exhibit a dramatically increased affinity to the cornea of living animals compared to pristine DNA. The best adhering system was found on the cornea even 4 hours after application of a single eye drop to conscious rats, which is significantly longer than medication in pristine eye drop-based dosage forms.

3.4 Experimental

3.4.1 Materials

All chemicals and reagents were purchased from commercial suppliers and were used without further purification, unless otherwise noted. The 1-dodecyne, copper(I)iodide, tetrakis(triphenylphosiphine)palladium(0) and diisopropylamine were purchased from Sigma-Aldrich and used as received. Other special chemicals acquired from different chemical sources were 5'-DMT-5-iodo deoxy uridine (Chemgenes). All lipid modified oligonucleotides (ODNs) were synthesized using standard automated solid-phase phosphoramidite coupling methods on an ÄKTA oligopilot plus (GE Healthcare) DNA synthesizer. All solvents and reagents for oligonucleotide synthesis were purchased from Novabiochem (Merck, UK) and SAFC (Sigma-Aldrich, Netherlands). Solid supports (Primer Support^{TM}, 200 µmol/g) from GE Healthcare were used for the synthesis of DNA. Oligonucleotides were purified by reverse-phase high performance liquid chromatography (HPLC) using a C15 RESOURCE RPC^{TM} 1 ml reverse phase column (GE Healthcare) through custom gradients using elution buffers (A: 100 mM triethylammonium acetate (TEAAc) and 2.5% acetonitrile, B: 100 mM TEAAc and 65% acetonitrile). Fractions were desalted using centrifugal dialysis membranes (MWCO 3000, Sartorius Stedim) or a HiTrap Desalting column (GE Healthcare). Afterwards the oligonucleotides were characterized by MALDI-TOF mass spectrometry using a 3-hydroxypicolinic acid matrix. Spectra were recorded on an ABI Voyager DE-PRO MALDI-TOF (delayed extraction reflector) Biospectrometry Workstation mass spectrometer. The concentrations of the DNA were measured on a SpectraMax M2 spectrophotometer (Molecular Devices, USA) using 1 cm light-path quartz cuvette. Fluorescently labeled oligonucleotides were purchased from Biomers.net at HPLC purification grade. H^1-NMR and P^{31}-NMR spectra were recorded on a Varian Mercury (400 MHz) NMR spectrometer at 25 °C. Column chromatography was performed using silica gel 60 Å (200-400 Mesh).

3.4.2 Synthesis and characterization of amphiphilic oligonucleotides

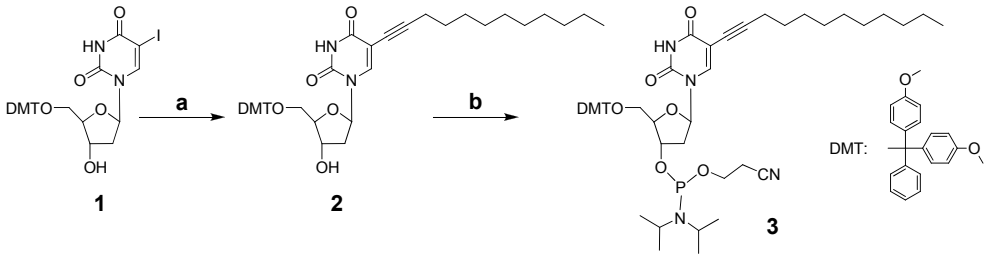

Figure 3.5. Synthesis scheme of 5-(dodec-1-ynyl) uracil phosphoramidite.

The modified 5-(dodec-1-ynyl)uracil phosphoramidite **3** was synthesized in two steps as previously reported in our group starting from **1** (See Fig. 3.5)[24]. The modified uracil phosphoramidite was dissolved in CH_3CN to adjust the concentration to 0.15 M, in the presence of 3 Å molecular sieves. The prepared solution was directly connected to the DNA synthesizer. All oligonucleotides were synthesized on a 10 μmol scale on an ÄKTA oligopilot plus (GE Healthcare) DNA synthesizer using standard β-cyanoethylphosphoramidite coupling chemistry. Deprotection and cleavage from the PS support was carried out by incubation in concentrated aqueous ammonium hydroxide solution for 5 h at 55 °C. Following deprotection, the oligonucleotides were purified by using reverse-phase chromatography, using a C15 RESOURCE RPC^{TM} 1 ml reverse phase column (GE Healthcare) through custom gradient elution (A: 100 mM triethylammonium acetate (TEAAc) and 2.5% acetonitrile, B: 100 mM TEAAc and 65% acetonitrile). Fractions were desalted using centrifugal dialysis membranes (MWCO 3000, Sartorius Stedim). Oligonucleotide concentrations were determined by UV absorbance using extinction coefficients. Finally, the identity and purity of the oligonucleotides were confirmed by MALDI-TOF mass spectrometry and analytical anion exchange chromatography using a linear gradient elution, respectively (See Fig. 3.6 and Fig. 3.7).

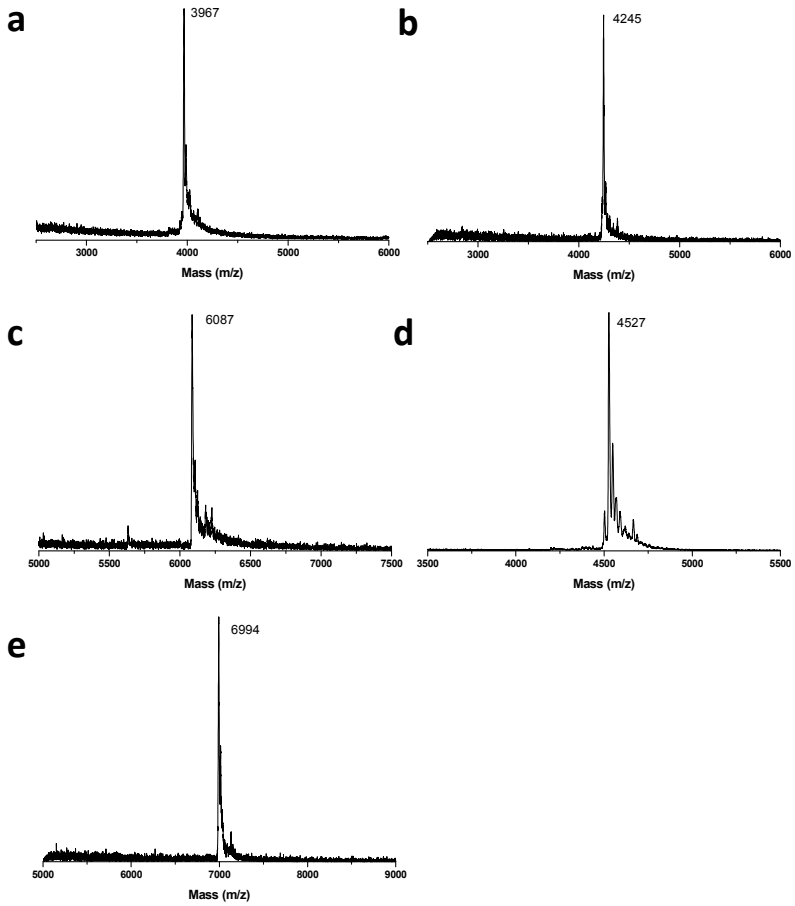

Figure 3.6. Characterization of amphiphilic oligonucleotides by MALDI-TOF mass spectrometry. (a) Spectrum of U2-12 (calc. 3968 g/mol, found 3967 g/mol), (b) U4-12 (calc. 4243 g/mol, found 4245 g/mol), (c) U4-18 (calc. 6089 g/mol, found 6087 g/mol), (d) U6-12 (calc. 4534 g/mol, found 4527 g/mol), (e) U6-20 (calc. 6998 g/mol, found 6994 g/mol).

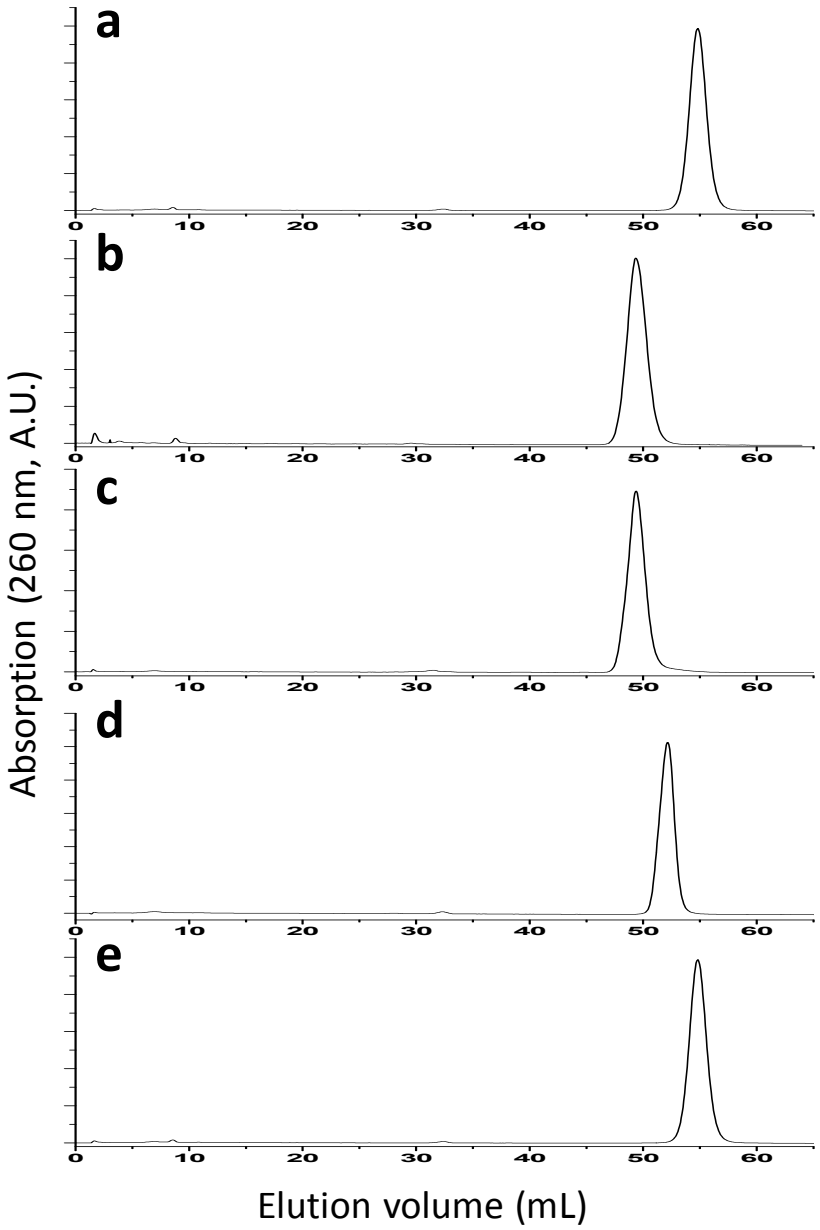

Figure 3.7. Characterization of the amphiphilic oligonucleotides by analytical anion exchange chromatography. A linear gradient to 100 %B in 62.5 ml was used. Chromatograms show (a) U2-12, (b) U4-12, (c) U4-18, (d) U6-12 and (e) U6-20.

3.4.3 Preparation of functionalized NPs

Micelles were prepared in low bind tubes (Eppendorf) in 1x TAE buffer (40 mM Tris-Acetate, 1 mM EDTA, 20 mM NaCl, 12 mM MgCl2, pH 8.0) at a concentration of 20 μM. The lipid modified oligonucleotide of interest was prepared at the desired concentration and one equivalent of the complementary DNA was added and hybridized using a thermal gradient (90 °C, 30 min; -1 °C/2 min until room temperature (RT)). When nanoparticles were used for fluorescent imaging a 5' Atto488 functionalized complementary DNA was used.

3.4.5 Critical micelle concentration determination

For CMC determination, firstly 10 pmol of 1,6-diphenyl-1,3,5-hexatriene (DPH) was loaded in Eppendorf DNA low-bind tubes using a 1 μM solution in acetone. The solvent was allowed to evaporate at room temperature (RT) for 5 h after which 100 μl of DNA amphiphile solution was added. The oligonucleotides were prepared at concentrations ranging from 0.0025 to 1 g/L in 1x TAE buffer (10 mM Tris-Acetate, 0.2 mM EDTA, 20 mM NaCl, 12 mM MgCl2, pH 8.0) and thermally cycled (90 °C, 30 min; -1 °C/2 min until RT) before use. After addition to the DPH containing tubes, the solutions were incubated overnight at 37 °C. Subsequently, fluorescence spectra (375 – 500 nm) were recorded on a Varian Cary Eclipse fluorimeter (Varian Nederland B.V.) at RT using an excitation wavelength of 350 nm (See Fig. 3.8).

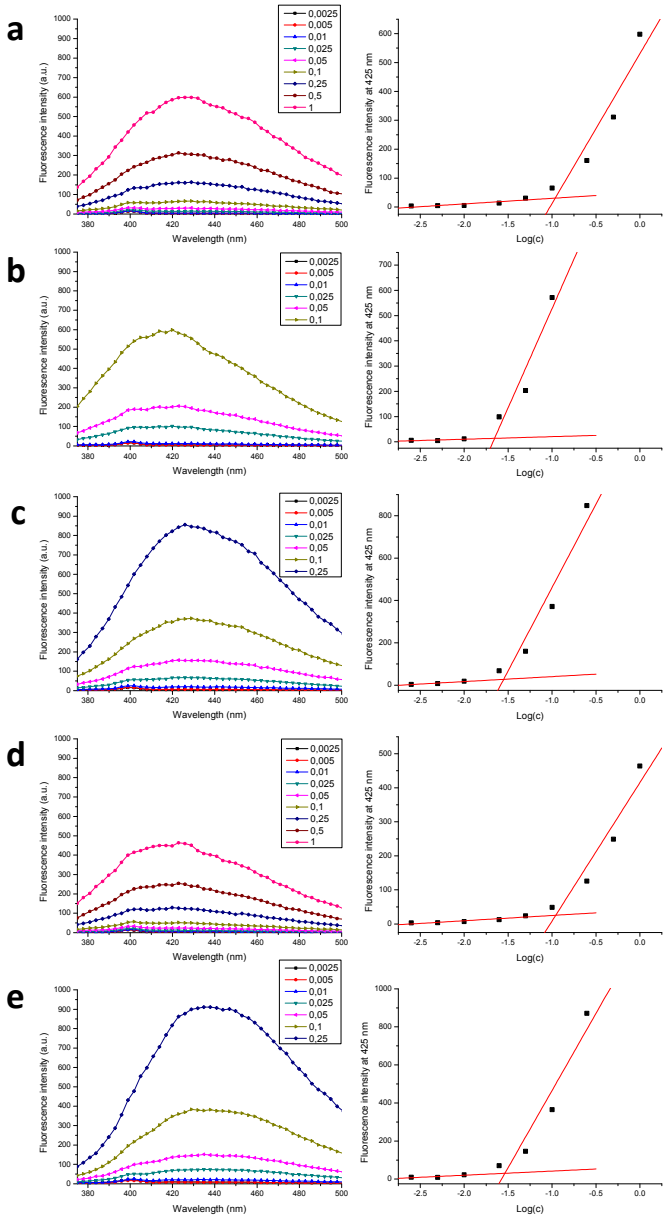

Figure 3.8. Determination of critical micelle concentrations of the amphiphilic oligonucleotides. Fluorescence spectra of micelle-incorporated 1,6-diphenyl-1,3,5-hexatriene (DPH) at different concentrations (g/L)(Left) and intensity at 425 nm (maximum) plotted against the logarithm of the concentration (right) for (a) U2-12, (b) U4-12, (c) U4-18, (d) U6-12 and (e) U6-20.

3.4.4 Determination of adherence to porcine eye

Pig eyes were obtained from a local slaughterhouse and kept humidified at 4°C until further use. Before applying the NPs the eyes were washed and allowed to adjust to room temperature. For NP application, the eyes were placed on 6-well plates with the cornea facing up and 2 rubber rings (a smaller one in the center of the cornea and a larger one around the cornea) were used to prevent spillage of the solution. To every eye 50 µl of NP solution (20 µM) was applied and the eyes were incubated for the designated time (15 minutes). Afterwards the rings were removed and the eyes were washed in excess PBS buffer. Then the eyes were frozen in Tissue-Tek O.C.T. (Sakura Finetek) in liquid nitrogen. Frozen sections were longitudinally cut (12 µm) on a cryostat (Leica CM 1900), thaw-mounted onto glass slides (Superfrost plus, R. Langenbrinck Labor- & Medizintechnik) and stored at -30 °C until further use. For visualisation sections were fixed with methanol and to stain nuclei the sections were further incubated in a solution containing 0.2 µg/ml DAPI for 1 min. Stained sections were embedded in FluorSave (Calbiochem) and imaged using a fluorescent microscope (Axioplan2, Zeiss with Openlab software, Improvision)[25].

3.4.5 Selection of best adhering NP and evaluation of adherence time on the cornea

Adult Lister Hooded Rats were obtained from Harlan Winkelmann (Germany). Nanoparticles, prepared as described above, were administered to conscious rats at a concentration of 20 µM using a single drop of approximately 30 µl. For the eye drop applications the conscious rats were very shortly fixated and a drop was administered to the eye using a single drop device as in medical applications. Blinking of the eyes was not hindered during drop application or afterwards. After the designated incubation time, the rat was sacrificed with carbon dioxide inhalation. After sacrificing the animal, the eyes were enucleated and frozen in Tissue-Tek O.C.T. (Sakura Finetek, Germany) using liquid nitrogen. The samples were stored at -30 °C until further use and processed as described in section 3.4.4. Animals were treated according to the Principles of laboratory animal care

(NIH publication No. 85-23, revised 1985), the OPRR Public Health Service Policy on the Human Care and Use of Laboratory Animals (revised 1986) and the German animal protection law (Research permission AK3/11 to Sven Schnichels).

3.5 References

[1] A. C. Amrite, H. F. Edelhauser, U. B. Kompella, *Invest. Ophthalmol. Vis. Sci.* **2008**, *49*, 320-332.

[2] W. Zhang, M. R. Prausnitz, A. Edwards, *J. Control. Release* **2004**, *99*, 241-258.

[3] M. M. Hermann, A. M. Bron, C. P. Creuzot-Garcher, M. Diestelhorst, *J. Glaucoma* **2011**, *20*, 502-508.

[4] D. L. Budenz, *Ophthalmology* **2009**, *116*, S43-47.

[5] J. C. Tsai, *Curr. Opin. Ophthalmol.* **2006**, *17*, 190-195.

[6] C. Baudouin, A. Labbe, H. Liang, A. Pauly, F. Brignole-Baudouin, *Prog. Retin. Eye Res.* **2010**, *29*, 312-334.

[7] M. Lai Becker, N. Huntington, A. D. Woolf, *Pediatrics* **2009**, *123*, e305-311.

[8] S. Y. Liu, L. Jones, F. X. Gu, *Macromol. Biosci.* **2012**, *12*, 608-620.

[9] J. G. Souza, K. Dias, T. A. Pereira, D. S. Bernardi, R. F. Lopez, *J. Pharm. Pharmacol.* **2014**, *66*, 507-530.

[10] R. C. Nagarwal, P. N. Singh, S. Kant, P. Maiti, J. K. Pandit, *Chem. Pharm. Bull.* **2011**, *59*, 272-278.

[11] R. S. Bhatta, H. Chandasana, Y. S. Chhonker, C. Rathi, D. Kumar, K. Mitra, P. K. Shukla, *Int. J. Pharm.* **2012**, *432*, 105-112.

[12] E. Vega, F. Gamisans, M. L. Garcia, A. Chauvet, F. Lacoulonche, M. A. Egea, *J. Pharm. Sci.* **2008**, *97*, 5306-5317.

[13] J. Chen, N. C. Seeman, *Nature* **1991**, *350*, 631-633.

[14] P. W. K. Rothemund, *Nature* **2006**, *440*, 297-302.

[15] E. S. Andersen, M. Dong, M. M. Nielsen, K. Jahn, R. Subramani, W. Mamdouh, M. M. Golas, B. Sander, H. Stark, C. L. P. Oliveira, J. S. Pedersen, V. Birkedal, F. Besenbacher, K. V. Gothelf, J. Kjems, *Nature* **2009**, *459*, 73-75.

[16] J. C. Mitchell, J. R. Harris, J. Malo, J. Bath, A. J. Turberfield, *J. Am. Chem. Soc.* **2004**, *126*, 16342-16343.

[17] M. Chang, C. S. Yang, D. M. Huang, *ACS Nano* **2011**, *5*, 6156-6163.

[18] Y. X. Zhao, A. Shaw, X. H. Zeng, E. Benson, A. M. Nystrom, B. Hogberg, *ACS Nano* **2012**, *6*, 8684-8691.

[19] S. Dhar, W. L. Daniel, D. A. Giljohann, C. A. Mirkin, S. J. Lippard, *J. Am. Chem. Soc.* **2009**, *131*, 14652-14653.

[20] K. Zhang, L. L. Hao, S. J. Hurst, C. A. Mirkin, *J. Am. Chem. Soc.* **2012**, *134*, 16488-16491.

[21] F. E. Alemdaroglu, N. C. Alemdaroglu, P. Langguth, A. Herrmann, *Adv. Mater.* **2008**, *20*, 899-902.

[22] Z. Y. Xiao, C. W. Ji, J. J. Shi, E. M. Pridgen, J. Frieder, J. Wu, O. C. Farokhzad, *Angew. Chem. Int. Edit.* **2012**, *51*, 11853-11857.

[23] D.-M. Anaya, M. Kwak, A. J. Musser, K. Müllen, A. Herrmann, *Chem. Eur. J.* **2010**, *16*, 12852-12859.

[24] M. Kwak, I. J. Minten, D.-M. Anaya, A. J. Musser, M. Brasch, R. J. M. Nolte, K. Muellen, J. J. L. M. Cornelissen, A. Herrmann, *J. Am. Chem. Soc.* **2010**, *132*, 7834-7835.

[25] M. Schultheiss, K. Januschowski, H. Ruschenburg, C. Schramm, S. Schnichels, P. Szurman, K. U. Bartz-Schmidt, M. S. Spitzer, *Graefes Arch. Clin. Exp.* **2013**, 1613-1619.

4. Preclinical evaluation of DNA nanoparticles for ophthalmic drug delivery

4.1 Introduction

Treatment of eye diseases is accompanied with many problems. Therefore, improvement in efficacy of eye drops has been an important goal for many years. By increasing the duration time of the medication a lower regime can be attained, resulting in an improved compliance. In addition, it allows for a lower drug concentration, what results in fewer side effects and therefore gives the possibility to use medication that is currently harmful to apply.

In the past, the effectiveness of eye drops has been slightly increased by changing the viscosity and composition of the drops. Examples are formulations containing hyaluronic acid[1-2] or a carbomer solution composed of several lipids[3]. However, this resulted in very little improvement and causes reduced vision when the medicine is applied, which in turn leads to a lack of compliance. As such improvement of eye drops has been pursued through the use of different nanoparticles (NPs)[4-5]. Among several different systems, liposomes and micelles are the most popular ones due to the ease of fabrication and commercial availability of the building blocks. Micellar NPs are typically comprised of diblock copolymers that are biocompatible and

biodegradable. Commonly used polymers include poly(lactic acid)(PLA)[6], poly(lactic-*co*-glycolic acid) (PLGA)[7-8], poly(ethylene oxide)(PEO)[9] and poly(*N*-isopropylacrylamide) (polyNIPAAm)[10]. The other frequently used nanocarriers, liposomes, are composed of lipids that have a hydrophobic tail and hydrophilic headgroup. These species self-assemble into spherical structures exhibiting an aqueous inner environment enveloped by a lipid bilayer membrane. Especially nanosystems with a positive charge at the surface have proven to increase the bioavailability of several drugs due to their interaction with the corneal mucin layer that is negatively charged[11-13].

Although the above mentioned delivery systems have great advantages over pristine formulations, they also have several limitations. These particles are not uniform in size or composition and surface functionalization often is cumbersome. In this respect DNA based nanoparticles have several advantages. Due to the complete control over the number and spatial orientation of the functional groups these particles can very easily be tailored [14-15]. Despite these benefits, NPs composed of nucleic acids have not been used in the field of ophthalmology. Therefore, we investigated the use of DNA nanoparticles containing lipid-modified nucleotides for ocular drug delivery.

As with other nanoparticulate systems loading of medication can be performed through hydrophobic interactions or by covalent attachment to the carrier (See Fig 4.1). The former strategy, however, is limited to hydrophobic drugs, which excludes a large number of compounds such as most antibiotics. The latter method requires chemical modification of the drug which might impair with binding of the drug to the target and requires cleavage from the carrier. Therefore, we proposed a more elegant strategy that allows for specific loading without the need of alteration of the target molecule. This can be achieved through the use of aptamers[16] that are elongated with the complementary sequence and simply hybridized to the single stranded corona of the DNA NPs. This method enables the loading of virtually any molecule of interest as aptamers can reliably be developed

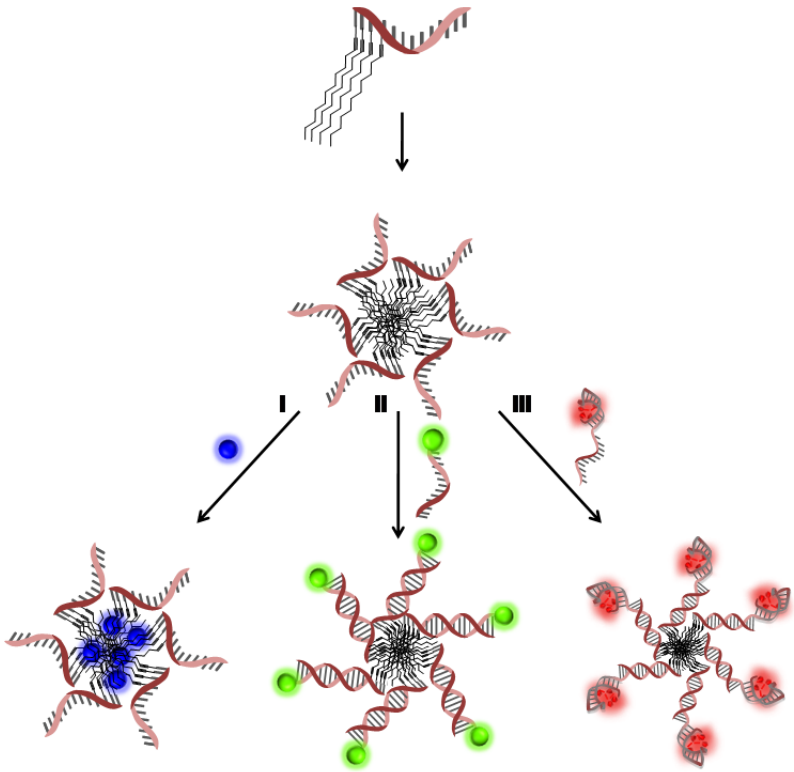

Figure 4.1. Schematic drawin of possible loading stratigies for DNA based NPs using hydrophobic interactions (I), covalent attachment to the complementary strand (II) or employing an extended aptamer seequence (III).

using systematic evolution of ligands by exponential enrichment (SELEX)[17-19]. In short, this process involves the exposure of a library of oligonucleotides to the immobilized target. After a washing step the binding sequences are eluted and amplified by the use of PCR. The amplified binders are then again exposed to the target and the procedure is repeated. Through multiple selection cycles and with more stringent washing conditions throughout the repetitions the strongest binding sequences are selected.

In this chapter, the translation from adherent NPs to true drug delivery vehicles is presented. To this end, the best adhering NP system developed in chapter 3 was loaded with two well-known antibiotics, i.e., neomycin B and kanamycin B. These are currently used in the clinic for treatment of ocular inflammation. To incorporate drug molecules, a DNA aptamer binding

kanamycin B[20] and a RNA aptamer binding neomycin B[21] were extended at the 3' end with the complementary sequence of the U4-12 DNA amphiphile. Watson-Crick base pairing of aminoglycoside-complexed aptamers and DNA nanoparticles resulted in two antibiotic-loaded nanocarrier systems (See Fig. 4.1, III), proving the general drug loading strategy. With one of the first *in-vivo* delivery examples of DNA nanotechnology we show that the long residence time of the nanoparticles can be translated into improved efficiency compared to the pristine drug, even demonstrating applicability with human tissue.

4.2 Results and discussion

4.2.1 Delivery of antibiotic-loaded NPs to the cornea

After completion of proof-of-concept experiments we investigated aptamer-functionalized U4-12 carriers loaded with neomycin B and kanamycin B. These two antibiotics are widely used for treatment of ocular infections and can be anchored to a DNA NP via well characterized high affinity aptamers[20-21]. To compare the time-dependent clearance of the antibiotic and the drug-loaded carrier they were administered *in-vivo* to rats. As control, the same antibiotics were labeled with a green fluorescent dye (fluorescein) at one of the amine groups. For imaging of the NPs the aptamer was functionalized with a red fluorescent dye (Cy3) at the 5' end. Eye drops of approximately 30 µl and containing equal amounts of either NP-bound antibiotic or free antibiotic were administered to live rats at a concentration of 20 µM and the adherence to the cornea was studied 5, 15, 30 minutes, 1, 2 and 4 hours after application (See Fig. 4.2).

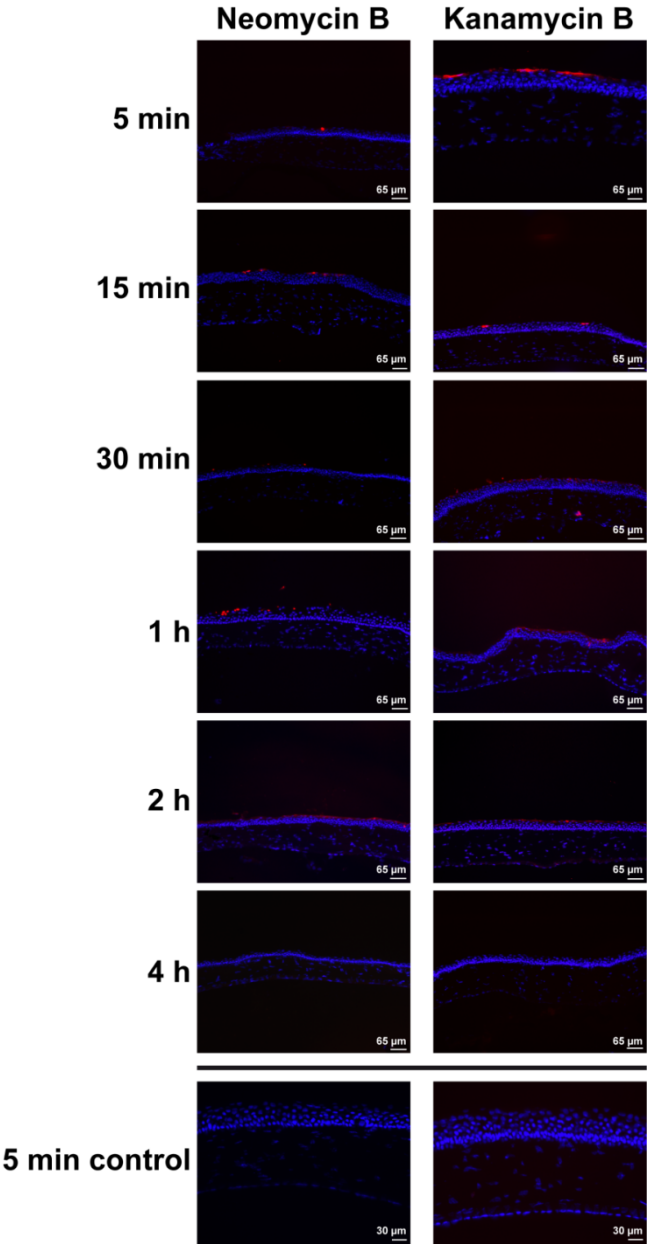

Figure 4.2. Fluorescence images demonstrating adhesion of neomycin B- (left) and kanamycin B-loaded (right) NPs (red) to the rat cornea (blue). In the images in the bottom row, a fluorescently labelled form of the free antibiotic was used as a control (green). The time point after administration of the antibiotic-loaded NP or free antibiotic is indicated on the left.

Both neomycin B- and kanamycin B-loaded NPs are effectively attached to the cornea for a period of at least 2 hours, whereas the fluorescent antibiotics are not detectable after only 5 min. These experiments indicate that adhesion to the cornea is greatly enhanced by the carrier system, which allows the loading of different cargoes and their close contact to the corneal surface. It is important to mention in this context that the chemical structure of the drugs was not modified due to the non-covalent nature of NP loading. Since RNA and DNA aptamers are known to bind a large variety of molecular structures[16-17] these vehicles represent a general delivery platform for diseases of the anterior section of the eye that can be loaded with drugs in a modular fashion.

4.2.2 Adherence of antibiotic loaded NPs to the human cornea

To demonstrate the translatability of this nanocarrier system from the rat model to humans, we examined the adherence of antibiotic-loaded particles to human corneal tissue. The experiments were performed on discarded tissue from corneal transplantations. Eye drops containing nanoparticles loaded with fluorescently labeled aptamers were administered to the corneal epithelium, the tissue was incubated for five minutes and afterwards the cornea was washed. Similar to previous experiments, fluorescently labeled antibiotics were used as control. Washing times after incubation were varied between five minutes and two hours (See Fig. 4.4). Both neomycin B- and kanamycin B-loaded NPs showed a remarkable attachment to the human cornea, while the free drugs were displaced at the first time point. A slow decrease in intensity was observed for increasing washing times for particles containing neomycin B. This can be due to detachment of the NPs from the corneal surface or because of degradation of the aptamer. In contrast, for kanamycin B this effect was not notable.

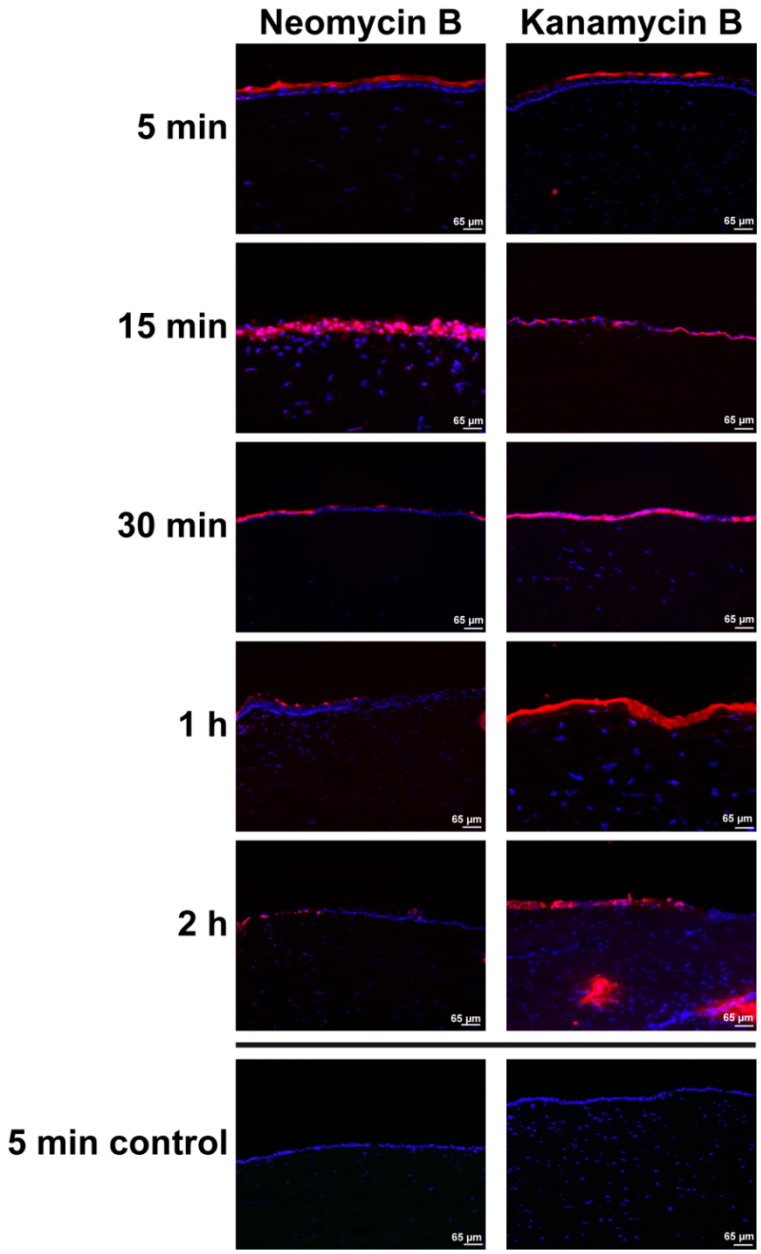

Figure 4.3. Adhesion of neomycin B- (left) and kanamycin B- (right) loaded NPs (red) to human cornea(blue), as monitored by fluorescence microscopy. After administration of the NP, the tissue was washed for the times indicated on the left. In the images in the far right column, a fluorescently labelled form of the free antibiotic was used as a control (green).

4.2.3 Antimicrobial activity of loaded NPs in medium

Next, we investigated whether an improved adherence half-life of the NPs translates into better activity and efficacy compared to the pristine drug. To do so, we first demonstrated that the antibiotic can be liberated from the NP by subjecting antibiotic-loaded NPs to a minimum inhibitory concentration test (MIC-test) using Escherichia coli (E. coli)(See Fig. 4.4). For this purpose, the action of antibiotic loaded NPs was compared to the free drugs. To mimic nuclease containing body fluids on the ocular surface, RNAse and DNAse were added to the cell suspension containing neomycin B- and kanamycin B-loaded NPs, respectively. The growth progress was determined by measuring the optical density of the cell suspension at 600 nm after 5 hours incubation at 37 °C

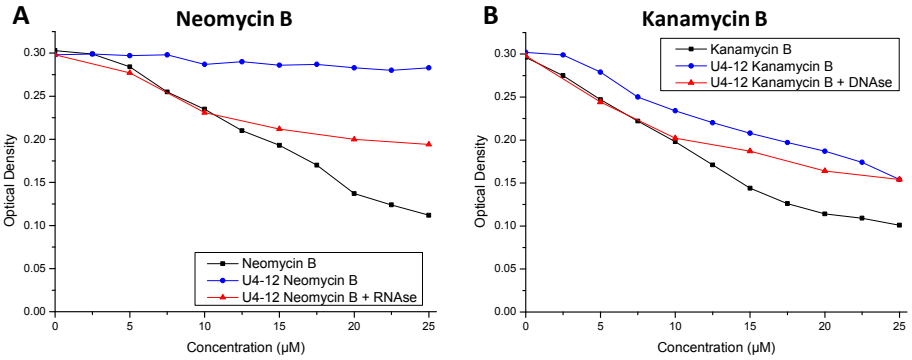

Figure 4.4. E. coli growth dependence on antibiotic concentration after 5 hours of incubation at 37°C with (A) neomycin B and (B) kanamycin B, for the free compound (black), the antibiotic loaded in the NP (blue) and the antibiotic loaded in the NP in the presence of DNA/RNAse (red).

The MIC tests clearly demonstrate that under *in-vivo*-like conditions, both nanocarrier-loaded antibiotics are active. As expected, for the free aminoglycosides a clear decrease in cell growth was observed with increasing antibiotic concentration. Neomycin B-loaded NPs, however, require the presence of RNAse to release the drug and induce bactericidal effects while the presence of DNAse has little impact on the effectiveness of

kanamycin B-loaded NPs. In the context of *in-vivo* applications, neither the RNAse-dependent release of the neomycin B nor the DNAse-independent release of the kanamycin B presents an obstacle because nucleases are prevalent in biological fluids[22].

4.2.4 Activity and Efficacy of antibiotic-loaded NPs

Having demonstrated that the NPs exhibit excellent adhesive properties on the cornea and that the antibiotic activity is retained in an *in-vivo*-like environment, in a next step we determined whether a clear antibiotic effect can be observed at the site of action. To this end, growth studies of E. coli were performed on porcine corneas where the efficacy of antibiotic-loaded NPs was compared to that of the free drugs. Growth inhibition was first evaluated without washing by incubating the cornea from porcine eyes with antibiotic-loaded NPs for 5 minutes. At the end of the incubation period, excess solution was removed and the corneas were placed on petrifilms containing growth medium. A total of on average 50 E.coli bacteria were applied to the cornea and were allowed to grow for 48 hours, after which the number of bacterial colonies was determined (See Fig. 4.5).

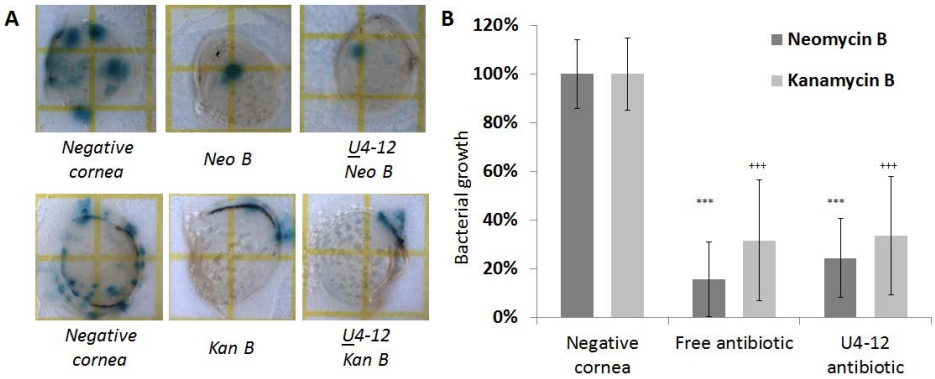

Figure 4.5. Bacterial growth experiments on porcine corneas treated with buffer (Negative cornea), free antibiotic and antibiotic-loaded NPs (U4-12) without washing. (A) Representative photographs of E. coli growth on unwashed porcine corneas. (B) Growth experiment without washing (n = 4-5). Control (Negative cornea) is set to 100% growth. Statistical differences are shown as * for neomycin B and +++ for kanamycin B, with p<0.001 compared to negative cornea. Comparison between the loaded U4-12 NPs and the free antibiotics did not show significant differences.**

The growth experiments clearly show the antibacterial activity after incubation of the cornea with free antibiotics. The antibiotics bound to the NPs show a similar growth inhibition, suggesting that the aptamers are degraded by nucleases or that the drugs are otherwise fully released from the NPs within the timeframe of the experiment.

After confirming the antibiotic activity on the cornea further growth experiments were performed where tearing was simulated by washing the porcine corneas with an excess of buffer to evaluate the efficacy of the kanamycin B-loaded NPs that are bound tightly to the cornea. Therefore, the same setup was utilized, but after incubation with the NPs the porcine cornea was washed with a large excess of PBS for 5, 30 and 60 minutes (See Fig. 4.6). The results of the E.coli growth experiment on corneas washed for 5, 30 and 60 minutes after exposure to kanamycin B-loaded NPs illustrate one of the shortcomings of current ophthalmic medication. No significant growth inhibition is found for the free antibiotic after 5 minutes of washing, indicating that the drug molecule is washed away within this short period of time. This is in good agreement with results from experiments where fluorescently labeled free antibiotics were not detected by fluorescence microscopy 5 minutes after application to the rat cornea *in-vivo* and the human cornea *in-vitro*. In contrast, the porcine corneas treated with the NPs containing kanamycin B exhibited bactericidal activity after up to 30 minutes of washing. Again, this is in good agreement with the extended NP adhesion time observed on the rat cornea. These experiments establish that the long adherence time of the NPs can be translated into a higher efficiency of the antibiotic treatment when employing the nanocarrier compared to the free drug.

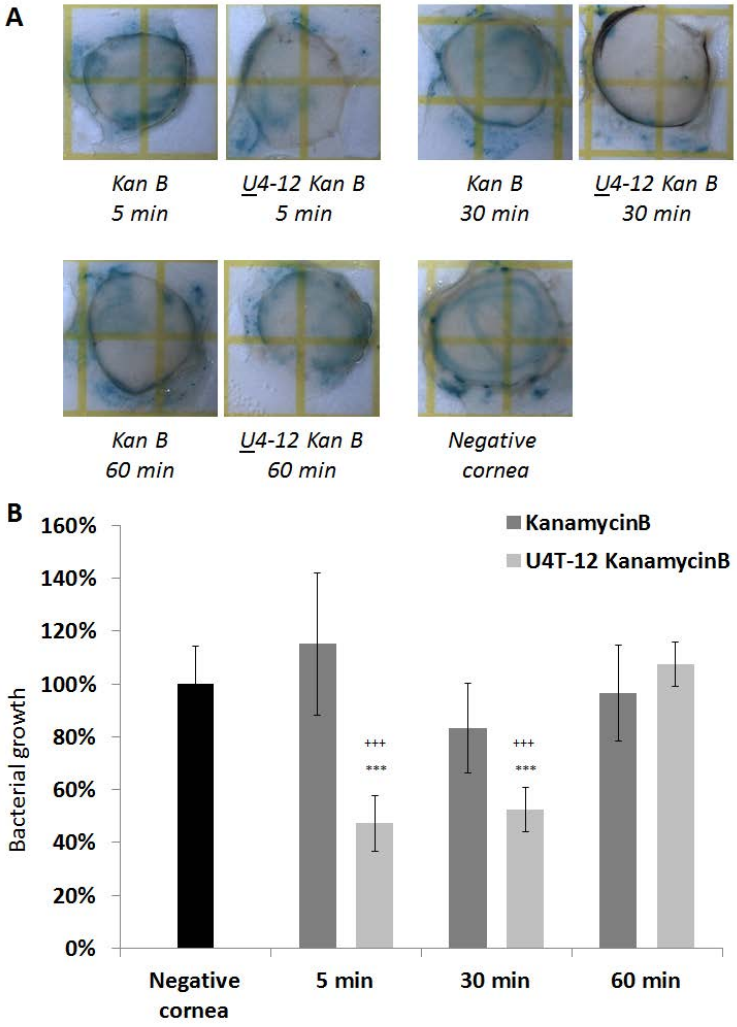

Figure 4.6. Bacterial growth experiments on porcine corneas treated with buffer (Negative cornea), free kanamycin B and kanamycin B-loaded NPs (U4-12) with washing. (A) Representative photographs of E. coli growth with varying washing times. (B) Growth experiment with varying washing times (n = 3-4). Control (Negative cornea) is set to 100% growth. Statistical differences are shown as * with p<0.001 compared to negative cornea. Comparison between kanamycin B and kanamycin B-loaded U4-12 NPs are shown as +++ with p<0.001. Unmarked time-points were not significantly different. Differences between the time-points were not evaluated.**

4.3 Conclusion

Treatment of eye diseases by eye drops is complicated by several means and improving efficacy of eye drops has been an important goal for many years[23]. By increasing the exposure time of the target tissue to the active compound in the drops, less frequent administration of less concentrated drops would be required. As a consequence, improved compliance is to be expected alongside lower levels of side effects, providing the opportunity to administer medication that is toxic at the concentrations currently required[24].

Here, we have shown a novel, powerful and general approach for treating eye infections using DNA nanotechnology that can be easily extended to treat other ocular indications. A paramount feature is the use of aptamers for drug loading, which enables specific binding of virtually any drug to the carrier without chemical modification or alteration of the pharmaceutical function. Because aptamers can be evolved against molecules with very diverse structures, this approach represents a truly modular drug delivery platform. We have demonstrated functionalization of the DNA carrier with therapeutically active agents, imaging units or a combination of the two by simple mixing of components and hybridization to generate multifunctional nanoobjects. The NPs have proven to dramatically increase the adherence time of antibiotics on the cornea in living animals and human tissue. Furthermore, antibiotic-loaded NPs have shown to be more effective than free antibiotics in preventing bacterial growth on porcine corneal tissue under conditions simulating tear fluid production, with an increased residence time at least 10-fold higher than the pristine drug. These findings open a variety of possibilities for utilization of DNA-based materials in ophthalmic drug delivery.

4.4 Experimental

4.4.1 Preparation of functionalized NPs

Antibiotic-loaded NPs were prepared at the needed concentration (20 µM) in 1x TAE buffer (40 mM Tris-Acetate, 1 mM EDTA, 20 mM NaCl, 12 mM MgCl2, pH 8.0). For loading of neomycin B and kanamycin B a RNA and DNA aptamer was used, respectively, both were elongated with the complementary sequence of the carrier (See Table 4.1). The lipid modified oligonucleotide U4-12 and the complementary DNA-aptamer (1 eq.) were loaded in a tube at the desired concentration and hybridized using a thermal gradient (80 °C, 30 min; 1°C/2 min until RT). When nanoparticles were used for fluorescent imaging a 5' Cy3 functionalized aptamer was used. Subsequently, for neomycin B two equivalents of antibiotic were added and for kanamycin B one equivalent (10 mM stock solution in ultrapure water). The solution was incubated at RT for a minimum of 30 minutes and used without further dilution.

Name	Sequence (5' → 3')
cU4-neo	GGACUGGGCGAGAAGUUUAGUCCGCGAAUCCGCAAAA
cU4-kan	TGGGGGTTGAGGCTAAGCCGATTGAATCCGCAAAA

Table 4.1. Sequence of extended aptamers used for antibiotic loading of NPs.

4.4.2 Adherence of antibiotic-loaded NPs to living rat eyes

The adherence of antibiotic-loaded NPs was determined as described in Chapter 3, section 3.4.5. In short, a single eye drop of approximately 30 µl of the NP containing solution was administered to the fixated rat. Blinking of the eyes was not hindered during drop application or afterwards. After the designated incubation time the rat was sacrificed with carbon dioxide inhalation. After sacrificing the animal, the eyes were enucleated and frozen in Tissue-Tek O.C.T. (Sakura Finetek, Germany) using liquid nitrogen. Frozen sections were longitudinally cut (12 µm) on a cryostat (Leica CM 1900, Germany), thaw-mounted onto glass slides (Superfrost plus, R. Langenbrinck Labor- und Medizintechnik, Germany) and stored at -30 °C until further use. For visualization, sections were fixed with methanol and to

stain nuclei sections were further incubated in a solution containing 0,2µg/ml 4`,6-diamidino-2-phenylindol (DAPI) for 1 min. Stained sections were embedded in FluorSave (Calbiochem, Germany) and imaged using a fluorescent microscope (Axioplan2 imaging®, Zeiss, Germany with Openlab software, Improvision, Germany)[25]. Animals were treated according to the principles of laboratory animal care (NIH publication No. 85-23, revised 1985), the OPRR Public Health Service Policy on the Human Care and Use of Laboratory Animals (revised 1986) and the German animal protection law (research permission AK3/11 to Sven Schnichels)

4.4.3 Human cornea experiments

Five human cornea rims were kindly provided by the eye bank of the University Eye Hospital Tübingen after approval of the planned experiments. These rims are leftover tissue after a corneal transplantation. Informed consent was obtained from all human subjects. After the transplantation the cornea rims were returned to the cornea media (KM1, Biochrom, Deutschland) until further use. Before applying the nanoparticles the corneas were cut into 3-4 equal sized pieces, transferred to a 24-well plate and washed with PBS (PAA, Germany). Afterwards, 100 µl of the nanoparticles were applied on top of the cornea and incubated at room temperature for the designated time. Then the corneas were transferred to another well containing 2 ml of PBS and washed for the designated time at room temperature. Next the corneas were frozen in Tissue Tek, cut on a cryostat, stained with DAPI and photographed as described previously.

4.4.4 Minimum inhibitory concentration tests

For inhibitory test Escherichia coli (E. coli), kindly donated by Sukirthini Balendran, Molecular Genetics Laboratory, Centre for Ophthalmology, Institute for Ophthalmic Research, Tübingen was grown in 1x LB medium (0.5% yeast extract, 1% tryptone, 1% NaCl) at 37 °C. Obtained solution was diluted to 0.3 OD_{600} units using 1x LB medium and loaded in a 96 well plate (200 µL/well). The antibiotic or antibiotic-loaded NPs were added and the

OD600 was monitored every 5 minutes while incubating at 37 °C. When nanoparticles were used, they were prepared as described above at 800 µM. For studies including DNAse or RNAse 2 µL of 10 mg/mL RNAse or DNAse was added to each well.

4.4.5 Evaluation of antibiotic activity on porcine cornea

Corneas were taken from porcine eyes obtained from the local slaughterhouse and placed in a petridish. Kanamycin B- or neomycin B-loaded NPs were prepared at a concentration of 100 µM as described above. A rubber ring was placed around the cornea to prevent spillage and 100 µl of NP or free antibiotic solution was placed on top of the cornea. After 5 minutes incubation time, excess liquid was removed or the cornea was washed in a large excess of PBS (typical volume 10 ml) for the designated time. Subsequently, the corneas were placed on petrifilms (3M) prepared as recommended by the manufacturer. E. coli were grown at 37 °C overnight after which the amount of bacteria per ml LB medium was determined. Subsequently the suspension was diluted to obtain a final concentration of 10^4 E. coli/ml LB medium. On top of the corneas, on average 50 E. coli bacteria in 5 µl 1x LB medium were placed. For experiments with neomycinB 0.5 mg/ml RNAse was added to the medium. The petrifilms were incubated at 37 °C for 48 h after which pictures were taken. The number of colonies was determined in duplo by three persons with the pictures being blinded. Data are represented as mean +/- SD. Statistical analysis was performed using JMP® (version 10.0.0, SAS Institute Inc.). ANOVA analysis with Tukey-Kramer post-hoc test was used for statistical evaluation of the individual time-points and the negative cornea samples. Differences were considered to be significant at $p<0.05$.

4.4.6 Fluorescent labeling of aminoglycoside antibiotics

5-Carboxyfluorescein (5-FAM, 22.6 mg, 60 µmol) was dissolved in 250 µL of anhydrous DMF and activated by adding 1.2 eq of N-hydroxysuccinimide (NHS; 8.3 mg, 72 µmol) and dicyclohexylocarbodiimide (DCC; 14.96 mg,

72 µmol). The reaction mixture was gently shaken at room temperature for 3 h. The precipitate that was formed (dicyclohexylurea) was removed by centrifugation (5 min, 15k rpm) and crude supernatant containing 5-carboxyfluorescein succinimidyl ester was used without further purification. To ensure monomodification of the aminoglycosides, 1 eq (62.5 µL) of NHS-activated 5-FAM was subsequently added to 15 µmol of antibiotic in free base form (9.21 mg neomycin B; 7.24 mg kanamycin B) dissolved in 200µL of a water:dioxane mixture (2:1). After a reaction time of 2 h, 5-FAM-modified neomycin B (5-FAM-neomycin B) and kanamycin B (5-FAM-kanamycin B) were purified on Shimadzu VP series HPLC system with PDA detector using Zorbax SB-C18 3.5 µm column 75 x 4.6 mm (Agilent®). A linear gradient from 0 to 75% buffer B in 20 min was applied (A: 0.5% trifluoroacetic acid (TFA) and 5% CH_3CN in ultra-pure water, B: 100% CH_3CN). Purification was monitored at a wavelength of 440 nm. The purity and identity of the products was confirmed using RPC HPLC and ESI-MS (See Fig. 4.7 and Fig. 4.8). 5-FAM-neomycin B was obtained as TFA salt with 41% yield; ESI-MS (pos.) *m/z* 973.366 $[M+H]^+$ calc. 973.367 $[M+H]^+$. 5-FAM-kanamycin B was obtained as TFA salt with 35% yield; ESI-MS(pos.) *m/z* 842.308 $[M+H]^+$ calc. 842.309 $[M+H]^+$

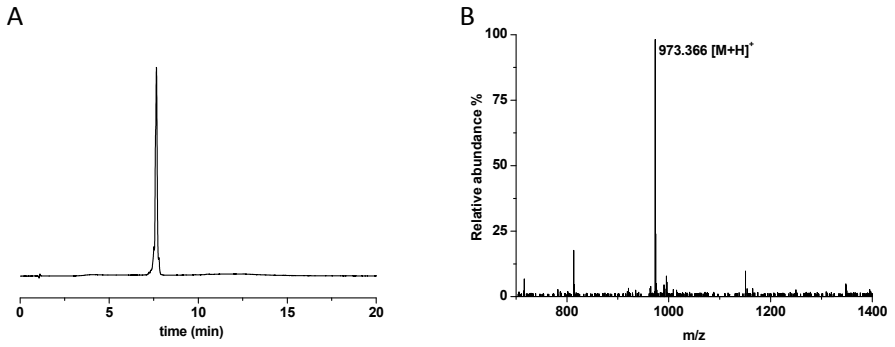

Figure 4.7. Characterization of 5-FAM-neomycin B conjugate. (A) HPLC chromatogram of purified product, (B) ESI-MS spectrum of purified product (calc. 973.367 [M+H]+, found m/z 973.366 [M+H]+).

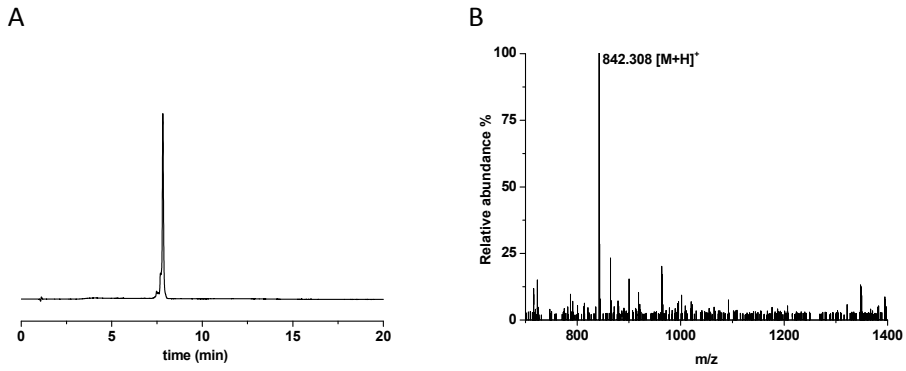

Figure 4.8. Characterization of 5-FAM-kanamycin B conjugate. (A) HPLC chromatogram of purified product, (B) ESI-MS spectrum of purified product (calc. 842.309 [M+H]+, found m/z 842.308 [M+H]+).

4.4.7 Nanoparticle (NP) imaging by transmission electron microscopy (TEM)

The amphiphiles were prepared at a concentration of 20 µM in 1x TAE buffer and thermally cycled (85°C, 30 min; -1°C/2 min until RT). Subsequently, 5 µl of NP solution was deposited on a glow-discharged carbon coated copper grid. Excess NP solution was blotted on a filter paper and the grid was washed once with ultrapure water and stained twice with a 2% uranyl acetate solution. Images were recorded using a CM12 transmission electron microscope (Phillips) at 120 kV. For size determination the diameter of 60 NPs was measured using ImageJ software (See Fig. 4.9).

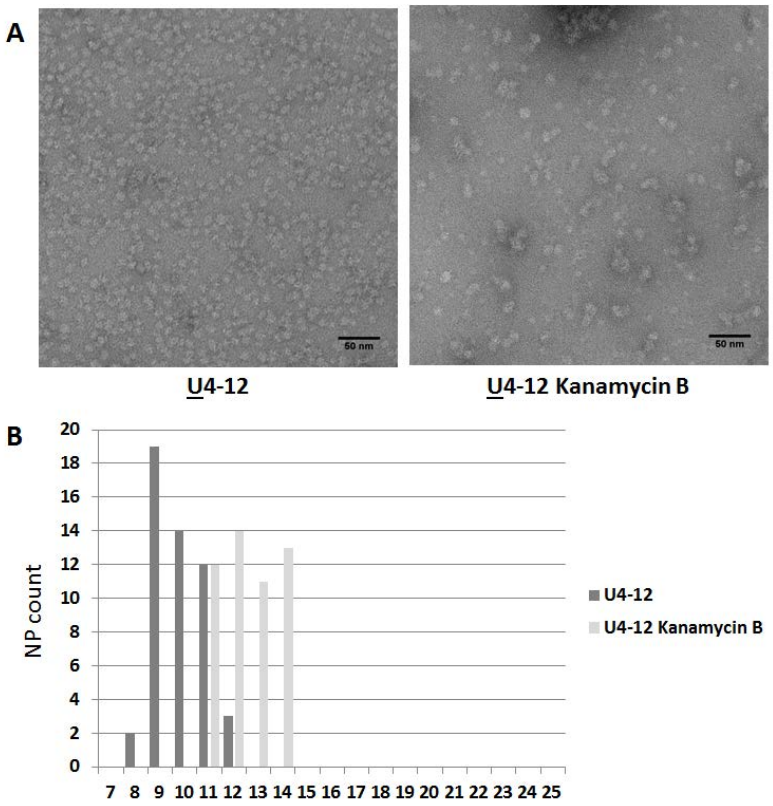

Figure 4.9. Transmission electron microscopy (TEM) images and size determination of bare and aptamer functionalized U4-12 micelles. (A) TEM images of bare U4-12 nanoparticles (left) and kanamycin B aptamer functionalized U4-12 carriers (right) and (B) size histogram of both NPs. Calculated average diameters are 10.0 ± 1.3 nm and 12.5 ± 1.4 nm for pristine and aptamer-functionalized NPs, respectively.

4.5 Acknowledgement

For the help with the TEM analysis of the pristine and aptamer functionalized NPs I would like to acknowledge the efforts of Agnieszka Gruszka. For the help with the statistical analysis of the bacterial growth on the cornea I would like to thank Sven Schnichels, Jose Hurst and Lisa Strudel.

4.6 References

[1] S. Shimmura, M. Ono, K. Shinozaki, I. Toda, E. Takamura, Y. Mashima, K. Tsubota, *Brit. J. Ophthalmol.* **1995**, *79*, 1007-1011.

[2] M. E. Johnson, P. J. Murphy, M. Boulton, *Graefes Arch. Clin. Exp.* **2006**, *244*, 109-112.

[3] M. E. Johnson, P. J. Murphy, M. Boulton, *Optometry Vision. Sci.* **2008**, *85*, 750-757.

[4] H. Y. Zhou, J. L. Hao, S. Wang, Y. Zheng, W. S. Zhang, *Int. J. Ophthalmol.* **2013**, *6*, 390-396.

[5] S. Y. Liu, L. Jones, F. X. Gu, *Macromol. Biosci.* **2012**, *12*, 608-620.

[6] C. Di Tommaso, A. Torriglia, P. Furrer, F. Behar-Cohen, R. Gurny, M. Moller, *Int. J. Pharm.* **2011**, *416*, 515-524.

[7] S. P. Ayalasomayajula, U. B. Kompella, *Eur. J. Pharmacol.* **2005**, *511*, 191-198.

[8] J. L. Cleland, E. T. Duenas, A. Park, A. Daugherty, J. Kahn, J. Kowalski, A. Cuthbertson, *J. Control. Release* **2001**, *72*, 13-24.

[9] I. Pepic, N. Jalsenjak, I. Jalsenjak, *Int. J. Pharm.* **2004**, *272*, 57-64.

[10] A. K. Gupta, S. Madan, D. K. Majumdar, A. Maitra, *Int. J. Pharm.* **2000**, *209*, 1-14.

[11] S. L. Law, K. J. Huang, C. H. Chiang, *J. Control. Release* **2000**, *63*, 135-140.

[12] N. Li, C. Y. Zhuang, M. Wang, X. Y. Sun, S. F. Nie, W. S. Pan, *Int. J. Pharm.* **2009**, *379*, 131-138.

[13] I. P. Kaur, D. Aggarwal, H. Singh, S. Kakkar, *Graefes Arch. Clin. Exp.* **2010**, *248*, 1467-1472.

[14] F. A. Aldaye, A. L. Palmer, H. F. Sleiman, *Science* **2008**, *321*, 1795-1799.

[15] J. W. de Vries, F. Zhang, A. Herrmann, *J. Control. Release* **2013**, *172*, 467-483.

[16] L. Gold, B. Polisky, O. Uhlenbeck, M. Yarus, *Annu. Rev. Biochem.* **1995**, *64*, 763-797.

[17] R. Stoltenburg, C. Reinemann, B. Strehlitz, *Biomol. Eng.* **2007**, *24*, 381-403.

[18] A. D. Ellington, J. W. Szostak, *Nature* **1990**, *346*, 818-822.

[19] C. Tuerk, L. Gold, *Science* **1990**, *249*, 505-510.

[20] K.-M. Song, M. Cho, H. Jo, K. Min, S. H. Jeon, T. Kim, M. S. Han, J. K. Ku, C. Ban, *Anal. Biochem.* **2011**, *415*, 175-181.

[21] L. Jiang, A. Majumdar, W. Hu, T. J. Jaishree, W. Xu, D. J. Patel, *Structure* **1999**, *7*, 817-827.

[22] T. N. Yusifov, A. R. Abduragimov, K. Narsinh, O. K. Gasymov, B. J. Glasgow, *Mol. Vis.* **2008**, *14*, 180-188.

[23] J. G. Souza, K. Dias, T. A. Pereira, D. S. Bernardi, R. F. Lopez, *J. Pharm. Pharmacol.* **2014**, *66*, 507-530.

[24] F. Lallemand, O. Felt-Baeyens, K. Besseghir, F. Behar-Cohen, R. Gurny, *Eur. J. Pharm. Biopharm.* **2003**, *56*, 307-318.

[25] M. Schultheiss, K. Januschowski, H. Ruschenburg, C. Schramm, S. Schnichels, P. Szurman, K. U. Bartz-Schmidt, M. S. Spitzer, *Graefes Arch. Clin. Exp.* **2013**, 1613-1619.

5. Stability and toxicity of lipid DNA nanoparticles

5.1 Introduction

In recent years researchers have explored the use of nanomaterials in the fields of biomedicine due to the numerous potential advantages they exhibit over administration of the free drug or larger sized alternatives. In multiple cases, the use of these carriers has shown to result in improved efficacy with better pharmacokinetics and toxicity profiles. A major advantage of these nanometer sized constructs is that they allow for incorporation of multiple functionalities in the same nanoparticle (NP), thereby opening the possibility to employ targeting molecules, drug loading and imaging units in a single system[1-3]. Due to intense efforts, currently there are several NP based formulations on the market or in clinical trials[4-6]. For NP application in humans, several challenges need to be solved, including body clearance, toxicity and stability of the carrier.

The majority of all NPs is removed from the body through the reticuloendothelial system (RES) or through renal excretion. Here, various factors play an important role, like size and surface charge[7-9]. Nanoobjects that are smaller than 5 nm generally exhibit a short half-life as they are

rapidly cleared by the kidneys[10]. Particles with larger diameters generally have longer circulation times and show increased absorption of RES proteins with increasing size, resulting in even further increased half-life times[11]. Additionally, surface charge of the NPs also plays an essential role in clearance. In this respect, charged NPs (either positive or negative) are more rapidly cleared than neutral ones, mainly due to lower protein adhesion on the latter species[12-13]. To overcome short half-life times nanoobjects are commonly coated with biocompatible polymers such as poly(ethylene glycol)(PEG). Decoration of the NP with such moieties dates back to the early 1970s and decreases protein adsorption on the NPs due to steric hindrance[14-17]. Unfortunately, PEGylation also has disadvantageous as it can impair with the targeting and delivery abilities of the NPs due to shielding of any functional groups. This might inhibit cellular uptake and therefore drastically reduces the efficiency of the system[18-19]. Additionally, it has been reported that repeated intravenous injection of carriers comprising a PEG shell caused stronger immune responses compared to the unfunctionalized particles, which actually leads to an increased clearance rate[20].

Although many NPs have found to be non-toxic in preclinical and clinical trials, it is still a very common show-stopper for development of novel carrier systems[5-6, 21]. Similar to the circulation time of these objects, induced toxic effects are strongly dependent on the structures from which the carriers are made, i.e. their size, concentration and the exposed surface. In addition, the route of administration plays an important role. Here, a clear distinction between systemic and local toxicity has to be made. Naturally, the use of nanoparticles intravenously will result in a different toxicity profile compared to utilization of the same carrier on the outside of the body, e.g. as eye drop or skin cream. Hence, the needed safety testing is strongly dependent on the final application. Unfortunately, as the field is still developing rapidly there are no standardized methods to test toxicity of nanometer sized objects and a large discrepancy is found between *in-vitro* and *in-vivo* toxicity data[22]. For example, citrate coated gold nanoparticles showed no toxic effects in several cell lines, but under *in-vivo* conditions caused severe side effects such as weight loss or even death of the animals[23-25]. In stark contrast, gold nanorods and NPs exhibiting a PEG

shell proved to have limited toxicity while greatly improving treatment[26-27]. As is apparent from the examples above and other literature, the obtained data can hardly be compared among different carriers and mostly concerns a specific NP in a specific setting. Moreover, due to the many different parameters involved, small changes in the carrier can induce drastic alterations in the toxicity profile of the system. Thus, application tailored toxicity testing of such particles is needed before conducting further clinical trials.

Another crucial aspect determining the success of NPs in medicine is the *in-vivo* stability of the nanoformulation. In this respect several factors need to be considered. One of these is aggregation of the carrier that can occur before complete clearance of the NPs, which can result in e.g. clogged blood vessels. To stabilize the particles of interest, several FDA approved polymers like PEG or poly(vinyl alcohol) (PVA) can be used to prevent aggregation through steric hindrance[28-29]. Aside from colloidal stability, degradation of the building blocks can also have severe impact on the performance of the system and cause significant side effects. In this respect, some block copolymer based NPs have shown to cause the release of toxic by-products upon degradation[30]. As such, investigating the stability and possible degradation of the NPs and its building materials is another crucial factor for the success of the delivery platform.

In this chapter, preliminary toxicity evaluation of the NPs used in chapter 4 will be presented. In a first assessment, possible toxic effects of the pristine carrier on different ocular cell lines will be evaluated. Afterwards, the induction of apoptosis *in-vivo* will be considered for pristine and antibiotic loaded NPs. Additionally, the stability of the carriers over prolonged periods of time will be analyzed with denaturating polyacrylamide gel electrophoresis (PAGE) and reversed phase high performance liquid chromatography (RPC HPLC).

5.2 Results and discussion

5.2.1 Evaluation of toxicity profile in cell cultures

When using the DNA NPs presented in earlier chapters as ophthalmic formulation, the systemic exposure is limited by the digestive system. Therefore, obtaining knowledge about local toxicity is of greater importance due to the direct exposure to the eye. Hence, possible cytotoxic properties of the U4-12 NPs were first investigated using three different ocular cell lines. Three critical parameters - cell number, cell viability and apoptosis induction - were taken into account by performing MTS viability assay, crystal violet staining and determining the caspase 3/7 activity, respectively (See Fig. 5.1). The selected cell lines, 661W, RGC-5 and ARPE-19, originate from rodent and human eyes. Cells were incubated with DNA NPs at an amphiphile concentration of 20 µM for 24 h.

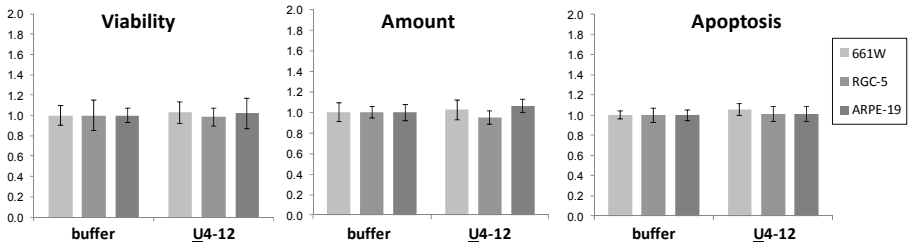

Figure 5.1 Toxicity studies on U4-12 and the vehicle buffer for 661W, RGC-5 and ARPE-19 cells. Cultures were screened for cell viability, cell amount and apoptosis induction after 24h of incubation (n = 6). Data is presented relative to the buffer, which was set to 1.0.

As is evident from the results, no difference in the reaction of the cells under all measured parameters was observed between cells treated with NPs and the cells treated with the same amount of vehicle buffer alone. This clearly indicates that the NPs do not show any toxic effect under these conditions. In the past, several promising nanoparticles used for drug delivery have been put aside due to toxicity of the carrier[31-32].

5.2.2 *In-vivo* toxicity study

The absence of toxicity is thus an important finding and allows for further screening of possible toxic effects *in-vivo*. To this end, the NPs with the complementary sequence containing a fluorescent label (Atto488) or functionalized with an aptamer containing a Cy3 fluorophore and loaded with the antibiotic kanamycin B were applied as eye drops. The toxicity was investigated after a single or multiple eye drops at concentrations of 20µM and 100 µM. The latter concentration was taken to gauge the effect of a higher exposure to the NPs. When administering multiple times, four installations were performed with one hour between each drop. The rats were sacrificed 24 hours after the first exposure and apoptosis was visualized through terminal deoxynucleotidyl transferase mediated dUTP nick end labeling (TUNEL). This particular staining is commonly used to detect apoptosis in cells, a process during which nicks are formed in the nuclear DNA. The nicks are recognized by terminal deoxynucleotidyl transferase (TdT) which will add fluorescently labeled dUTPs to the cleaved strand. For screening upon exposure to Atto488 labeled U4-12 NPs a red fluorophore was used, whereas for screening of kanamycin B loaded NPs a green fluorescent probe was employed. After staining, apoptosis induction was evaluated using fluorescence microscopy (See Fig. 5.2). As can be seen from the micrographs, no apoptosis was observed in any of the application conditions for the pristine U4-12 and the kanamycin B loaded NPs. They prove that no negative effects are present at higher concentrations and also after multiple installations no apoptotic stress is exerted by the DNA carrier. These results confirm the non-toxic character of the carrier and open the way for further testing of this drug delivery platform for ophthalmology.

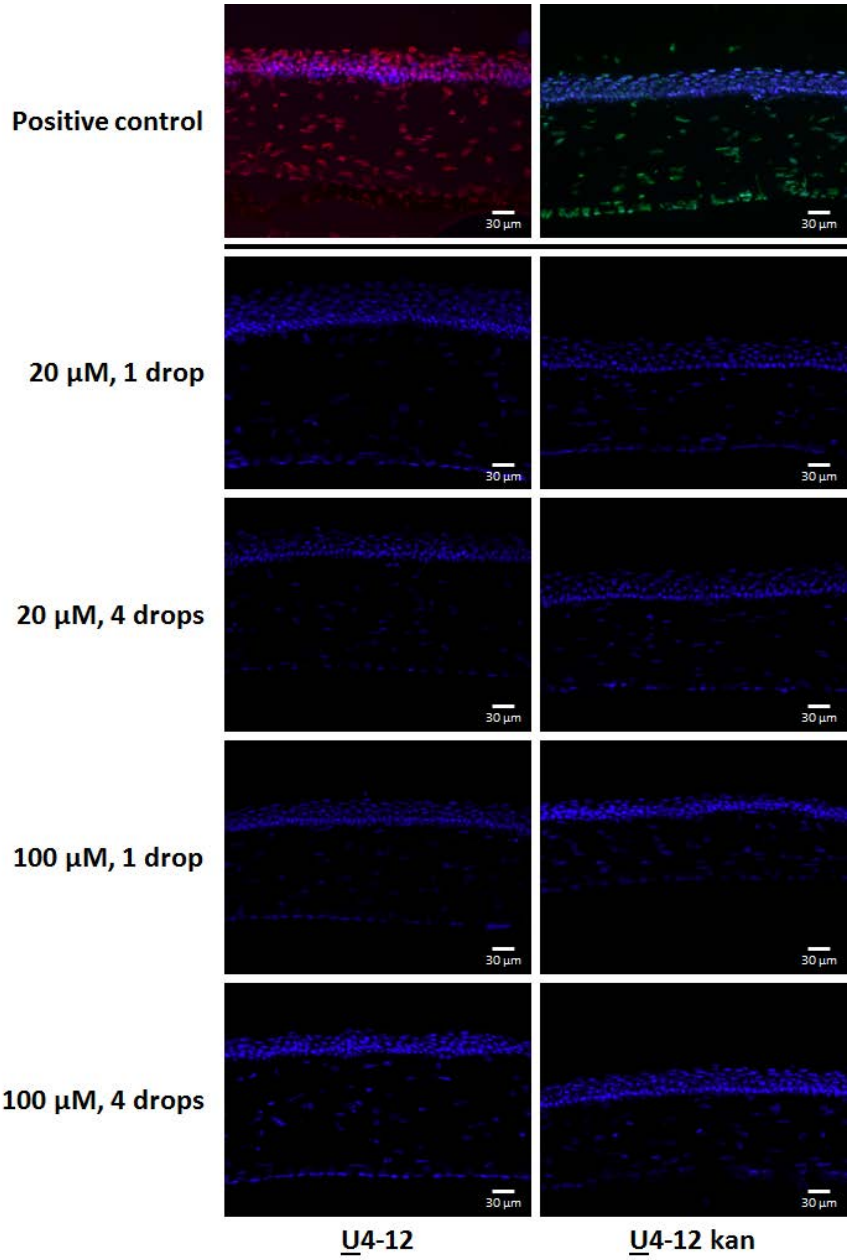

Figure 5.2. Evaluation of apoptosis induction in the cornea (blue) upon exposure to fluorescently labeled U4-12 NPs and kanamycin B loaded NPs. For the prior NPs apoptosis is shown in red, for antibiotic loaded NPs it is visualized in green. Positive staining controls were generated using DNAse.

5.2.3 Stability determination by gel electrophoresis.

Another crucial parameter for successful use of a drug delivery platform is the stability of the NP formulation. However, before testing this, the structural integrity of the building blocks needs to be assessed. Hence, after evaluating the toxicity of the NPs, the stability of the compounds was investigated over prolonged periods of time under different conditions. To this end, aliquots of pristine and aptamer functionalized U4-12 NPs were stored in the dark in the cold (4 °C) or at room temperature (RT) for a period of 6 months. Samples were taken every month and evaluated using PAGE and RPC HPLC. The electrophoretic assessment was performed using 8% denaturing polyacrylamide gels in order to judge possible degradation of the individual components (See Fig. 5.3).

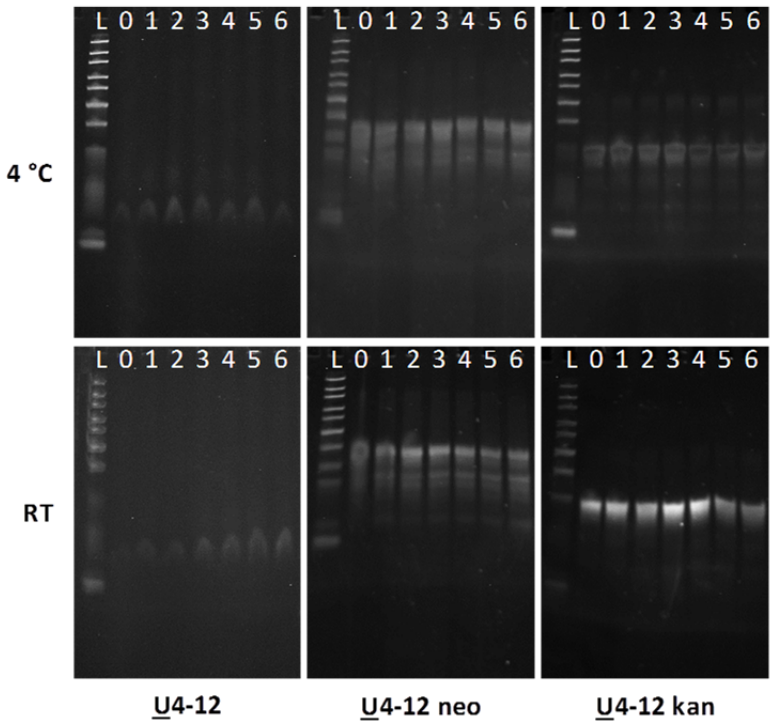

Figure 5.3. Denaturate PAGE analysis of pristine U4-12 NPs and neomycin B- and kanamycin B-loaded U4-12 NPs (8% TBE-Urea, 120 V, 90 min) stored at 4 °C or at room temperature (RT). In all gels the first lane was loaded with a ladder, the lanes right to the ladder contain the control (0 months) and samples with increasing age from left to right (1 to 6 months).

When comparing the electrophoretic mobility of the samples stored under different conditions, several observations can be made. A closer look at the pristine U4-12 NPs reveals that the different storage conditions seem to have little effect on the materials. The electrophoretic mobility and intensity of the samples does not or change very little over time, indicating that there is no degradation of the amphiphiles.

For the neomycin B loaded NPs stored at 4 °C two bands can clearly be identified. As their intensity does not vary over time, no degradation of the carrier and aptamer is observed. However, for the PAGE results of the storage of the same carrier at RT several bands with higher electrophoretic mobility become visible for longer storing periods. This indicates that the RNA aptamer is subject to degradation. This fragmentation is probably due to hydrolysis of the phosphodiester backbone induced by attack of the 2' OH group which is absent in the DNA carrier.

In contrast to NPs functionalized with a RNA aptamer, the samples exhibiting kanamycin B binding sequences hybridized on the NP show little degradation over time for the different storage conditions. Similar to the pristine carrier, little variation in electrophoretic mobility and in intensity of the bands is observed, indicating both building blocks are stable under the applied conditions.

5.2.4 Evaluation of NP stability by liquid chromatography

Despite the results obtained from the electrophoretic evaluation, identification of possible smaller or uncharged byproducts is not possible using this method. Therefore, the samples were also characterized by RPC HPLC. To confirm the absence of degradation for the carrier system, the pristine U4-12 NPs were analyzed first (See Fig. 5.4).

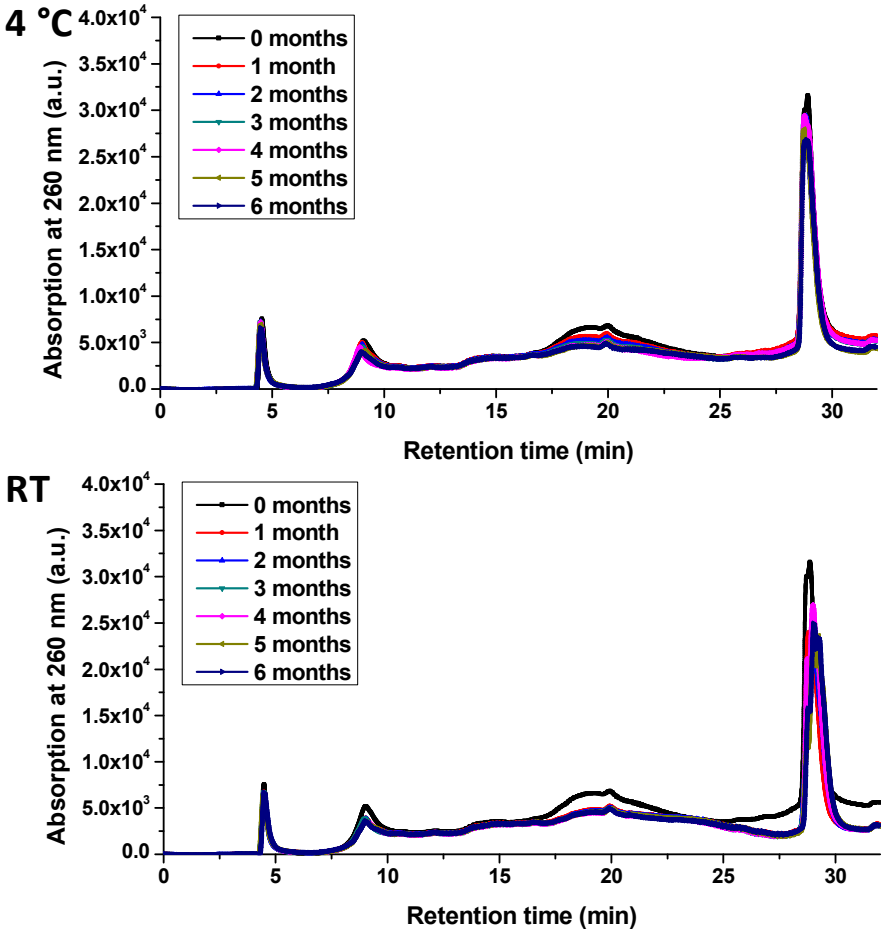

Figure 5.4. RPC HPLC analysis of pristine U4-12 NPs. A linear gradient 0 – 80% isopropanol (iPrOH) in 32 min was applied.

As observed in the chromatograms of the pristine NPs, several peaks can be identified. First, unbound materials elute at around 5 minutes, which corresponds to approximately 1 column volume. Secondly, around 9 and 19 minutes two other peaks are observed that is part of the baseline. These were also observed when injecting water and do not correspond to signal originating from the sample (data not shown). Both peaks are visible due to

the relatively low signal coming from the amphiphile, which is a result of the concentration and short sequence. The peak corresponding to the NPs is found at 29 minutes. The shape and elution time of the product peak is similar for all samples of different storage conditions, indicating that there are no large changes in the NP building blocks. Additionally, the intensity of the peak is constant. Both observations indicate that the NPs are stable for a period of at least 6 months, which is in good agreement with the results found by PAGE.

After confirming the stability of the pristine carrier, the influence of storage conditions on neomycin B-loaded NPs was investigated (See Fig. 5.5). In the RPC HPLC analysis of the stored neomycin B-loaded U4-12 NPs, the peak corresponding to the amphiphiles is also observed at an elution time of 29 minutes. Also here no obvious change in peak shape and intensity is observed. The RNA aptamer employed for binding of neomycin B is eluted after 9.25 minutes. For storage in the cold no changes in the peak intensity and shape are found. However, when keeping the nanoparticles at RT for prolonged periods of time a shoulder occurs before the RNA aptamer. Additionally, when looking carefully multiple smaller peaks can be identified that elute before the aptamer. This indicates that the RNA is degrading slowly when kept at RT for longer time periods, as was also observed by PAGE.

For a complete evaluation also the NPs functionalized with the kanamycin B binding aptamer and stored under different conditions were characterized by RPC HPLC (See Fig. 5.6).

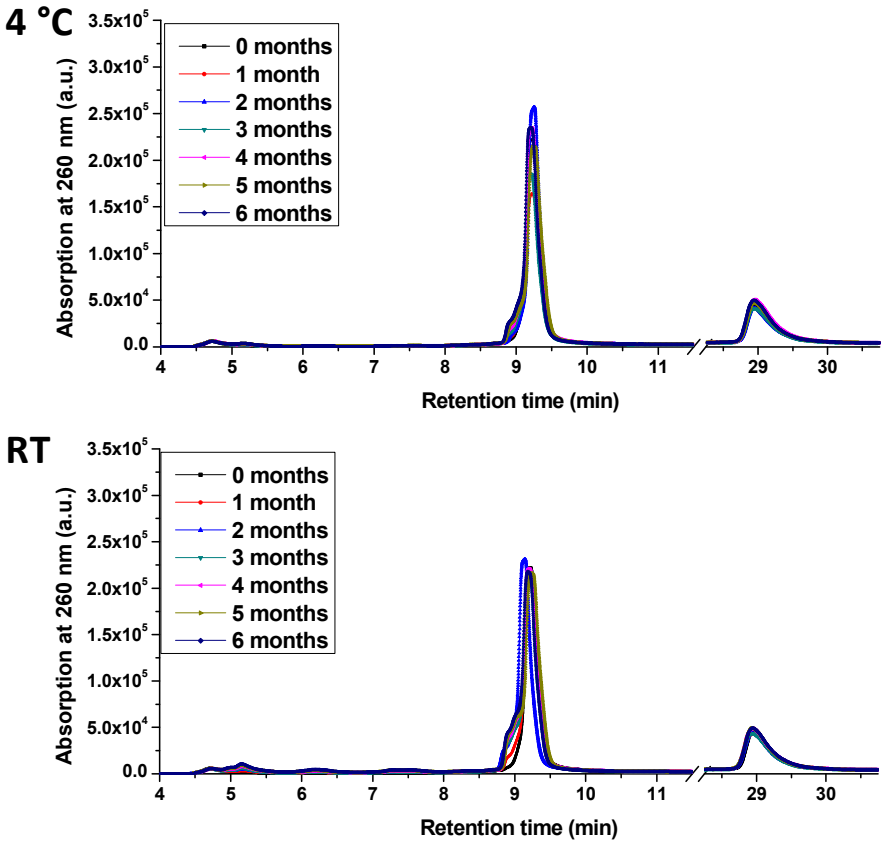

Figure 5.5. RPC HPLC analysis of neomycin B-loaded U4-12 NPs. A linear gradient 0 – 80% iPrOH in 32 min was applied.

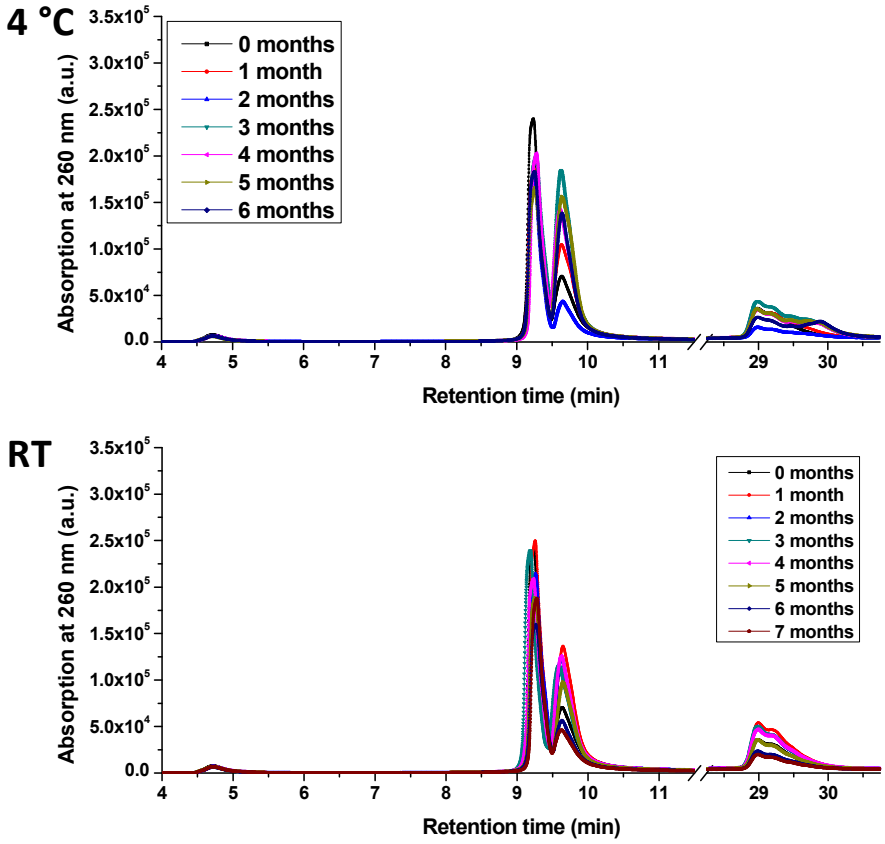

Figure 5.6. RPC HPLC analysis of kanamycin B-loaded U4-12 NPs. A linear gradient 0 – 80% iPrOH in 32 min was applied.

As can be seen, in all cases the aptamer elutes as two peaks that are found at a retention time of 9.25 and 9.65 minutes, respectively. The ratio between the two peaks changes between different samples and storage conditions but does not seem to follow a trend, what indicates the presence of non-covalent interactions and dynamic changes in the folding of the molecules but no degradation. To investigate the purity of the starting material, the pristine DNA aptamer was also analyzed by RPC HPLC (See Fig. 5.7). A gradient with a lower slope was used for this purpose in order to have a better separation between the two peaks observed earlier.

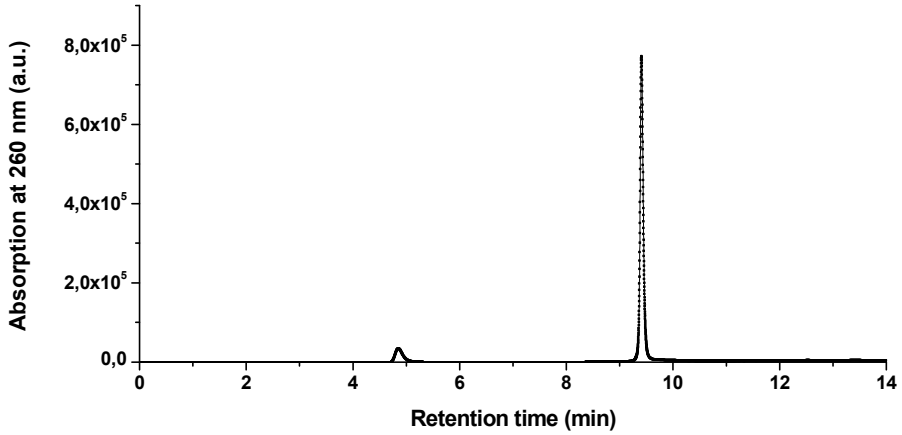

Figure 5.7. RPC HPLC characterization of cU4-kan DNA aptamer. A linear gradient 0 – 30% B in 12 min was applied.

As is visible, the pristine aptamer elutes as a single peak at 9.4 minutes and no second peak is observed. These results confirm that the observed splitting is due to the secondary structure of the aptamer or interaction with the amphiphile. As aptamers are selected to bind the specific molecule of interest they have strong secondary structures and hence it is not unexpected that the product does not elute as a single peak.

In figure 5.6 the U4-12 amphiphiles are observed at later elution times. For NPs kept at 4 °C only little change in the peak shape and intensity are observed, showing no clear trend over time. In case of storage at RT, after 3 months formation of a second peak eluting after 30 minutes is observed. However, for elution of amphiphiles with a highly hydrophobic character, loss of a conventional nucleotide would result in a less drastic change in the elution profile. Therefore, it is expected that the additional peak is the result of secondary interactions or change in the NP aggregation number. In order to exclude decomposition of the amphiphile several selected samples were characterized by UPLC coupled with a mass spectrometer. Here no degradation was observed in the samples and for both peaks the correct mass corresponding to the U4-12 molecule was found (data not shown).

5.3 Conclusion

In this chapter, the toxicity of the NPs used in the earlier chapters was elucidated. In three different ocular cell lines, the cell number, cell viability and apoptosis induction was investigated for the pristine NP that showed best adherence in chapter 3, i.e. U4-12. For none of the evaluated parameters and in none of the investigated cell lines a negative effect was seen, indicating no toxic effects of the nanoobjects under the employed conditions. To further evaluate the toxicity profile, *in-vivo* studies were conducted where the animals were exposed to the vehicle in a single or multiple exposure experiment at different concentrations. Also here, screening for apoptosis by TUNEL staining showed that no negative effects of the NPs are visible. These findings are of high importance as toxicity of drug delivery platforms is a common show-stopper for successful development.

After verifying the non-toxic nature of the delivery platform, the stability of the building blocks used for NP formation was investigated under different storage conditions. Both PAGE and RPC HPLC of the pristine amphiphiles showed that they are stable for at least 6 months in a fridge or at RT. For vehicles functionalized with the neomycin B aptamer no degradation of the carrier was apparent. The RNA sequence also proved to be relatively stable over a long period of time as only slight degradation was observed both in electrophoretic analysis and in the HPLC chromatograms. For NPs exhibiting the kanamycin B binding aptamer little degradation was found in PAGE. However, a large shift in the peak corresponding to the aptamer was found during chromatographic evaluation due to secondary structure formation or aggregation. To conclude, storage under refrigerated conditions shows minimal degradation with all three NPs being stable for a period of at least 6 months.

5.4 Experimental

5.4.1 Materials

All chemicals and reagents were purchased from commercial suppliers and were used without further purification, unless otherwise noted. The triethylamine, acetic acid, neomycin B trisulfate hydrate and kanamycin B sulfate were purchased from Sigma-Aldrich and were used as received. Isopropanol was purchased at VWR. The lipid modified oligonucleotide was synthesized as described in section 3.4.2. The concentrations of the DNA were measured on a SpectraMax M2 spectrophotometer (Molecular Devices, USA) or JASCO V-630 (Jasco Benelux, The Netherlands) using 1 cm light-path quartz cuvette. Fluorescently labeled and unmodified oligonucleotides were purchased from Biomers.net in HPLC purification grade. For cell culture assays a Synergy HT multi-mode microplate reader (BioTek, Bad Friedrichshall, Germany) was used.

5.4.2 Preparation of functionalized NPs

For loading of neomycin B and kanamycin B a RNA and DNA aptamer was used, respectively[33-34]. Both were elongated with the complementary sequence of the carrier (See Table 5.1).

Name	Sequence (5' → 3')
cU4-neo	GGACUGGGCGAGAAGUUUAGUCCGCGAAUCCGCAAAA
cU4-kan	TGGGGGTTGAGGCTAAGCCGATTGAATCCGCAAAA

Table 5.1.Sequence of extended aptamers for antibiotic loading of NPs

All micelles were prepared in sterile low bind tubes (Eppendorf) in 1x TAE buffer (40 mM Tris-Acetate, 1 mM EDTA, 20 mM NaCl, 12 mM $MgCl_2$, pH 8.0) at a concentration of 20 μM. The lipid modified oligonucleotide of interest was prepared at the desired concentration and thermally cycled (90 °C, 30 min; -1 °C/2 min until RT). For functionalized NPs the same amount of U4-12 and the complementary DNA-aptamer (1 eq.) were loaded in a tube at the desired concentration and hybridized using a thermal gradient (80 °C, 30 min; 1°C/2 min until RT).

5.4.3 Toxicity studies on ocular cell lines

Cell culture studies were performed as previously described in detail.[35-36] All cell lines were maintained in Dulbecco's modified eagle medium (Invitrogen) supplemented with 1% penicillin, 1% streptomycin and 5% (RGC-5 and 661W) or 10% (ARPE-19) fetal bovine serum (Invitrogen). The RGC-5 (passage 5) and 661W (passage 78) cells were seeded at a density of 5000 cells/well whereas ARPE-19 cells (passage 5) were seeded at 10000 cells/well in 96-well plates having a surface of 0.32 cm^2. Subsequently, 24 h after seeding the pristine NPs were added to obtain a final concentration of 20 µM of the amphiphile. After 24 h of incubation their toxicity was evaluated. A description of the conducted assays is found below.

MTS Viability Assay

24 h after NP addition, 20 µl of the CellTiter 96® AQueous One Solution Reagent (Promega) was directly added to the culture wells and incubated for 90 minutes. Then the absorbance was recorded at 490 nm with a Microplate Reader (BioTek, Synergy HT, Bad Friedrichshall, Germany) with the correction of interference at 690 nm.

Crystal violet staining

After the MTS assay, medium was removed and the cells fixed overnight with 4% paraformaldehyde. After washing the cells three times, they were stained with crystal violet solution (Sigma Aldrich, Steinheim, Germany) washed again and incubated with 1% SDS for 1h. Absorbance was determined at 595 nm (BioTek, Synergy HT, Bad Friedrichshall, Germany).

Caspase 3/7 activity assay

24 h after supplementation, caspase 3/7 activity was determined using CaspaseGlo 3/7 activity kit (Promega, Madison, USA) according to the manufacturer's protocol. Luminescence was measured with a luminometer (BioTek, Synergy HT, Bad Friedrichshall, Germany).

Statistical analysis of cell culture assays

Data are represented as mean +/- SD. With every assay five-six different experiments were conducted per cell line and U4-12 or buffer, respectively

(n=5-6). Statistical analysis was performed using JMP® (version 11.1.1, SAS Institute Inc., Cary, NC, USA). Student's ANOVA analysis with Dunnett's post-hoc test was used for comparison between buffer and NP. Differences were considered to be significant at $p<0.05$.

5.4.4 *In-vivo* toxicity evaluation

For *in-vivo* toxicity testing NPs were prepared using the complementary sequence of U4-12 labeled with an Atto488 dye or using cU4-kan aptamer labeled with a Cy3 dye. NPs were prepared as described above and administered to conscious Lister Hooded rats (Charles River, Germany) at a concentration of 20 µM or 100 µM using a single drop or four drops with an interval of 1 hour. Each drop had a volume of approximately 30 µl. For the eye drop application, the conscious rats were very shortly fixated and a drop was administered to the eye using a single drop device as in medical applications. Blinking of the eyes was not hindered during drop application or afterwards. After 24 hours the rats were sacrificed with carbon dioxide inhalation. Afterwards, the eyes were enucleated and frozen in Tissue-Tek O.C.T. (Sakura Finetek, Germany) using liquid nitrogen. Frozen sections were longitudinally cut (12 µm) on a cryostat (Leica CM 1900, Germany), thaw-mounted onto glass slides (Superfrost plus, R. Langenbrinck Labor- und Medizintechnik, Germany) and stored at -30 °C until further use. For TUNEL staining the sections were fixated in 4% paraformaldehyde for 20 minutes at RT. Subsequently the samples were washed and stained using an In-Situ Cell Death Detection Kit, (Roche, Germany) according to the manufacturer's protocol. Stained sections were embedded in FluorSave (Calbiochem, Germany) and imaged using a fluorescent microscope (Axioplan2 imaging®, Zeiss, Germany with Openlab software, Improvision, Germany)[35].

5.4.5 Stability assessment of pristine and antibiotic loaded U4-12 NPs

For stability measurement 1000 µl of each NP was prepared and aliquots of 25 µL were made. Of these, 12 were stored in the dark in a fridge (4 °C) and 12 were kept at RT. For each NP one was stored at -80 °C from the start of the experiment. Every month 1 aliquot was taken from each condition for each NP and stored at -80 °C.

Electrophoretic analysis of the NPs was performed using an 8% TBE-Urea self-cast polyacrylamide gel. The samples were run at 120V for 60 min followed by staining of the bands using 1x SYBR Gold (Life Technologies Europe BV).

RPC HPLC analysis of the products was done on a Shimadzu VP series HPLC equipped with PDA detector using a Jupiter C4 5 µm column 4.6 x 250 mm (Phenomenex). A linear gradient 0 – 80% B in 32 min was applied at 30 °C using buffer A: 100 mM triethylammonium acetate (TEAAc) and 5% acetonitrile, B: 100% isopropanol. The DNA was monitored at a wavelength of 260 nm. For further investigation of the cU4-kan aptamer a linear gradient 0 – 30% B in 12 min was applied using the same column and buffers.

5.5 Acknowledgement

For their help with the RPC HPLC analysis I would like to acknowledge the efforts of Eliza Warszawik and Agnieszka Gruszka. For the help with the toxicity studies on ocular cell lines I would like to thank Johanna Hofmann and Sven Schnichels.

5.6 References

[1] D. E. Lee, H. Koo, I. C. Sun, J. H. Ryu, K. Kim, I. C. Kwon, *Chem. Soc. Rev.* **2012**, *41*, 2656-2672.

[2] G. Y. Tonga, K. Saha, V. M. Rotello, *Adv. Mater.* **2014**, *26*, 359-370.
[3] Z. L. Cheng, A. Al Zaki, J. Z. Hui, V. R. Muzykantov, A. Tsourkas, *Science* **2012**, *338*, 903-910.
[4] G. Bao, S. Mitragotri, S. Tong, *Annu. Rev. Biomed. Eng.* **2013**, *15*, 253-282.
[5] T. M. Allen, P. R. Cullis, *Science* **2004**, *303*, 1818-1822.
[6] D. Peer, J. M. Karp, S. Hong, O. C. FaroKHzad, R. Margalit, R. Langer, *Nat. Nanotechnol.* **2007**, *2*, 751-760.
[7] J. W. Yoo, E. Chambers, S. Mitragotri, *Curr. Pharm. Design* **2010**, *16*, 2298-2307.
[8] J. W. Yoo, N. Doshi, S. Mitragotri, *Adv. Drug Deliv. Rev.* **2011**, *63*, 1247-1256.
[9] R. A. Petros, J. M. DeSimone, *Nat. Rev. Drug. Discov.* **2010**, *9*, 615-627.
[10] H. S. Choi, W. Liu, P. Misra, E. Tanaka, J. P. Zimmer, B. I. Ipe, M. G. Bawendi, J. V. Frangioni, *Nat. Biotechnol.* **2007**, *25*, 1165-1170.
[11] S. Nagayama, K. Ogawara, Y. Fukuoka, K. Higaki, T. Kimura, *Int. J. Pharm.* **2007**, *342*, 215-221.
[12] F. Alexis, E. Pridgen, L. K. Molnar, O. C. Farokhzad, *Mol. Pharmaceut.* **2008**, *5*, 505-515.
[13] M. J. Ernsting, M. Murakami, A. Roy, S. D. Li, *J. Control. Release* **2013**, *172*, 782-794.
[14] J. V. Jokerst, T. Lobovkina, R. N. Zare, S. S. Gambhir, *Nanomedicine-Uk* **2011**, *6*, 715-728.
[15] H. Otsuka, Y. Nagasaki, K. Kataoka, *Adv. Drug Deliv. Rev.* **2003**, *55*, 403-419.
[16] A. Abuchowski, J. R. Mccoy, N. C. Palczuk, T. Vanes, F. F. Davis, *J. Biol. Chem.* **1977**, *252*, 3582-3586.
[17] A. Abuchowski, T. Vanes, N. C. Palczuk, F. F. Davis, *J. Biol. Chem.* **1977**, *252*, 3578-3581.
[18] H. Hatakeyama, H. Akita, H. Harashima, *Adv. Drug Deliv. Rev.* **2011**, *63*, 152-160.
[19] K. Remaut, B. Lucas, K. Braeckmans, J. Demeester, S. C. De Smedt, *J. Control. Release* **2007**, *117*, 256-266.
[20] T. Ishida, X. Wang, T. Shimizu, K. Nawata, H. Kiwada, *J. Control. Release* **2007**, *122*, 349-355.
[21] S. Arora, J. M. Rajwade, K. M. Paknikar, *Toxicol. Appl. Pharm.* **2012**, *258*, 151-165.
[22] A. Nel, T. Xia, L. Madler, N. Li, *Science* **2006**, *311*, 622-627.
[23] Y. S. Chen, Y. C. Hung, I. Liau, G. S. Huang, *Nanoscale Res. Lett.* **2009**, *4*, 858-864.
[24] E. E. Connor, J. Mwamuka, A. Gole, C. J. Murphy, M. D. Wyatt, *Small* **2005**, *1*, 325-327.

[25] X. D. Zhang, H. Y. Wu, D. Wu, Y. Y. Wang, J. H. Chang, Z. B. Zhai, A. M. Meng, P. X. Liu, L. A. Zhang, F. Y. Fan, *Int. J. Nanomed.* **2010**, *5*, 771-781.
[26] G. Zhang, Z. Yang, W. Lu, R. Zhang, Q. Huang, M. Tian, L. Li, D. Liang, C. Li, *Biomaterials* **2009**, *30*, 1928-1936.
[27] G. von Maltzahn, J. H. Park, A. Agrawal, N. K. Bandaru, S. K. Das, M. J. Sailor, S. N. Bhatia, *Cancer Res.* **2009**, *69*, 3892-3900.
[28] A. K. Gupta, M. Gupta, *Biomaterials* **2005**, *26*, 3995-4021.
[29] Z. Amoozgar, Y. Yeo, *Wires Nanomed. Nanobiotechnol.* **2012**, *4*, 219-233.
[30] R. P. Singh, P. Ramarao, *Toxicol. Sci.* **2013**, *136*, 131-143.
[31] M. A. Dobrovolskaia, S. E. McNeil, *Nat. Nanotechnol.* **2007**, *2*, 469-478.
[32] Y. Diebold, M. Calonge, *Prog. Retin. Eye Res.* **2010**, *29*, 596-609.
[33] L. Jiang, A. Majumdar, W. Hu, T. J. Jaishree, W. Xu, D. J. Patel, *Structure* **1999**, *7*, 817-827.
[34] K.-M. Song, M. Cho, H. Jo, K. Min, S. H. Jeon, T. Kim, M. S. Han, J. K. Ku, C. Ban, *Anal. Biochem.* **2011**, *415*, 175-181.
[35] S. Schnichels, M. Schultheiss, J. Hofmann, P. Szurman, K. U. Bartz-Schmidt, M. S. Spitzer, *Neurochem. Int.* **2012**, *60*, 581-591.
[36] M. Schultheiss, S. Schnichels, K. Miteva, K. Warstat, P. Szurman, M. S. Spitzer, S. Van Linthout, *Graefes Arch. Clin. Exp. Ophthalmol.* **2012**, *250*, 1221-1229.

Summary

The field of DNA nanotechnology has progressed rapidly in recent years and hence a large variety of 1D-, 2D- and 3D DNA nanostructures with various sizes, geometries and shapes is readily accessible. DNA-based nanoobjects are fabricated by straight forward design and self-assembly processes allowing the exact positioning of functional moieties and the integration of other materials. At the same time some of these nanosystems are characterized by a low toxicity profile. As a consequence, the use of these architectures in a biomedical context has been explored. In **Chapter 1** the progress and possibilities of pristine nucleic acid nanostructures and DNA hybrid materials for drug delivery was discussed. For the latter class of structures, a distinction was made between carriers with an inorganic core comprised of gold or silica and amphiphilic DNA block copolymers (DBCs) that exhibit a soft hydrophobic interior.

In **Chapter 2**, the synthesis and purification of several DBCs architectures using RPC HPLC was presented. This method is the current gold standard to obtain oligonucleotides (ODNs) with high purity but is rarely used for more complex hybrid materials despite its many advantageous. As described here, three different diblock copolymers containing a poly(propylene oxide)(PPO) unit and 22mer ODNs can readily be purified by RPC HPLC in a single step. To obtain a triblock copolymer with the same polymer, however, additional purification by AEX HPLC was needed. Characterization of the DBCs by MALDI-TOF mass spectrometry showed several products that correspond well to the DNA conjugated to a PPO polymer comprising different number of monomer units, representing the typical polydisperse character of a synthetic polymer. To investigate the influence of the polymer on the hybridization characteristics also the melting temperatures of different double stranded DBC architectures were determined. Here, no changes were observed, indicating that the polymer does not influence Watson-Crick base pairing despite its large size and hydrophobic nature.

In the next chapter, the application of similar amphiphilic nucleic acid materials as DBCs in a biomedical context is explored. Treatment of ophthalmic diseases by eye drops is impaired by the short survival time of the drug on the eye surface. As a consequence, topical administration of ocular therapeutics requires high drug doses and frequent administration but rarely provides high drug bioavailability. Therefore, in **Chapter 3** several nanoparticle systems were developed that aim to increase the half-life of drugs on the ocular surface. The nanoparticles (NPs) were composed of lipid-modified DNA strands and mostly showed good adherence to the corneal surface both *in-vitro* and *in-vivo* experiments. Through optimization of the total length of the ODN and the number of modified nucleotides the binding to the ocular surface was optimized. The best adhering NP showed a greatly improved survival time on the eye of up to 4 hours, which is significantly longer than currently used drugs.

After optimizing adsorption to the ocular surface, **Chapter 4** deals with the translation of the well adhering lipid DNA NPs into a novel and general drug delivery system. Through the use of aptamers elongated with the complementary sequence, these carriers were equipped with two different antibiotics using only a single assembly step. *In-vivo* evaluation of the adherence showed that after 2 hours the loaded NPs were still detected on the cornea whereas the fluorescently labeled control was already washed out after 5 minutes. This highlights one of the major shortcomings of treatment of ophthalmic indications. The long survival time of the antibiotic-loaded NPs was then translated into improved efficacy with the functional carrier showing antibacterial activity at least 10-fold longer compared to the pristine antibiotics. Finally, functionality of the NPs was even demonstrated for human tissue.

In **Chapter 5** the toxicity and stability of the NPs employed for ocular drug delivery was evaluated. No toxic effects were found in *in-vitro* cell culture studies on three ocular cell lines. Further evaluation of possible apoptosis induction *in-vivo* also showed no negative outcome, even when applying the NPs multiple times at concentrations of 100 μM. Afterwards, the long term stability of the building blocks of the NPs was evaluated using gel

electrophoresis and RPC HPLC. In both methods, the pristine amphiphiles proved to be stable for a period of at least 6 months when stored at 4 °C and at room temperature. Moreover, the aptamer functionalized NPs showed little to no degradation during the monitoring time period, strongly suggesting their further development into a general drug delivery platform for ophthalmology.

Samenvatting

Onderzoek naar DNA nanotechnologie heeft de laatste jaren veel vooruitgang geboekt met als resultaat dat een grote variëteit aan 1D, 2D en 3D DNA structuren met verschillende afmetingen en vormen beschikbaar zijn. DNA gebaseerde nanoobjecten worden gemaakt door een eenvoudig design en zelf-montage processen die de exacte positionering van functionele groepen en de integratie van ander materialen mogelijk maken. Tegelijkertijd hebben sommige van deze nanosystemen een lage toxiciteit. Als gevolg daarvan is geprobeert deze materialen in een biomedische context te gebruiken. In **Hoofdstuk 1** is de vooruitgang hierin beschreven en worden de mogelijkheden tot gebruik van zuivere nucleïne zuren en hybride DNA materialen voor drug delivery bediscussieerd. Voor de laatst genoemde materialen word een scheiding gemaakt tussen dragers met een anorganische kern zoals goud of silica en amfifiele DNA blok copolymeren (DBCs) die een zacht binnenste hebben.

In **Hoofdstuk 2** is de synthese en opwerking van verschillende DBCs door RPC HPLC gepresenteerd. Deze methode is de huidige standaard om oligonucleotiden (ODNs) met hoge zuiverheid te verkrijgen, maar wordt zelden benut voor complexe hybride materialen ondanks de vele voordelen. Hier wordt beschreven hoe drie verschillende diblok copolymeren bestaande uit een poly(propylene oxide)(PPO) blok en een 22 basen lange ODN gemakkelijk kunnen worden opgewerkt met RPC HPLC in een enkele zuiverings stap. Om een triblok copolymeer met hetzelfde PPO blok te verkrijgen was echter een additionele purificatie nodig met AEX HPLC. Karakterisatie van de producten met MALDI-TOF massa spectrometrie toonde verschillende producten die goed overeenkomen met het DNA geconjugeerde PPO polymeer. Ook kon onderscheidt worden gemaakt tussen verschillend aantal monomeer eenheden in de PPO keten, wat representatief is voor het typisch polydispers karakter van synthetische polymeren. Om de invloed van het polymeer op de hybridisatie te onderzoeken is ook de smelttemperatuur van verschillende dubbelstrengige DBC architecturen

bepaalt. Hier werden geen verschillen gemeten, wat aangeeft dat het polymeer geen invloed heeft op de Watson-Crick base paring, ondanks zijn grootte en hydrofobe karakter.

In het volgende hoofdstuk wordt het gebruik van soortgelijke amfifiele materialen in een biomedische context verzocht. Behandeling van oogheelkundige ziekten door oogdruppels wordt bemoeilijkt door de korte verblijftijd van het medicijn op het oogoppervlak. Als gevolg daarvan is een hoge concentratie van het geneesmiddel en zeer frequente toediening nodig wat desalniettemin maar zelden in hoge beschikbaarheid resulteert. Daarom werden in **Hoofdstuk 3** verschillende nanoparticle systemen ontwikkelt die als doel hebben om de halfwaardetijd van medicatie op het oogoppervlak te verhogen. De nanoparticles (NPs) waren opgebouwd uit lipide gemodificeerde DNA strengen en toonden goede binding aan het hoornvlies in zowel *in-vitro* als *in-vivo* experimenten. Door verandering in de lengte van de ODN en het aantal gemodificieerde nucleotiden is de binding aan het oogoppervlak geoptimaliseerd. Het best hechtende NP toonde een sterk verhoogde overlevingstijd op het oog tot 4 uur, wat behoorlijk langer is dan medicijnen die nu gebruikt worden.

Na optimalisatie van de binding aan het oogoppervlak werd in **Hoofdstuk 4** de vertaling van een goed hechtend lipide DNA NP naar een nieuw en algemeen drug delivery stysteem gemaakt. Door gebruik van aptameren die verlengd zijn met de complementaire sequentie zijn de dragers in een enkele stap voorzien van twee verschillende antibiotica. *In-vivo* evaluatie van de binding liet zien dat de beladen NPs na 2 uur nog steeds detecteerbaar zijn op het hoornvlies terwijl het controlemonster al na 5 minuten weg gewassen was. Dit belicht tevens een van de grootste tekortkomingen in behandeling van oogziektes. De hoge halfwaardetijd van de antibiotica beladen NPs is daarna vertaalt in een verbeterde werkzaamheid waar de functionele drager een 10 keer langer antibacteriële werking liet zien in vergelijking tot het zuivere antibioticum. Als laatste is ook de functionaliteit van de NPs voor menselijk weefsel laten zien.

In **Hoofdstuk 5** is de toxiciteit en stabiliteit van de eerder gebruikte NPs geëvalueerd. Geen toxische effecten werden gevonden in *in-vitro* experimenten aan drie cellijnen die gevonden worden in het oog. Ook

verdere evaluatie van eventuele apoptose inductie *in-vivo* liet geen negatieve uitkomsten zien, zelfs niet wanneer de NPs meerder keren toegediend werden bij concentraties van 100 μM. Na deze eerste beoordeling is de stabiliteit van de NP componenten over langere periode bepaalt met behulp van gel electroforese en RPC HPLC. Bij beide methoden bleken de oorspronkelijke NPs stabiel voor een periode van minimaal 6 maand wanneer ze op 4 °C of op kamer temperatuur bewaard werden. Verder vertoonden ook de aptameer gefunctionaliseerde NPs weinig tot geen degradatie gedurende deze periode. Deze resultaten impliceren een verder ontwikkeling tot een algemeen drug delivery platform voor behandeling van oogheelkundige indicaties.

Acknowledgement

After having finished writing this thesis I'm very glad to acknowledge those that have helped me realizing it.

First of all, I want to thank my supervisor Prof. Andreas Herrmann. Almost 7 years ago I entered your lab as inexperienced student and now I'm very happy to be your first Dutch PhD candidate. I want to thank you for the endless support, patience and guidance and for the great trust you have placed in me. I've always appreciated the freedom that I was given and your advices, also on non-scientific content, have been of enormous importance. From start to end, I have enjoyed my time working with you and in your lab. I'm looking forward to establishing the company with you in the team.

I would also like to express my deep gratitude to the members of my reading committee. Dear Prof. Dömling, Prof. Molema and Prof. Otto, thank you for your efforts in correcting my work. Your comments and suggestions have greatly helped me to improve my thesis.

Then I have arrived at the point where I like to thank the many (former) colleagues that have helped me through the days. My dearest Deepak, you have been a great colleague and supervisor. You have introduced me into the world of DNA synthesis and I have enjoyed working with you so much. Thank you for explaining me so many things and for making my time in the lab so enjoyable. Dear Minseok, also you have been of great importance during my time in Groningen, together with Deepak you were the guys running the chemistry part of our lab and introducing me into many different techniques. Thanks a lot for all your help. Also I want to especially thank Jur Wildeman. I have spent quite some time in your lab and learned a lot from you. Whenever I had a problem regarding synthesis you were helping out to find a solution, thanks a lot. Also Jan Zimmermann and Tobias Schnitzler deserve special mentioning, we had enormous fun and I always enjoyed our evenings/nights in the lab or at home. Alberto, thanks for the many nice lunches and coffee breaks and the fun in the office. I will never forget your

state of bananate. Diego, your salsa lessons were great and I always enjoyed them. Andreas, thank you for the many barbeque parties, they were always a pleasure. Lifei, Kai and Qing, we had a lot of laughter in the lab and always very fruitful discussion. Thank you for the great dinners that contained so many nice dishes; I will never be able to make them myself. Dear Eliza, thanks a lot for the nice time and your help in the last run towards finishing my thesis! Mark, thanks for taking care of the lab and helping me with many things. I hope your beers turn out really well! My Indian friends, Kamlesh, Swati and Avishek, thanks for the amazing food and great times. Bart, although we did not share a lot of time working together, I have enjoyed our discussions and talks a lot. Of course there are too many people to thank. With all of my colleagues I had loads of fun and very good days in the lab. Andrew, Alessio, Pavlo, Wei, Manfred, JingYi, Jing, Zhoujun, Lei, Yun, Pei, Barbara, Philipe, Tiancai, Stefano, Chao, Gert-Jan, Jennifer, Hongyan, Gurudas and Alina, thank you all for the great times and support when needed. I hope you have enjoyed working together as much as I have.

Many things I would not have been able to do without the help of the students of which I had the pleasure to work with. Especially Daniel Gautier has been a great support and has helped me so many times. Daniel, although the start was probably strange for the both of us, I have greatly enjoyed our time! Also I want to thank Niels Klement for helping me out in the lab. Despite your limited experience you have greatly impressed me with your capabilities. Finally, Andrey, Kranthi, Goutham, Sjoerd, Simone, Bob, Tycho, Marlies and Corinne thanks for your help and nice time in the lab.

Aside from my group I had the pleasure to work in a great department. Despite the many differences, the doors have always been open and I have always felt welcome in case of questions or problems. Prof. Schouten, Prof ten Brinke, Prof. Loos and Prof. Loontjens, thank you very much for your counseling and help. Special mentioning also goes to the many great colleagues from the department and the outstanding secretaries. Karin, Yvonne and Martine, I could always drop in for a small thing or just a nice chat. Thanks a lot for your support and help.

I also want to gratefully acknowledge the many collaborators for their input and sharing their knowledge. Many thanks to Prof. Thorben Cordes, Jasper

van der Velde, Jochem Smit, Prof. Sijbren Otto, Piotr Nowak, Prof. Anna Hirsch, Yun Liu, Prof. Ryan Chiechi, Davide Fracasso, Prof. Jeroen Cornelissen, Dr. Koay, Melanie Brasch, Dr. Deepak Veeregowda, Dr. Anna Salvati, Valentina Francia, Prof. Rachel O'Reilly, Dr. Thomas Wilks, Prof. Horst Weller, Anna Marlena Kreuziger, Prof. Itamar Willner and Dr. Bauke Albada.

Then there is one group of collaborators that deserves very special mentioning. Dear Martin, Sven, Kai, Jose, Max, Johanna, Marina, Lisa (Strudel), David, Katharina, Lisa (Pohl), Aileen, Karin, Heike, Maren, Melanie, Sarah, Sebastian and Matze, the many times I have been traveling from Groningen to Tübingen it always felt good to arrive. I want to thank all of you for the great time I had, am having and hopefully will have. Dear Sven and Martin, I think back of our many adventures with fond memories and I'm very happy to have joined your lab for the upcoming two years. Martin, thank you for the many useful discussion and great input. It has been a great experience to work with you and I'm thankful for the tremendous amount of knowledge you have shared with me. Sven, right from the start we had so much fun and yet we have been very productive. I have greatly enjoyed my time with you and want to thank you so much for that and the many fruitful discussions. Jose, I also want to thank you for the great help and support you have given, it's always a real pleasure to work with you.

At this point I would also like to thank the people that helped me keeping the lab running. Bert, Hans, Maarten, Jan Dirk, Klaas, Johan, Gert, Stijntje and all the others from technical department and the store, thanks for your support! I always could ask either one of you to help me out when things were not running the way they should.

Of course there is also a life outside the lab. Sometimes it is good to relax the brain in the presence of your friends. This gives the energy to start freshly the next morning and look at things from a different perspective. It feels very good to be able to say that the friends I have in Groningen have been a true comfort in this respect. Dear Willem, Jaap, Martijn, Maria, Sjoerd, Sebas, Lex, Alice, Esther, Erik, Menen, Biya, Keri and Candela, thank you for all the fun we had. I always enjoyed our parties, drinks on Thursdays, the LAN parties and all the other things we did together.

Then we come to my dear study friends, “de Jannen”. Lieuwe Jan, Vincent, Steven, Sjoerd, Thomas and Rienk, thanks a lot for all the great days in the lab and the nice parties. We had enormous amounts of fun, with the necessary collateral damage. I’m also very thankful for the amounts of food I still find in my room when cleaning up.

For physical relaxation I have always enjoyed going to sports on Tuesdays and Thursdays. Dojo Kokoro gave me the possibility to lose all my energy, be it positive or negative. I have had the great pleasure of teaching the kids and my own training was always a nice balance of technique, fighting and exhaust. Dear Raymond, Ludwig, Christian, Samantha and all the others, thanks a lot for all the time you have shared with me and the energy you gave me!

Alderliefste Heit, Mem, Tina, Roelie en Thijs. Ook jullie mogen hier natuurlijk niet ontbreken. Jullie onvoorwaardelijke liefde, steun en hulp heeft mij op veel momenten goed gedaan en soms er doorheen geholpen. Of het nu leuke onderwerpen waren of niet, ik heb altijd genoten van onze discussies en er veel van geleerd. Bij deze groep hoor natuurlijk ook tante Minke. Zonder haar zou ik waarschijnlijk nog steeds niet weten hoe met mes en vork tee ten. Heel erg bedankt voor alle fijne momenten en goede zorgen!

Up to now one of the most important persons is still missing. My dearest Agnieszka, it is hard to believe that is mere luck that made you decide to come to exactly my lab in Groningen. From the first day onwards we had enormous amounts of fun and yet could have very serious discussions as well. Thank you for your infinite support, love and help. You are probably one of the very few on this world that know me inside out and yet can keep up with me. I’m extremely happy to have you by my side and I’m looking forward to the many adventures to come!

After writing this I’m pretty sure I forgot some people that should have been mentioned. For this I’m truly sorry. I’ve enjoyed my time in Groningen a lot and look back with fond memories. Thanks everybody for making it such a pleasure.

Curriculum vitae

Personalia

Address:	Schlossbergstr. 20, 72070 Tübingen (GE)
Date of Birth:	26-05-1987
Tel:	+31625088923, +4917645637504
Email:	jan_willem_de_vries@hotmail.com
Nationality:	Nederlands/Dutch

Education and Training

Nov 2010 – Nov 2014: PhD Thesis in the Polymer Chemistry and Bioengineering group at the University of Groningen, Groningen, The Netherlands. Supervisor: Prof. Dr. Andreas Herrmann. Topics involved:

- Use of DNA nanoparticles for topical ophthalmic drug delivery
- Synthesis, purification and characterization of DNA hybrid materials

Sep 2008 – Sep 2010: Master, Polymer Chemistry, University of Groningen, Groningen, The Netherlands, Thesis Title: Novel Fluorescence Based Assay for the Detection of Small Molecules Using Transcriptional Regulators.

Sep 2005 – Aug 2008: Bachelor, Chemistry, University of Groningen, Groningen, The Netherlands, Thesis Title: Ultrasensitive DNA Diagnostics Based on DNA Block Copolymers.

Work experience

Dec 2014 – current: Postdoctoral research, Center for Ophthalmology, University Eye Hospital Tübingen, Tübingen, Germany

Nov 2010 – Nov 2014: PhD Thesis in the Polymer Chemistry and Bioengineering group at the University of Groningen, Groningen, The Netherlands.

Feb 2010 – Mar 2010: "Practicum Macromoleculaire Chemie voor BMT". Teaching laboratory classes for undergraduate students biomedical technology.

Sep 2008 – Apr 2009: Laboratory Research Assistant at the Polymer Chemistry and Bioengineering group, University of Groningen, Groningen, The Netherlands. Scope of research: Ultrasensitive DNA Diagnostics Based on DNA Block Copolymers.

Sep 2007 – Mar 2010: Guidance of first year students in their development and studies, University of Groningen, Groningen, The Netherlands.

Specialties and Qualities

- Synthesis of modified and native DNA, their purification and characterization: solid phase DNA synthesis, HPLC, LCMS and PAGE.
- Experienced in a wide variety of fields: protein binding assays (biology), labeling of DNA (biochemistry) and the synthesis of polymers (polymer chemistry).
- Experienced in organizing of events and symposia. (Two years board experience, VvP Netwerk, Chairman. Organized yearly symposium for study-association, 140 visitors).
- Motivated, quick-learning, technically skilled, responsible and reliable.
- Communicative capable, experienced in working in an international team.

Awards and prices

- Winner of the NGI Venture Challenge Fall 2012. A Netherlands Genomics Initiative (NGI) activity to support and stimulate life science researchers in translating their inventions into a viable business.
- Winner of the poster price at the Deutsche Ophthalmologische Gesellschaft (DOG) yearly meeting 2013. Poster title "Enhanced antibiotic delivery through a new class of nanoparticles"
- Winner of the poster price at the Deutsche Ophthalmologische Gesellschaft (DOG) yearly meeting 2014. Poster title "Efficacy and functionality of antibiotic delivery through DNA based nanoparticles"
- Winner of the poster price at the Bioinspired Materials & Functionalities symposium. Poster title "Optical Detection of Small Molecules using Transcriptional Regulators"
- Second place in science2start competition by BioRegio STERN

Publications

1. P. Gordiichuck, D. Rimmerman, A. Paul, D. Gautier, A. Gruszka, M. Saller, J.W. de Vries, G.-J. Wetzelaer, M. Manca, W. Gomulya, M. Matmor, E. Gloukhikh, M. Loznik, N. Ashkenasy, P. Blom, M. Rögner, M.A. Loi, S. Richter, A. Herrmann, Increasing the Activity of a Megadalton Photosystem I Complex by Conjugation of Organic Dyes, submitted.
2. B. Santos de Miranda, C. van Nisselroy, B.-J. Hoogenberg, S. Dantuma, F. Hollman, J.W. de Vries, E. Warszawik, R. Fischer, U. Commandeur, P. van Rijn, Virus-Polymer Hybrid Nanoparticles via Biocatalytic Surface-induced Polymerization, under consideration.
3. P. Wagler, G.A.S. Minero, U. Tangen, J.W. de Vries, D. Prusty, M. Kwak, A. Herrmann, J.S. McCasckill, Sequence-specific nucleic acid mobility using a reversible block copolymer gel matrix and DNA amphiphiles (lipid-DNA) in capillary and microfluidic electrophoretic separations, accepted.

4. K. Liu, L. Zheng, Q. Liu, J.W. de Vries, J.Y. Gerasimov, A. Herrmann, Nucleic Acid Chemistry in the Organic Phase: From Functionalized Oligonucleotides to DNA Side Chain Polymers, *J. Am. Chem. Soc.*, **2014**, 136, 14255.
5. M.C. Wamberg, R. Wieczorek, S.B. Brier, J.W. de Vries, M. Kwak, A. Herrmann, P.A. Monnard, Functionalization of Fatty Acid Vesicles through Newly Synthesized Bolaamphiphile−DNA Conjugates, *Bioconjug. Chem.*, **2014**, 25, 1678.
6. P. Gordiichuck, G.-J.A.H. Wetzelaer, D. Rimmverman, A. Gruszka, J.W. de Vries, M. Saller, D.A. Gautier, S. Catarci, D. Pesce, S. Richter, P.W.M. Blom, A. Herrmann, Solid-State Biophotovoltaic Cells Containing Photosystem I, *Adv. Mater.*, **2014**, 26, 4863.
7. J.H.M. van der Velde, E. Ploetz, M. Hiermaier, J. Oelerich, J.W. de Vries, G. Roelfes, T. Cordes, Mechanism of Intramolecular Photostabilization in Self-Healing Cyanine Fluorophores, *ChemPhysChem*, **2013**, 14, 4084.
8. T.R. Wilks, J. Bath, J.W. de Vries, J.E. Raymond, A. Herrmann, A.J. Turberfield, R.K. O'Reilly, 'Giant Surfactants' Created by the Fast and Efficient Functionalization of a DNA Tetrahedron with a Temperature-Responsive Polymer, *ACS Nano*, **2013**, 7, 8561.
9. R. Keller, M. Kwak, J.W. de Vries, C. Sawaryn, J. Wang, M. Anaya, K. Müllen, H.-J. Butt, A. Herrmann, R. Berger, Properties of amphiphilic oligonucleotide films at the air/water interface and after film transfer, *Colloid Surface B*, **2013**, 111, 439.
10. J.W. de Vries, F. Zhang, A. Herrmann, Drug delivery systems based on nucleic acid nanostructures, *J. Control. Release*, **2013**, 172, 467.
11. J. Ciric, J. Oostland, J.W. de Vries, A.J.J. Woortman, K. Loos, Size Exclusion Chromatography with Multi Detection in Combination with MALDI-ToF MS as a Tool for Unraveling the Mechanism of the Enzymatic Polymerization of Polysaccharides, *Anal. Chem.*, **2012**, 84, 10463.
12. M. Kwiat, R. Elnathan, M. Kwak, J.W. de Vries, A. Pevzner, Y. Engel, L. Burstein, A. Khatchtourints, A. Lichtenstein, E. Flaxer, A. Herrmann, F. Patolsky, Non-covalent monolayer-piercing anchoring of lipophilic nucleic acids: preparation, characterization, and sensing applications, *J. Am. Chem. Soc.*, **2012**, 134, 280.

Patents

- A. Herrmann; J.W. de Vries; M.S. Spitzer; S.O. Schnichels, Means and Methods for Ocular Drug Delivery, PCT/NL2014/050634, world patent application.

Selected presentations

- J.W. de Vries, "DNA nanotechnology for biomedicine and ophthalmology", Deutsche Ophthalmologische Gesellschaft (DOG) yearly meeting, Leipzig, Germany, 2014.
- L. Strudel, J.W. de Vries, M. Kwak, J. Hofmann, K. Frößl, K.U. Bartz-Schmidt, A. Herrmann, M.S. Spitzer, S. Schnichels, "Comparison of different DNA-based nanoparticles for the treatment of anterior segment diseases", Deutsche Ophthalmologische Gesellschaft (DOG) yearly meeting, Leipzig, Germany, 2014.
- S. Schnichels, J.W. de Vries, S. Dammeier, L. Strudel, K.U. Bartz-Schmidt, A. Herrmann, M.S. Spitzer, "Efficacy and functionality of antibiotic delivery through DNA based nanoparticles", Deutsche Ophthalmologische Gesellschaft (DOG) yearly meeting, Leipzig, Germany, 2014.
- M. Kwak, J.W. de Vries, A. Herrmann, "Biomedicinal application of DNA-based nanostructures", ChemCYS 2014 conference, 2014.
- J.W. de Vries, S. Schnichels, L. Strudel, J. Hofmann, K.U. Bartz-Schmidt, A. Herrmann, M.S. Spitzer, "Enhanced antibiotic delivery through a new class of nanoparticles", Deutsche Ophthalmologische Gesellschaft (DOG) yearly meeting, Berlin, Germany, 2013.
- S. Schnichels, J.W. de Vries, L. Strudel, M. Kwak, J. Hofman, K.U. Bartz-Schmidt, A. Herrmann, M. Spitzer, "A new class of nanoparticles as potential drug carriers for the treatment of anterior segment diseases", Deutsche

Ophthalmologische Gesellschaft (DOG) yearly meeting, Berlin, Germany, 2013.

- M.S. Spitzer, J.W. de Vries, A. Herrmann, K.U. Bartz-Schmidt, S. Dammeier, “Clouding of Intraocular Silicone Oil in the Absence of Emulsification”, Deutsche Ophthalmologische Gesellschaft (DOG) yearly meeting, Berlin, Germany, 2013.
- J.W. de Vries, D.K. Prusty, D.A. Gautier, E. Christen, J. Menz, W. Weber, A. Herrmann, “Optical Detection of Small Molecules using Transcriptional Regulators and catalytically active aptamers”, Dutch polymer days, Veldhoven, The Netherlands, 2012.
- D.A. Gautier, J.W. de Vries, A. Herrmann, “Closing the green-gap in photosystem I with organic dyes”, Dutch polymer days, Veldhoven, The Netherlands, 2012.
- D.K. Prusty, J.W. de Vries, A. Herrmann, ”Carrying out Fluoregenic reactions on the Biomarcomolecule DNA“, Dutch polymer days, Veldhoven, The Netherlands, 2010.

Languages:

Dutch: Native proficiency
English: Full working proficiency
German: Limited working proficiency
Spanish: Elementary proficiency
Polish: Elementary proficiency